THE REGULATORY DOMAIN OF CTP: PHOSPHOCHOLINE CYTIDYLYLTRANSFERASE (CCT): STRUCTURE, MEMBRANE INTERACTIONS, AND SIMILARITY TO α-SYNUCLEIN.

by

Joseph Lee
B.Sc., University of British Columbia, 2006

THESIS SUBMITTED IN PARTIAL FULFILLMENT OF
THE REQUIREMENTS FOR THE DEGREE OF

MASTER OF SCIENCE

In the
Department
of
Molecular Biology and Biochemistry

SIMON FRASER UNIVERSITY
Spring 2011

APPROVAL

Name: **Joseph Lee**

Degree: **Master of Science**

Title of Thesis: **The Regulatory Domain of CTP: phosphocholine cytidylyltransferase (CCT): Structure, Membrane Interactions, and Similarity to α-Synuclein.**

Examining Committee:

Chair: **Dr. David Baillie**
Professor, Department of Molecular Biology and Biochemistry

_____

Dr. Rosemary Cornell
Senior Supervisor
Professor, Department of Molecular Biology and Biochemistry

_____

Dr. Lisa Craig
Supervisor
Associate Professor, Department of Molecular Biology and Biochemistry

_____

Dr. William S. Davidson
Supervisor
Professor, Department of Molecular Biology and Biochemistry

_____

Dr. Jennifer Thewalt
Internal Examiner
Professor, Department of Molecular Biology and Biochemistry

Date Defended/Approved: 31 March 2011

Declaration of
Partial Copyright Licence

ABSTRACT

α-Synuclein, a synaptic vesicle protein whose mis-folding is linked to Parkinson's Disease, and CTP: phosphocholine cytidylyltransferase (CCT), a key regulatory enzyme in phosphatidylcholine synthesis, share a common structure and function. Both contain lipid-inducible, amphipathic helical (AH) membrane binding motifs followed by unstructured acidic tails. Circular dichroism and tryptophan fluorescence studies comparing membrane-binding properties showed that α-synuclein has weaker affinity for anionic phospholipids than CCT tail regions, and a more stringent lipid compositional selectivity for binding. This may reflect the lower propensity of α-synuclein for helical conformation. However, both proteins can penetrate the lipid bilayer to a similar depth. A phospho-mimic version of the CCT tail had lower α-helicity than wildtype CCT upon membrane binding, suggesting phosphorylation affects the secondary structure of the adjacent AH domain. These studies provide a foundation for exploring the usefulness of CCT tails to promote the α-helical character of α-synuclein, thus promoting its non-toxic folding pathway.

DEDICATION

For my Parents and Shirley

Thank you for your encouragement

ACKNOWLEDGEMENTS

I would like to thank my senior supervisor, Rosemary Cornell, for her excellent supervision and suggestions on my thesis work. Your enthusiasm in science and research has motivated me to walk thru the difficulties in life. Thanks also to my committee members, Dr. Lisa Craig and Dr. William S. Davidson for their inputs.

Thanks to all my lab mates, past and present, for being such a great group of people to work with. Special thanks to Ziwei Ding. Thank you for teaching me the use of many lab equipments and the techniques of cell work during the early stages of my research. Thanks also to Svetla Taneva, Melissa Dennis, Harris Huang, and Jaeyong Lee for discussions and ideas about experiments.

Thanks to all the MBB labs for sharing reagents, equipment and ideas, especially the Paetzel and Leroux labs for sharing their equipments and the Pio and Unrau labs for sharing their cuvettes.

Special Thanks to Dr. Neale Ridgeway (Dalhousie University) for providing the original CCT(M+P)-phospho-mimic variant construct and Dr. David Eliezer (Weill Medical School of Cornell University) for providing the original α-synuclein construct.

TABLE OF CONTENTS

Approval ..... **ii**
Abstract ..... **iii**
Dedication ..... **iv**
Acknowledgements ..... **v**
Table of Contents ..... **vi**
List of Figures ..... **viii**
List of Tables ..... **xi**
Glossary ..... **xii**
1 Introduction **1**
1.1 CTP: Phosphocholine Cytidylyltransferase (CCT) 1
1.1.1 CCT and its Role in Phosphatidylcholine Metabolism 1
1.1.2 CCT Isoforms, Cellular Localization and Domain Organization. 3
1.1.3 Membrane Lipid Composition Regulates CCT Binding 8
1.2 α-Synuclein 10
1.2.1 α-Synuclein and its Role in Parkinson's Disease 10
1.2.2 The Folding Pathways of α-Synuclein 12
1.2.3 α-Synuclein Resemblance to CCT 14
1.3 Overview of Objectives 17
2 MATERIALS AND METHODS **19**
2.1 Materials 19
2.1.1 Plasmids 19
2.1.2 Rosetta™ Cells 20
2.2 Methods 20
2.2.1 Polymerase Chain Reaction 20
2.2.2 QuikChange Site-Directed Mutagenesis 21
2.2.3 Recombinant DNA General Methods 22
2.2.4 Preparation of CCT, CCT-phospho-mimic and α-Synuclein Constructs and Variants 24
2.2.5 Expression of Protein via IPTG Induction using pET Vectors 34
2.2.6 Protein Purification: His-tagged Protein Purification (Optimized Protocol) 34
2.2.7 Thrombin Digestion 36
2.2.8 Sample Concentration And/Or Buffer Exchange 36
2.2.9 Protein Biochemical Methods 36
2.2.10 Chemical Analysis of Detergent β-Octylglucoside Concentration 37
2.2.11 Gel Electrophoresis 38

2.2.12 Preparation of Small Unilamellar Vesicles (SUVs) 38
2.2.13 Circular Dichroism Spectroscopy and Deconvolution Protocol 39
2.2.14 Tryptophan Fluorescence Analyses 40

3 DEVELOPMENT OF A PURIFICATION PROTOCOL FOR HIS-TAGGED CCT TAILS AND α-SYNUCLEIN 42

3.1 Introduction 42
3.2 Results and Discussion 42
3.2.1 Expression protocol for CCT Tail Domains and α-Synuclein 42
3.2.2 Development of Nickel Affinity Chromatography Protocol 44
3.2.3 Development of Thrombin Digestion Protocol 50
3.2.4 Potential Pitfalls of Octyl ß-Glucoside 52
3.3 Concluding Discussion 52

4 COMPARATIVE INVESTIGATION OF THE LIPID INTERACTION OF CCT TAILS AND α-SYNUCLEIN 55

4.1 Introduction 55
4.2 Results 57
4.2.1 CCT Tail Domains Have Higher Affinity than α-Synuclein for Membranes Containing Anionic Lipids 57
4.2.2 Comparison of Lipid Compositional Selectivity of WT and Phospho-mimic CCT Tails, and α-Synuclein. 67
4.2.3 CCTs and α-Synuclein Bind with Similar Extent of Bilayer Penetration 72
4.2.4 How Does the Phospho-mimic Modification Affect CCT's Domain M? 76
4.3 Discussion 85
4.3.1 CCT Tail Domains and α-Synuclein Conversion to α-Helices, Promoted by Lipids, Occurs at the Expense of Beta Structure. 85
4.3.2 α-Synuclein and CCT Tails Differ in Their Response to Type II Lipids 89
4.3.3 Phospho-Mimic Modification Does Not Affect the Structure or Membrane Binding of the Proximal Portion of the M Domain 91
4.3.4 C-terminal Limit of Domain M Includes Residue 302 91

5 CONCLUDING DISCUSSION 93

References 98

Appendices 107

Appendix A: PCR And Thermocycling Reaction Conditions 107
Appendix B: Oligonucleotide Primers 109
Appendix C: Purification of WT and PM CCT Tails and α-Synuclein Tryptophan Variants 117

LIST OF FIGURES

Figure 1.1 PC metabolic pathway: CDP-choline pathway 2

Figure 1.2 The Domain Structure of CCTα 3

Figure 1.3 Model of the Soluble and Membrane Bound CCT dimer 7

Figure 1.4 Folding Pathway for α-Synuclein 13

Figure 1.5 11/3 Helical Wheel Representations of Domain M of Rat CCTα and Human α-Synuclein 15

Figure 1.6 Alignment of α-Synuclein with Domain M+P of CCTα 16

Figure 2.1 Construction of pET-14b-CCT237-367 25

Figure 2.2 Construction of pET-14b-CCT237-367-phospho-mimic 27

Figure 2.3 Construction of pET-14b-α-Synuclein 29

Figure 2.4 Construction of pET-14b-CCT237-367-W336F, pET-14b-CCT237-367- phospho-mimic-W336F, and pET-14b-α-Syn-V37W 31

Figure 2.5 Construction of pET-14b-CCT237-367-M302W and pET-14b-CCT237-367- phospho-mimic-M302W 33

Figure 3.1 Protein Expression Test of N-terminal His-tagged CCT(M+P) Varying Temperature and Time of IPTG Induction 43

Figure 3.2 Protein Expression of N-terminal His-tagged Proteins 44

Figure 3.3 Nickel-affinity Chromatography in the Absence of Detergent Results in Loss of Soluble Protein. 45

Figure 3.4 SDS Promotes α-Helix Formation in WT CCT Tail 47

Figure 3.5 Nickel-affinity Chromatography with the Use of the Detergent OG Generates High Recovery of Soluble Protein. 49

Figure 3.6 Thrombin Digestion of N-terminal His-tagged Proteins 51

Figure 3.7 Flow Chart for Expression and Purification of His-tagged Proteins 54

Figure 4.1 Effect of Protein/Lipid Incubation Time and the Effect of Freeze-Thaw Cycle on the Secondary Structure of α-Synuclein 58

Figure 4.2 Circular Dichroism Spectra of Proteins in the Absence and Presence of Increasing Concentration of Lipid. 60

Figure 4.3 Comparison of the Effect of Lipid to Protein Molar Ratio on the Secondary Structure of WT and Phospho-Mimic CCT Tail Domains and α-Synuclein 61

Figure 4.4 Replot of the Percent Structure Distribution Shown in Figure 4.3 for the CCT tail-PM and α-Synuclein Using the Same L/P Scale 62

Figure 4.5 Anionic Vesicles Induce Protein Tryptophan Fluorescence Enhancement and Blue-Shift. 65

Figure 4.6 Comparison of the Effect of Lipid-to-Protein Molar Ratio on the Tryptophan Blue Shift of WT and Phospho-mimic CCT Tail Domains and α-Synuclein to Anionic Lipid SUVs 66

Figure 4.7 Comparison of the Effect of Various Mol% PG on the Secondary Structure of WT and Phospho-mimic CCT Tail Domains and α-Syn. 68

Figure 4.8 Comparison of the Effect of the Mol% of Egg PG on the Tryptophan Blue Shift of WT and Phospho-mimic CCT Tail Domains and α-Syn 69

Figure 4.9 Comparison of the Effect of Different Anionic Lipid Vesicles on the Secondary Structure of CCT (M+P). 70

Figure 4.10 Comparison of the Effect of Type II Lipid (DOPE) on the Secondary Structure of WT and Phospho-mimic CCT Tail Domains and α-Synuclein. 71

Figure 4.11 Quenching of Tryptophan Fluorescence in CCT Tails and α-Synuclein by Aqueous Iodide. 73

Figure 4.12 Stern-Volmer Plot for Iodide Quenching of Tryptophan Fluorescence. 75

Figure 4.13 Amphipathic Helix Insertion Model vs. Domain M C-terminus Disorder Model 77

Figure 4.14 Anionic Vesicles Induce Protein Tryptophan Fluorescence Enhancement and Blue-Shift Indicating Membrane Penetration of Trp 302 79

Figure 4.15 Comparison of the Effect of Lipid-to-Protein Molar Ratio on the Tryptophan-302 Blue-Shift of WT and Phospho-mimic CCT(M+P)-M302W 80

Figure 4.16 Effect of Increasing Anionic Lipid on Trp-302 Fluorescence 81

Figure 4.17 Comparison of the Effect of Increasing PG Content on Trp-302 Blue-shifts in WT and Phospho-mimic CCTs. 82

Figure 4.18 Quenching of Tryptophan Fluorescence in CCT Domain M C-terminus by Aqueous Iodide. 83

Figure 4.19 Stern-Volmer Plot for Iodide Quenching of Tryptophan-302 Fluorescence..... 84

Figure 4.20 Binding Curve of CCT(M+P)-PM and α-Synuclein for PC/PG (1/1) vesicles] 88

Figure 4.21 ProfSec Secondary Structure Prediction of CCT(M+P) and α-Synuclein 89

LIST OF TABLES

Table 3.1 Yields of WT and Various Variants of CCT(M+P), CCT(M+P)-PM, and α-Syn Determined by Nanodrop and Amino Acid Analyses..... 54

Table 4.1 Stern-Volmer Iodide Quenching Constants for WT and Phospho-mimic CCTs: a Comparison of Quenching of Trp-278 with Trp-302. 85

GLOSSARY

AFM:	atomic force microscopy
AH:	amphipathic helix
bp:	base pair
CCT:	CTP:phosphocholine cytidylyltransferase
DAG:	diacylglycerol
DOPC:	dioleoylphosphatidylcholine
DOPE:	dioleoylphosphatidylethanolamine
DTT:	dithiothreitol
EDTA:	ethylenediaminetetraacetic acid
EM:	electron microscopy
ER:	endoplasmic reticulum
ESR:	electron spin resonance
IPTG:	isopropyl β-D-1-thiogalactopyranoside
LUVs:	large unilamellar vesicles
NLS:	nuclear localization sequence
NMR:	nuclear magnetic resonance
OG:	β-octylglucoside
PA:	phosphatidic acid
PAG(E):	polyacrylamide gel (electrophoresis)
PBS:	phosphate buffered saline
PC:	phosphatidylcholine
PCR:	polymerase chain reaction
PG:	phosphatidylglycerol

PI:	phosphatidylinositol
PM:	phospho-mimic
PMSF:	phenylmethylsulphonylfluoride
PS:	phosphatidylserine
SAP:	shrimp alkaline phosphatase
SDS:	sodium dodecyl sulphate
SNARE:	N-ethylmaleimide–sensitive factor attachment protein receptor
SUVs:	small unilamellar vesicles
Tris:	Tris(hydroxymethyl)methylamine
WT:	wild-type

1 INTRODUCTION

In this thesis I began a comparison of the structure and membrane-binding properties of two distinct proteins that share a common feature, a lipid-inducible amphipathic helix (AH) that functions in membrane binding. While laboratories have separately examined the structure and behaviour of cytidylyltransferase and α-synuclein, this is the first time they have been studied in parallel. In the introduction of my thesis, I review the relevant literature pertaining to the structure and function of these two proteins followed by an overview of my specific objectives.

1.1 CTP: Phosphocholine Cytidylyltransferase (CCT)

1.1.1 CCT and its Role in Phosphatidylcholine Metabolism

CTP: phosphocholine cytidylyltransferase (CCT) is the rate-limiting enzyme in the CDP-choline pathway (Kennedy pathway) for the production of phosphatidylcholine (PC) (Figure 1.1). Cells take in choline by facilitated transport. Choline is phosphorylated in a step catalyzed by choline kinase to form phosphocholine. In the rate-limiting step, CCT catalyzes the formation of the activated cytidine intermediate, CDP-choline, by transferring cytidine 5'-monophosphate from CTP onto the phosphocholine. Lastly, choline phosphotransferase catalyzes the condensation of CDP-choline with diacyglycerol (DAG) to generate PC.

CCT was first discovered by Kennedy and Weiss while studying the enzymatic synthesis of CDP-choline in rat liver (Kennedy and Weiss, 1956). Its activation by lipid fractions from cells was reported in 1966 (Fiscus and Schneider, 1966). It was particularly difficult to purify CCT due to its tendency to aggregate, leading to poor yields. In the 1980's, Weinhold *et al.* finally purified the protein from rat liver with the addition of lipids and detergents (Weinhold *et al.,* 1986). CCT is an amphitropic enzyme, i.e. it is active when membrane-bound but inactive in its soluble form (Cornell and Northwood, 2000; Kent, 1997). From much research in several labs during the 1980s, a model for regulation of PC synthesis emerged in which the PC synthesis rate is controlled by the translocation of CCT from a soluble to a particulate compartment (Cornell and Northwood, 2000; Kent, 1997).

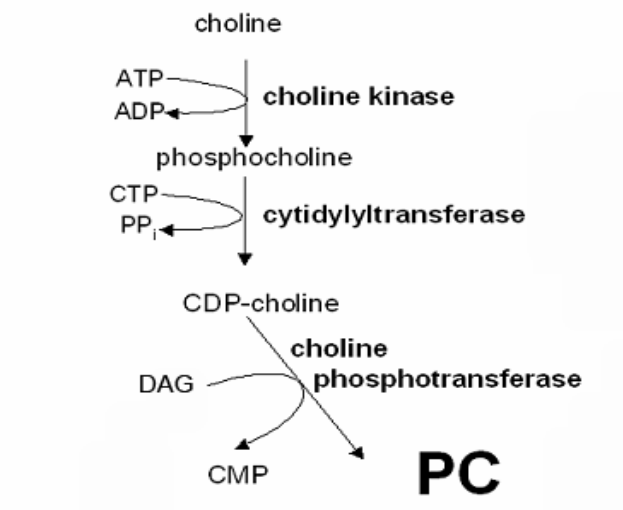

Figure 1.1 PC metabolic pathway: CDP-choline pathway

1.1.2 CCT Isoforms, Cellular Localization and Domain Organization.

CCT is encoded by an ancient and conserved gene (pcyt1), being found in eukaryotic organisms ranging from yeast and plasmodia to mammals. In mammals there are two CCT genes, pcyt1a and pcyt1b, encoding CCTα and β. CCTα is the major form ubiquitously expressed among mammalian tissues and developmental stages, and by far the best characterized. While CCTα is found in the nucleus of most cells (Houweling *et al.*, 1996), imported using its N-terminal nuclear localization sequence (NLS), CCTβ lacks an NLS and is cytoplasmic (Lykidis *et al.*, 1999). The rationale for a nuclear CCTα is not well understood, as the final step in PC synthesis occurs on the endoplasmic reticulum (ER).

CCTs are subdivided into 4 domains: the amino terminal domain (domain N, residues 1-72), the catalytic domain (domain C, residues 73-236), the membrane-binding domain (domain M, residues 237-299), and the carboxy terminal phosphorylation domain (domain P, residues 315-367) (Figure 1.2). Each of these CCT domains has its own specific function (reviewed in Cornell and Northwood, 2000).

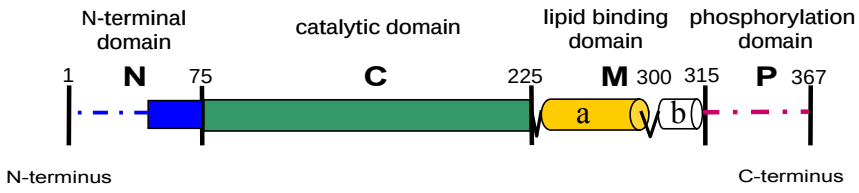

Figure 1.2 The Domain Structure of CCTα
The regions of the N and C-termini that are denoted by dashed lines indicate that they are intrinsically disordered. Portion (a) of domain M was determined to be a helix, whereas portion (b) has never been explored. The exact boundary of the structural domain M is not known.

1.1.2.1 Head Domain of CCT

The head domain of CCT consists of domain N and domain C. Domain N contributes, along with domain C, to form the CCTα dimer interface (Xie *et. al*., 2004, Lee *et al.*, 2009). The first 40 residues of the N region are not conserved between isoforms within a species nor in CCT orthologs. In CCTα, domain N houses an NLS sequence (a.a. 8-16) which is necessary and sufficient for nuclear import (Wang *et al.,* 1995). The catalytic domain C shows the highest homology with other members of the cytidylyltransferase superfamily and resembles the larger nucleotidyl-transferase superfamily in its fold and catalytic mechanism (Park *et al.,* 1997; Lee *et al.,* 2009). The structure of CCT1-236 was recently solved to 2.2 Á resolution (Lee *et al.,* 2009).

1.1.2.2 Tail Domains of CCT

The tail domain of CCT functions to regulate the catalytic domain and is comprised of domains M and P. Previous experiments using synthetic peptides have shown that domain M of the CCT tail is predominantly disordered when in buffer alone (Johnson and Cornell, 1994; Taneva *et al.,* 2003). Numerous algorithms for secondary structure prediction and for disorder/order prediction show that domain P has a high probability for disorder, while the prediction for domain M is highly disordered at the N-terminal portion and ordered at the C-terminal region (between residues 280-300) (Dennis *et al.,* 2011).

Domain M. This domain is responsible for binding CCT to membranes and thus activating the enzyme's catalytic function. The membrane binding domain was mapped onto amino acid residues 237-300 using many diverse approaches,

including chymotrypsin digestion followed by isolation of membrane-bound fragments via sucrose density gradient centrifugation (Craig *et al.*, 1994), mutagenesis experiments (Wang and Kent, 1995a; Cornell *et al.,* 1995), and vesicle binding assays with synthetic peptides derived from domain M sequence (Johnson and Cornell, 1994; Johnson *et al.,* 1998; Johnson *et al.,* 2003). Within this domain there are four 11-mer tandem repeats (residues 248-290), which I will discuss below, as they resemble the 11-mer motif repeat in α-synuclein. Although most literature predicted the C-terminal boundary of domain M to locate at the turn between amino acid residues 293-296, there is a region weakly predicted to be α-helical between residues 297-313. In this thesis I explored the possibility that domain M includes this second helix (Domain M *b*) as shown in Figure 1.2.

The membrane binding of domain M is regulated by the lipid composition (discussed in 1.1.3). Upon membrane binding, domain M converts from a mixture of conformations into an AH that intercalates into the hydrophobic zone of the bilayer (Dunne *et al.,* 1996; Johnson *et al.,* 1997; Taneva *et al.,* 2003; Figure 1.3). 2D homonuclear nuclear magnetic resonance analyses of domain M synthetic peptides in complex with sodium dodecyl sulphate (SDS) showed that the α-helix extends from residues 241-288 (Dunne *et al.,* 1996). The non-polar face within this amphipathic segment contains 18 hydrophobic residues, sufficient to drive hydrophobic interactions with the lipid bilayer and to promote membrane intercalation (Dunne *et al.,* 1996). In its AH structure, the interface between the polar and non-polar helical faces is rich in lysine residues. Substitution of groups of these lysines to glutamine in domain M peptides showed that they are essential

for the electrostatic component of binding (Johnson *et al.,* 2003). In addition, there are three glutamate residues flanking one of the interfaces. When these glutamates are near the surface of anionic membranes, they become protonated in the low pH environment hence increasing the hydrophobicity of domain M. When these glutamates were substituted with glutamines, it eliminated the pH dependence of *in vitro* vesicle binding and reduced anionic membrane selectivity. This showed that the glutamates are crucial charge sensors which make domain M dependent on membrane negative surface charge for binding (Johnson *et al.,* 2003). These two interactions, electrostatic interaction of lysine strips and protonation of three interfacial glutamates, generate selectivity for anionic membranes (Johnson *et al.*, 2003).

Domain M serves as the auto-inhibitory region for the catalytic domain (Figure 1.3). When CCT is in its soluble form, domain M interacts with the catalytic (or other) domain to create an inhibitory constraint on the active site (Friesen *et al.,* 1999). This inhibitory constraint is relieved upon binding of domain M to membranes. The key evidence for this mechanism is the creation of the constitutively active enzyme CCT236, a variant that lacks domain M + P and does not require membrane translocation for activation (Friesen *et al.*, 1999). A CCT variant with only domain P deleted remains as a lipid-requiring enzyme, thus confirming the inhibitory region maps onto domain M (Wang and Kent, 1995a; Yang *et al.*, 1995).

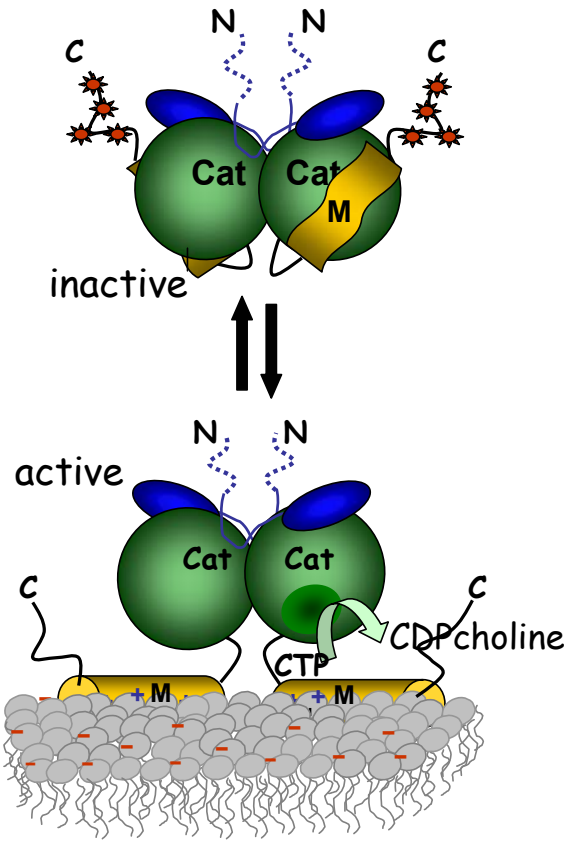

Figure 1.3 Model of the Soluble and Membrane Bound CCT dimer
In the soluble form, domain M is proposed to act as an auto-inhibitor of catalysis. The phosphorylation sites on domain P are indicated by red ¤ symbols. In the presence of anionic or type II lipid membranes, CCT interacts with the membrane via the amphipathic helix domain M, and this is sufficient to activate the enzyme.

Domain P. The phosphorylation domain P of CCT, which is approximately 50 residues long, is highly unstructured, proline-rich and susceptible to protease digestion (Bogan *et al.,* 2005). There are a total of 16 serines residues that may serve as phosphorylation sites. Of these 16 serines, seven are followed by prolines, leading to a hypothesis that proline-directed kinases are responsible for CCT phosphorylation (MacDonald and Kent, 1994, Wang and Kent, 1995b).

There is an inverse correlation between the extent of CCT phosphorylation on domain P and its membrane partitioning in cells (Houweling, 1994; Wang *et al.,* 1993; Walkins and Kent, 1991; Northwood *et al.,* 1999).

Based on *in vitro* studies showing an increase in membrane affinity upon dephosphorylation, Arnold *et al.* (1997) proposed that the phosphates on phosphorylated CCT might forge electrostatic interactions with basic residues on the membrane-binding domain. Hence, when phosphorylated, domain P antagonizes binding of CCT to the membrane. Upon addition of increasing activating lipids, these interactions would be out competed by negative charges on the membrane bilayer. Although the exact mechanism for antagonism of membrane binding by the phosphorylated P domain is unresolved, Dennis *et al.* (2011) showed that phosphorylation is an especially powerful modulator of the membrane affinity of the CCT beta isoform.

1.1.3 Membrane Lipid Composition Regulates CCT Binding

That CCT would have a built-in sensor of the membrane PC content makes metabolic sense. CCTs from diverse species have evolved a mechanism, via domain M conformational changes, to respond to the physical properties of PC-deficient membranes. *In vitro* purified CCT does not bind to pure PC vesicles (Arnold *et al.,* 1996; Arnold *et al.,* 1997). Two major classes of lipids have been identified that promote CCT-vesicle binding.

The first and most potent class of lipids is phospholipids with anionic head groups (charged lipids) such as phosphatidic acid (PA), phosphatidylglycerol (PG),

phosphatidylinositol (PI), and phosphatidylserine (PS). The second class includes Type II lipids with small head groups that promote negative curvature strain and packing defects in lipid bilayers (Davies *et al.*, 2001). These lipids consist of DAG and unsaturated phosphatidylethanolamine (PE). The combination of these two classes of lipids results in a synergistic effect of CCT binding to membranes and activation of its catalytic function (Arnold and Cornell, 1996).

Domain M binding to charged membranes is a two-step process. The first step involves electrostatic absorption, bringing CCT close to the membrane surface, followed by hydrophobic interactions which involve CCT intercalation into the non-polar core of the bilayer. The electrostatic absorption requires that the negatively charged phospholipid head groups attract basic amino acids situated on the interfacial boundary of domain M. This promotes membrane surface localization of CCT and hence facilitates the intercalation of the membrane-binding domain to the lipid bilayer. The degree of CCT binding to membranes is proportional to the net negative membrane surface charge (Arnold and Cornell, 1996; Cornell, 1991a).

Type II lipids also promote the insertion of CCT into the lipid bilayer (Davies *et al.*, 2001; Johnson *et al.*, 2003). However, the mechanism is quite different from that of anionic lipids. CCT binds bilayers enriched in type II lipids by responding to their interfacial packing defects, low lateral pressure, acyl chain disorder and negative curvature strain. Type II lipids, such as DAG and unsaturated PE, are characterized by their small head groups. This characteristic creates surface voids, cracks and other packing defects. Since these lipids have small head

groups, they are represented by an inverse cone shape which promotes the bilayer to curl and form a concave surface, creating negative curvature strain. This energetic tension is released when CCT inserts its membrane binding helix into the lipid bilayer (Davies *et al.*, 2001).

1.2 α-Synuclein

1.2.1 α-Synuclein and its Role in Parkinson's Disease

The synucleins are relatively new genes, arising with the evolution of chordates. There are three synucleins, α, β, and γ. α-Synuclein (α-Syn) is expressed primarily in the brain, and Parkinson's Disease associated degeneration occurs preferentially in the substantia nigra, leading to principle motor symptoms. Some studies have suggested a role for α-syn in trafficking synaptic vesicles carrying dopamine to the synaptic junction (Cabin *et al.,* 2002; Larsen *et al.,* 2006). Recently, new results have emerged to suggest how membrane-bound α-syn functions in regulating vesicle docking and fusion. Burré *et al.* (2010) showed that α-syn promotes the assembly of N-ethylmaleimide–sensitive factor attachment protein receptor (SNARE) - membrane fusion complex by simultaneously binding to the phospholipids with its N-terminus and synaptobrevin-2 (a component of the SNARE-complex) with its C-terminus.

Parkinson's disease is one of the most common neurodegenerative diseases caused by deterioration of dopaminergic neurons in substantia nigra of the human brain. A neuropathologic feature of Parkinson's disease is the presence of Lewy bodies composed of amyloid fibrillar deposits of α-syn

(Spillantini, 1997). The association of Parkinson's disease with elevated α-syn levels has been demonstrated in three distinct ways: over-expression via triplication of the α-syn gene SNCA in humans with early-onset PD (Singleton *et al.,* 2003), the impairment of efficient lysosomal degradation of α-syn (Cuervo *et al.,* 2004), and transgenic introduction of α-syn into Drosophilia (Feany and Bender, 2000) or mice that lack endogenous α-syn gene (Masliah *et al.*, 2000). These substitutions or manipulations lead to PD symptoms, such as amyloid fibrillar deposits and characteristic motor defects, which suggests that the accumulation of excess α-syn leads to the onset of PD.

Synuclein alleles linked to early onset Parkinson's Disease include single-site sustitutions, A30P, A53T, and E46K (Polymeropoulos *et al.,* 1997; Kruger *et al.,* 1998; Zarranz *et al.,* 2004). These site-specific substitutions alter α-syn's overall structure in various ways. First, A→P substitution at residue 30 disrupts the α-helical domain of α-syn resulting in the decrease in affinity for phospholipids and amyloid formation *in vitro* (Yonetani *et al.,* 2009). Alternatively, the A30P variant may promote aggregation by favoring the formation of stable, soluble toxic oligomers. Secondly, the A53T variant was discovered to destabilize the α-helical domain (Biere *et al*., 2000). This substitution expands the hydrophobic core and consequently promotes the protein's ability to adopt the β-sheet structure required for the formation of oligomeric species (Conway *et al*., 1998, Giasson *et al*., 1999). Lastly, the E46K substitution was shown to expose the hydrophobic surfaces. This alteration enhances the potential for intermolecular interactions hence accelerates dimer and toxic oligomer formation

(Rospigliosi *et al.,* 2009). These variants are more prone to aggregation *in vitro* and enhance fibrillation *in vivo*, supporting the idea that oligomerization of α-syn into β-amyloid fibrils is linked to the pathogenesis of PD (Li *et al.,* 2001; Fredenburg *et al.,* 2007; Giasson *et al.,* 2002).

1.2.2 The Folding Pathways of α-Synuclein

α-Syn is prone to several complex folding pathways and takes on different conformations *in vitro* (Figure 1.4; Lee *et al.,* 2002). α-Syn monomers in solution do not acquire any predominant secondary structure and are considered to be intrinsically disordered (Weinreb *et al*., 1996). The addition of detergent micelles (a good membrane-mimetic for analysis of peptide structure) induces an AH conformation in α-syn, which spans over residues 3-92 with a short interruption at residues ~41-44 (Chandra *et al*., 2003; Georgieva *et al*., 2008). Recently, Georgieva *et al.* (2010) showed that α-syn helix adopts either a broken or an extended helical conformation, depending on the detergent-to-protein ratio. However, the negatively charged C-terminal tail remains disordered and is proposed to act as a scaffold to recruit additional proteins to the membranes and bind to SNARE components (Eliezer et al., 2001). As illustrated in Figure 1.4, a large molar excess of anionic lipids would drive α-syn to adopt a helical character as it binds to the lipids. This mechanism slows the kinetics of aggregation and hence inhibits the formation of fibrils (Zhu and Fink, 2003). On the other hand, the monomeric α-syn will oligomerize when there is an increase in α-syn concentration (due to increased expression of the α-syn gene or an insufficiency of lipid vesicles) and eventually form amyloid fibrils that are β-sheet structure

(Fink, 2006). Interestingly, α-syn amyloid fibril formation proceeds through a series of discrete oligomeric intermediates, referred to as protofibrils, which disappear upon fibril formation. This intermediate is rich in β-sheet structure and appeared as spherical, chainlike, and annular morphologies in electron microscopy and atomic force microscopy images (Uversky *et al.*, 2001; Ding *et al*., 2002; Fink, 2006).

The α-syn missense variants that are related to early onset of PD affect the oligomerization rate. While the A30P and A53T variants accelerate the formation of α-syn protofibrils, the A30P substitution delays the formation of amyloid fibrils relative to wild-type (WT), suggesting that protofibrils, rather than fibrils, may be the pathogenic species (Conway *et al.*, 2000; Volles and Lansbury, 2003). Oligomers permeabilize lipid vesicles, whereas fibrils do not (Fredenberg *et al*., 2007)

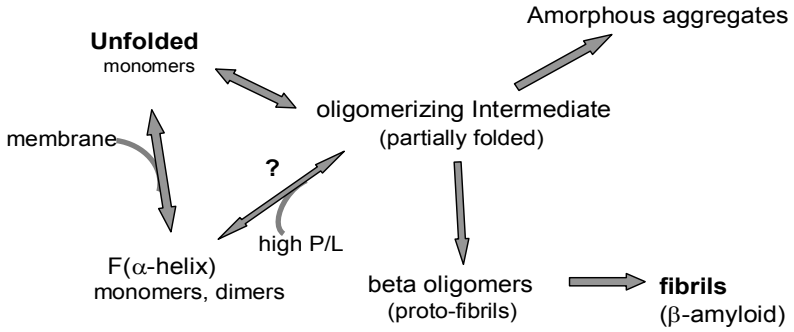

Figure 1.4 Folding Pathway for α-Synuclein
The complex folding pathway of α-synuclein is influenced by its concentration and also by the availability of a suitable membrane surface. At limiting membrane, the α-syn can concentrate on membrane surfaces leading to an *enhancement* of oligomerization

1.2.3 α-Synuclein Resemblance to CCT

1.2.3.1 Long Amphipathic Helix for Membrane Binding

The N-terminus (residues 3-92) of α-syn and domain M of CCT are well characterized membrane binding domains. Upon the addition of lipid vesicles, both of these proteins undergo a transition from disordered into α-helix conformation. Their long AHs bind to the vesicle surface with the helix axis parallel to the surface and penetrate deep into the hydrocarbon core (Figure 1.5). Studies have shown these two proteins share similar membrane binding properties. They show selectivity for anionic vesicles (Cornell, 1998; Arnold and Cornell, 1996; Jo *et al.,* 2000; Perrin *et al.,* 2000; Davidson *et al.,* 1998) and membranes at the gel / fluid phase transition (Cornell, 1991b; Nuscher, 2004). This suggests both proteins bind via a combination of electrostatic and hydrophobic interactions. Also, studies have shown that a high protein to lipid ratio tends to destabilize the bilayers (Taneva *et al.,* 2005; Zhu *et al.,* 2003) indicating that the proteins penetrate into the hydrocarbon core.

While it has been shown that α-syn prefers very small vesicles with high curvature (Middleton and Rhoades, 2010), this has not been investigated for CCT. Moreover, while binding to type II lipids has been demonstrated for CCT (Davies *et al.*, 2001; Taneva *et al.*, 2005), this has not been explored for α-syn.

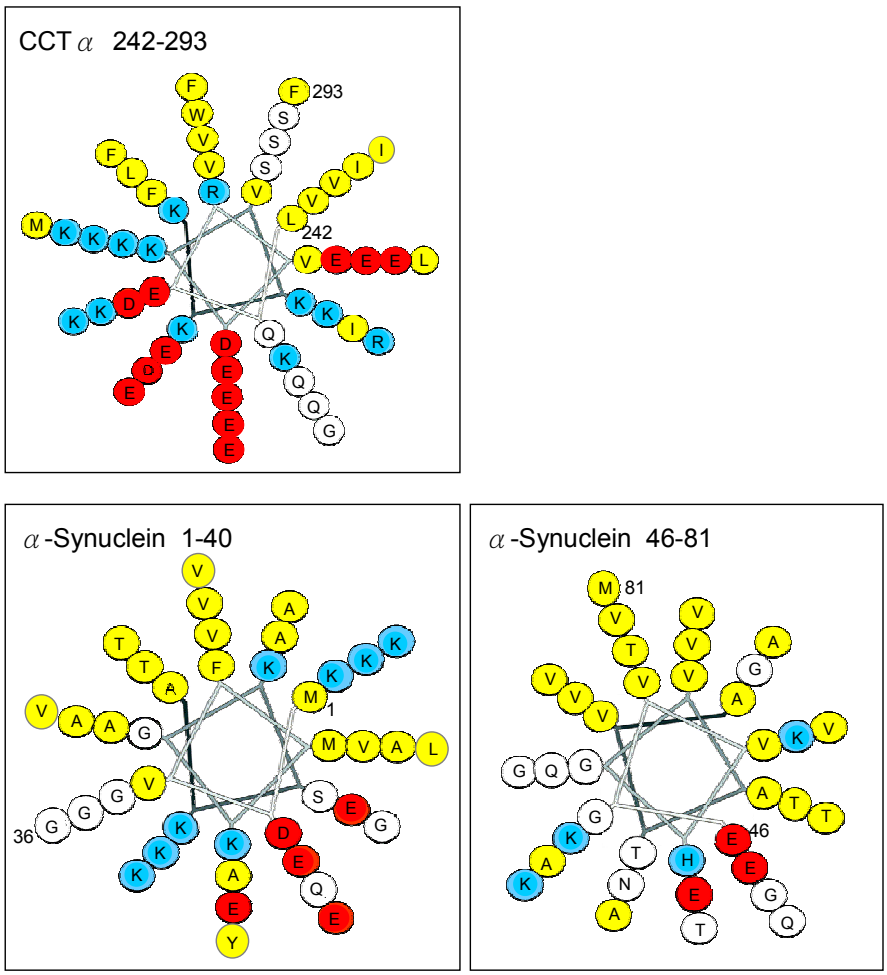

Figure 1.5 11/3 Helical Wheel Representations of Domain M of Rat CCTα and Human α-Synuclein
Acidic residues are Red. Basic residues are blue. Polar/hydrophilic residues are white. Non-polar/hydrophobic residues are yellow. Modified from Cornell and Taneva, 2006.

1.2.3.2 Membrane-Binding Region 11-mer Repeats

Domain M of CCT possesses four copies of 11-mer tandem repeats with the consensus motif **KSKEFVXKϕEE,** where ϕ represents hydrophobic residues (Figure 1.6). Residues 10-90 of α-syn also contain seven copies of imperfect 11-mer repeats that make up the AH. This whole region, especially the hydrophobic sequence between residues 71-82, is needed for oligomerization of

α-syn and fibril formation (Soper, 2008). Comparing the first five 11-mer repeats from α-syn (**KTKEGVϕXϕXX)** with those of CCT, there is a pattern similarity in position 1-4, 6, and 9 (Figure 1.6). Many other proteins have 11-mer-containing AHs such as apopliproteins, perilipins, and dehydrins (Bussell and Eliezer, 2003). However, only synucleins and CCTs exhibit a sequence match, as determined by a bioinformatics analysis that examined sequence matches to a profile generated from a combination of CCT and synuclein inputs (Semenec, Chen, Cornell, unpublished)

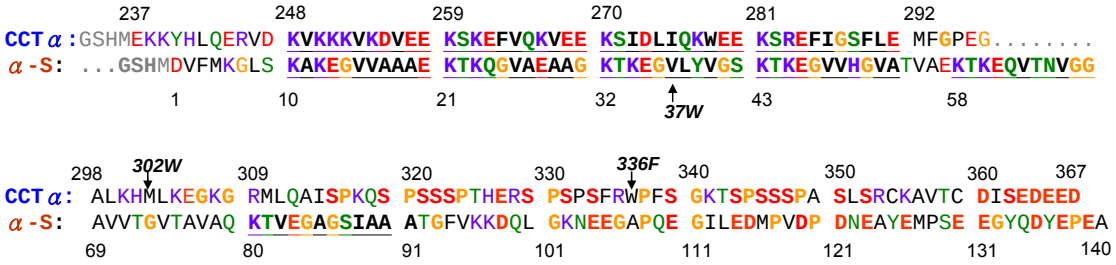

Figure 1.6 Alignment of α-Synuclein with Domain M+P of CCTα
Grey are linker residues. Red are acidic residues and phospho-serine sites. Basic residues are blue. Polar/hydrophilic residues are green. Non-polar/hydrophobic residues are black. Glycine and proline residues are orange. Bold and underlined residues refer to 11-mer motif**.** Residues with arrow and bold / *italics* numbers are sites for site-specific substitutions.

1.2.3.3 C-terminal tail of α-Synuclein Resembles that of CCT Domain P

α-Syn's C-terminal ~50 residues greatly resembles the phosphorylated CCT domain P in that it is acidic and disordered. Results from limited proteolysis, circular dichroism (C.D.), nuclear magnetic resonance, and electron spin resonance, have showed that domain P of CCT (Taneva *et al.*, 2003; Bogan *et al.*, 2005) and the α-syn tail (Eliezer *et al.,* 2001; Jao *et al.,* 2004; Ulmer *et al.,* 2005)

are highly disordered. CCT domain P has 16 potential phosphorylation sites (MacDonald and Kent, 1994), and the more heavily phosphorylated CCT species are in the soluble cell fraction while dephosphorylated CCT is more abundant in the membrane fraction (Watkins and Kent, 1991). By comparing phosphorylated and unphosphorylated α-syn at Ser-129, Paleologou *et al.* (2008) demonstrated that the phosphorylated species is more disordered and tends to inhibit fibrillation. These data suggest that phosphorylation of CCT and α-syn increases their solubility.

1.3 Overview of Objectives

My major goal has been to compare the membrane binding properties of the CCT tail domains with that of α-syn. I have also examined how the phospho-mimic (PM) substitution (16S→E) on the CCT tail domain affects membrane interactions.

Some of the specific questions asked are:

(1) Do CCT tail domains and α-syn have the same affinity for anionic lipids and type II lipids? Do they both penetrate the membrane upon binding?

(2) How does the phosphorylation-mimic (16S→E) of CCT's domain P affect the membrane binding domain?

(3) What is the C-terminal boundary of CCT's domain M?

I attempted to address these questions with the research presented in this thesis, largely using the approach of C.D. and tryptophan (Trp) fluorescence analysis. To compare CCT tail domains and α-syn affinity for anionic and type II

lipids, I investigated side-by-side the lipid composition and lipid-to-protein ratio requirements for induction of secondary structure elements and bilayer insertion using identical analytical methods, buffer systems, and lipid variants. Although many studies have been done using full length CCT and domain M peptides, the isolation and lipid interaction of complete CCT tail domain encompassing domains M+P has never been tested. To explore whether phosphorylation of domain P affects its structure, potential domain M interaction and membrane binding affinity, parallel studies were done using unphosphorylated and PM (16S→E) tails in the absence and presence of lipids. To examine the C-terminal extent of domain M, I selectively substituted M302 with a Trp residue to determine the effect of anionic lipid vesicles on its fluorescence.

2 MATERIALS AND METHODS

2.1 Materials

Restriction enzymes and accompanied buffers, gel purification kits, isopropylthio-β-galactoside (IPTG) and DH5α *E. coli* Competent Cells were from Invitrogen. Oligonucleotide primers were from Invitrogen and Integrated DNA Technologies (IDT). DpnI, *PfuTurbo* DNA polymerase and buffer, DNA ladder standards, and Rapid Ligation kit were from Fermentas. Thrombin protease, dNTPs and ECL Western Blotting detection kit were from GE Healthcare. *E. Coli* XL1-Blue® Supercompetent Cells were from Stratagene. Ampicillin, chloramphenicol, cytidine triphosphate (CTP), sodium dodecyl sulphate (SDS), and β-octylglucoside (OG) were from Sigma. Rosetta™ Competent Cells and pET-14b expression vector were from Novagen. Egg phosphatidylcholine (PC) and egg phosphatidylglycerol (PG) were from Northern Lipids. Dioleoylphosphatidylcholine (DOPC) and dioleoylphosphatidylethanoamine (DOPE) were from Avanti Polar Lipids. Plasmid DNA extraction kits and Ni-NTA agarose beads were from Qiagen. Shrimp Alkaline Phosphatase was from Roche. Amicon Ultra centrifugal filter devices were from Millipore. Sequencing was done by Operon.

2.1.1 Plasmids

The pET-14b vector is a bacterial expression plasmid that uses an IPTG-inducible T7 RNA polymerase promoter. It has a N-terminal His-tag

sequence followed by a thrombin cleavage site and three cloning sites. pET-14b also has a pBR322 origin and an ampicillin resistant gene.

pET-14b was propagated in either: 1) DH5α strain of *E. coli* (supE44ΔlacU169[Φ80lacZΔM15]hsdR17recA1endA1 gyrA96thi-1relA1) in LB (10 g NaCl, 10 g bacto-tryptone, 5 g yeast extract/L, pH 7.0) media supplemented with 100 µg/ml ampicillin) or 2) Rosetta™ host strains, a BL21 derivatives, of E. coli (F^- ompT $hsdS_B(r_B^- m_B^-)$ gal dcm pRARE (Cam^R)) in LB media supplemented with 100 µg/ml ampicillin and 32 µg/ml chloramphenicol.

2.1.2 Rosetta™ Cells

Rosetta cells are used for high-level expression of bacterial proteins with pET, pETBlue™, and pTriEx™ vectors. Rosetta™ host strains are BL21 derivatives (Wood, 1966) designed to enhance the expression of eukaryotic proteins that contain codons rarely used in *E. coli*. These strains supply eukaryotic tRNAs for AGG, AGA, AUA, CUA, CCC, GGA codons on a compatible chloramphenicol-resistant plasmid. Thus the Rosetta strains provide “universal” translation which is otherwise limited by the codon usage of *E. coli*. The tRNA genes are driven by their native promoters. Hence, Rosetta cells are commonly used for high-level expression of bacterial proteins.

2.2 Methods

2.2.1 Polymerase Chain Reaction

The standard molecular cloning techniques were used in polymerase chain reaction (PCR), sequencing, and plasmid construction (Sambrook *et al.,*1989).

PCR fragments were generated with *PfuTurbo* DNA polymerase, following Fermentas's recommendations for reaction conditions, using a Biometra T3000 Thermocycler. (See Appendix A for details on PCR reactions).

2.2.2 QuikChange Site-Directed Mutagenesis

Site-directed mutagenesis was performed using Stratagene QuikChange site-directed mutagenesis kit which incorporates a non-PCR based method of amplification that replicates only the original template DNA using a high fidelity polymerase. Double-stranded DNA plasmid with an appropriate insert is used as a template along with two complementary oligonucleotide primers containing the desired substitution. The primers are extended during thermocycling using *PfuTurbo* DNA polymerase resulting in a non-ligated circular daughter plasmid containing the incorporated substitution. DpnI is used to digest the methylated, non-mutated parental plasmid leaving only the daughter DNA that was copied *in vitro*. The daughter DNA is then transformed into XL1-Blue supercompetent cells that have the function to ligate the synthetic DNA.

The QuikChange protocol was performed using manufacturer's instructions, with the following exception: the XL1-Blue cells transformed with the mutated daughter DNA was grown in SOC (LB with 40 mM glucose, 10 mM $MgCl_2$, and 10 mM $MgSO_4$) media rather than NZY^+ broth.

All substitutions were confirmed by sequencing, as well as by diagnostic digests using restriction enzymes for sites silently substituted near the location of the desired substitution (See Appendix B for oligonucleotide primer sequences).

2.2.3 Recombinant DNA General Methods

2.2.3.1 Plasmid DNA Preparations

Plasmid isolations from bacterial cells were carried out using QIAGEN plasmid extraction kit, employing the alkaline lysis method, following QIAGEN's specific instructions.

2.2.3.2 Restriction Digests, Agarose Gels and Plasmid DNA Purification

Plasmid DNA was mixed with a variety of nucleases in the corresponding buffer and incubated at 37˚C for 1-2 h. Nuclease-digested plasmid DNA was run on 1% agarose gel (0.5 g agarose in 50 ml Tris-acetate buffer (40 mM Tris, 0.1% (v/v) glacial acetic acid, 1 mM EDTA, pH 8.0) 0.5 µg/ml ethidium bromide) at 100 volts on a E-C Apparatus Corporation EC-105 power supply for approximately 60 min (or until dye front reaches the end of the gel for maximal band separation), to separate fragments of different sizes. Gels were visualized on 360 nm long wave UV box from Alpha Innotech, or on a Typhoon 9410 Variable Mode Imager with a 532 nm green laser and a 610 nm filter.

Fragments of digested plasmid DNA were excised from agarose gels and purified according to instructions provided by Invitrogen PureLink™ Quick Gel Extraction Kit.

2.2.3.3 Ethanol Precipitation of DNA

To a sample size of 100µl, I added 2µl of linear polyacrylamide carrier (5 mg/mL), 12.5 µl of 8 M NH4Ac, and 200 µl of 95% EtOH on ice, quickly vortexed and incubated at -20°C for 60 min. Samples were centrifuged at 12470 x g, at 4°C

for 30 min. The supernatant was carefully aspirated from the sample and discarded. The DNA pellet was washed with ice cold 75% EtOH to remove the salt in the sample. After 10 min on ice, the sample was centrifuged for 5 min as above. The supernatant was discarded and the pellet washed with ice cold anhydrous EtOH before centrifuging for 5 min. The supernatant was discarded and the pellet was air dried at room temperature until all traces of EtOH had evaporated. DNA pellet was resuspended in 10 mM Tris pH 7.4 or ddH2O.

2.2.3.4 Phosphatase Treatment of Vector

The digested vector was mixed with one unit of shrimp alkaline phosphatase (SAP) per picomole of 5' ends in dephosphorylation buffer (50 mM Tris-HCl, 5 mM $MgCl_2$, pH 8.5) in a final volume of 10 µl. The reaction carried out for 10 min at 37°C and then deactivated by incubation at 65°C for 15 min.

2.2.3.5 Ligations

Ligation reactions were performed with a 6:1 molar ratio of insert to vector in Fermentas 5X Rapid Ligation Buffer (50 mM Tris-HCl pH 7.6, 10 mM $MgCl_2$, 1mM ATP, 1 mM DTT, 5% (w/v) polyethylene glycol-8000) with 5 units of T4 DNA ligase in a final volume of 20 µL, with 6 fmol of SAP vector and 36 fmol of insert DNA. The Fermentas Rapid Ligation Kit was used as per the manufacturer instructions, with a 1h incubation period.

2.2.3.6 Competent Cells Transformation

Competent cells (50 µl) were thawed on ice for 10 min prior to the gentle addition of 1.0 µg of plasmid DNA or 5 µl ligation product, and were then

incubated on ice for 20 min. The cells were heat-shocked in a 42°C water bath for 45 sec and transferred to ice for 2 min. 0.5 ml of prewarmed SOC or LB media was added and the culture was shaken at 250 rpm for 1 h at 37°C. 100 and 400 µls of transfected cells were plated on LB / agar plates containing the appropriate antibiotics, and grown overnight at 37°C.

2.2.4 Preparation of CCT, CCT-phospho-mimic and α-Synuclein Constructs and Variants

2.2.4.1 pET-14b-CCT237-367

The CCT tail domains, CCT237-367, was provided to me in an in-house modified pET-14b-Strep vector (with a Strep-tag instead of a His-tag). There are three major disadvantage to the Strep-tag: 1) low yield and purity; 2) no cut site between CCT237-367 and the Strep-tag (the additional amino acid sequence may affect the overall structure and membrane binding); and 3) the Strep-Tactin resin was relatively expensive for large scale expression and purification. Hence, I transferred the CCT tail region to a vector that would substitute a cleavable His-tag for a Strep-tag. A PCR fragment was generated using pET-14b-Strep-CCT237-367 as template. NdeI-CCT237-5F and modified-T7-terminator were used as 5' and 3' primers respectively. The 5' primer contains a *Nde*I site. The PCR product was digested with *Nde*I and *Bam*H1 to form a fragment 550 bp long, and was ligated into the 4661 bp fragment of pET14b-(His_6)-(thrombin)-CCT236K122A, which had also been digested with *Nde*I and *Bam*H1 (Figure 2.1).

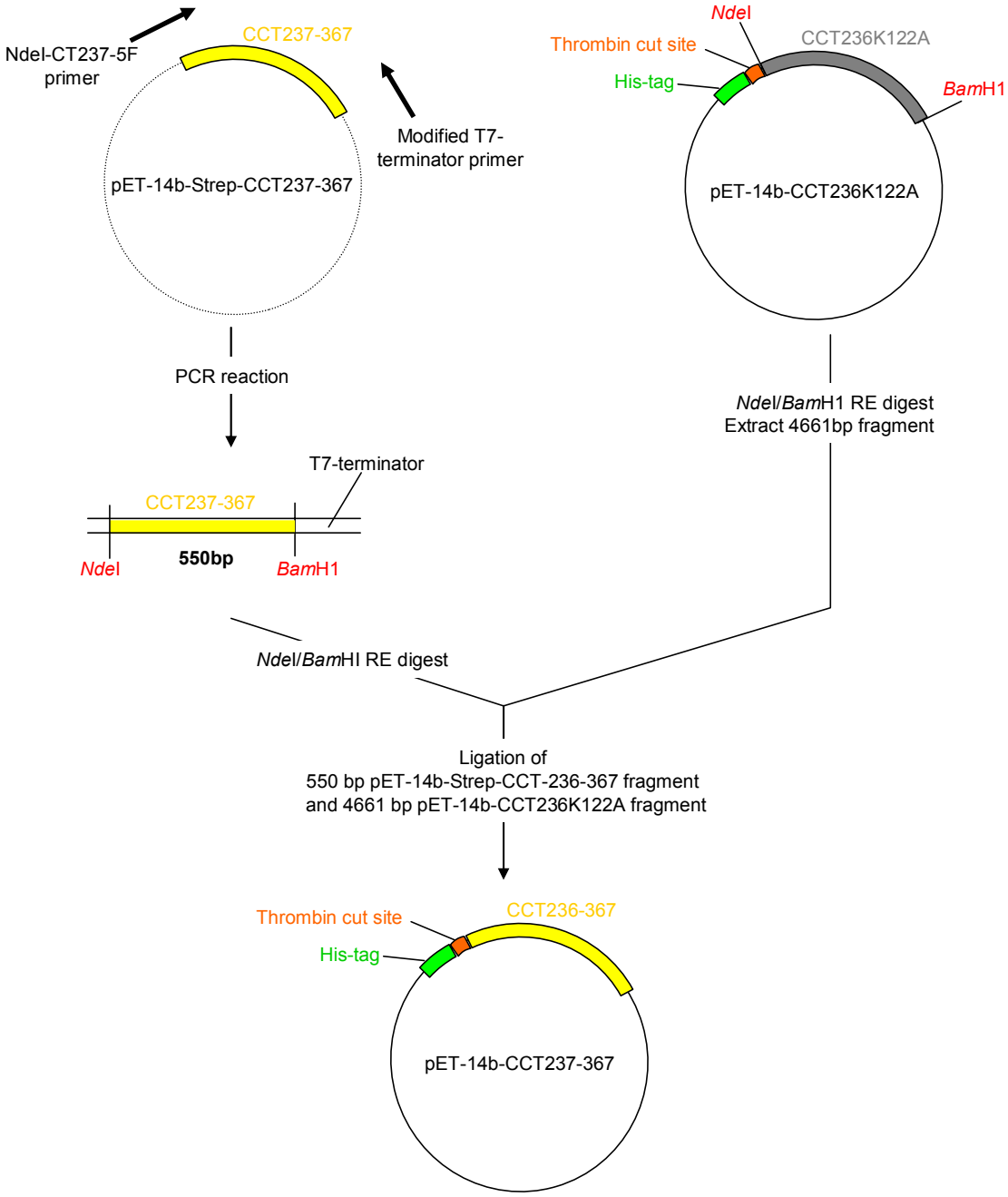

Figure 2.1 Construction of pET-14b-CCT237-367

2.2.4.2 pET-14b-CCT237-367-phospho-mimic

This PM variant (16S→E) was prepared similarly to the WT above. The PCR fragment was generated using CCT-16SE-GFP (provided by Dr. Neale Ridgeway (Dalhousie University) as template. NdeI-CCT237-5F and BamH1-Stop-CT367-phospho-mimic-3R were used as 5' and 3' primers respectively, to engineer *Nde*I and a *Bam*H1 sites flanking the CCT sequence. The PCR product was digested with *Nde*I and *Bam*H1 restriction enzymes to form a fragment 400 bp long, and was ligated into the 4661 bp fragment of pET14b-(His_6)-(thrombin)- CCT236K122A, which had also been treated with the same restriction enzymes (Figure 2.2).

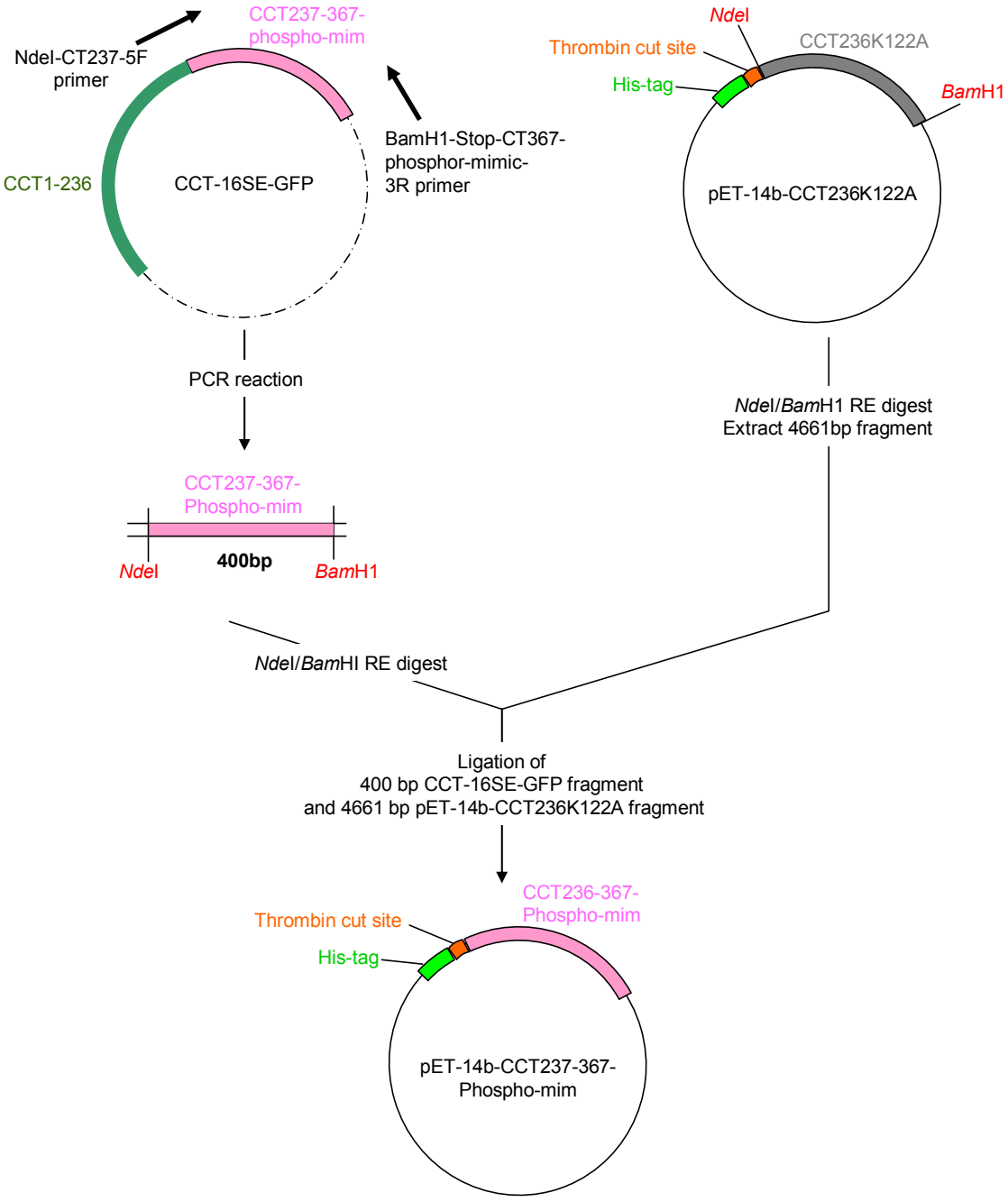

Figure 2.2 Construction of pET-14b-CCT237-367-phospho-mimic

2.2.4.3 pET-14b-α-Synuclein

The α-syn construct was engineered with a cleavable, N-terminal His-tag, similar to the above constructs, by PCR. The template PT7-7-AS was provided by Dr. David Eliezer (Weill Medical School of Cornell University). A *Nde*I site and a *Xho*I site was engineered into the 5' and 3' primer, respectively, using T7prom20-5F and pT7-7ClaI-3R. The PCR product was digested with *Nde*I and *Xho*I restriction enzymes to form a fragment 600 bp long, and was ligated into pET-14b empty vector (4665 bp) opened with the same restriction enzymes (Figure 2.3).

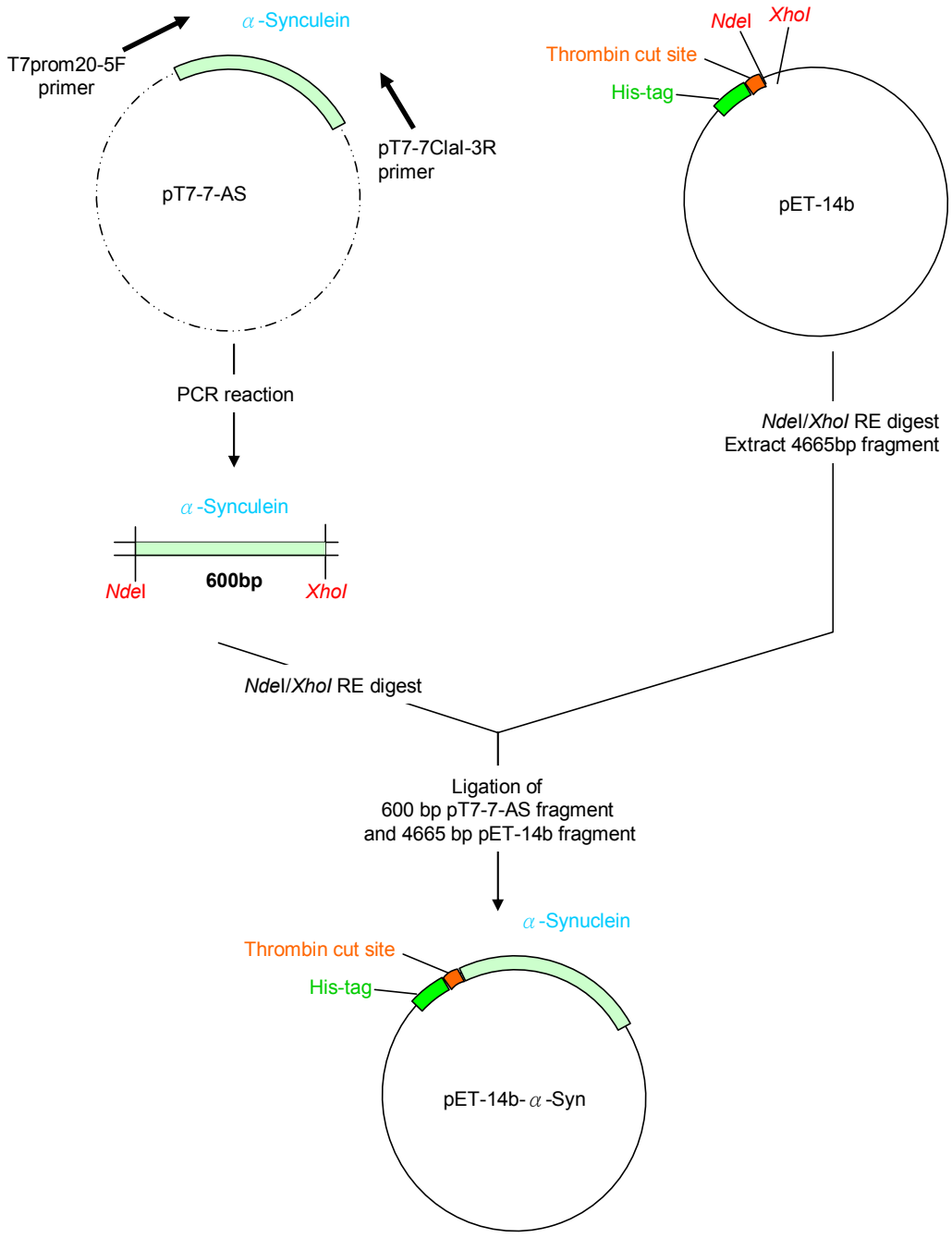

Figure 2.3 Construction of pET-14b-α-Synuclein

2.2.4.4 pET-14b-CCT237-367-W336F and pET-14b-CCT237-367-phospho-mimic-W336F (single Trp CCT variants at position 278)

This substitution eliminated the Trp in domain P so that the only Trp available is in domain M (position 278). This engineering facilitated the analysis of Trp fluorescence to measure domain M interaction with lipid vesicles. These variants were made using the QuikChange Site-Directed Mutagenesis protocol with pET-14b-CCT237-367 and pET-14b-CCT-237-367-phospho-mimic as templates. The Trp at position 336 was mutated to phenylalanine using CCT-W336F-5F / 3R primers and CCT-PM-W336F-5F / 3R primers for the WT and phospho-mimic, respectively (Figure 2.4).

2.2.4.5 pET-14b-α-Syn-V37W (single Trp α-synuclein variant at position 37)

α-Synuclein lacks Trp residues. To insert a Trp into the hydrophobic face in the middle of the AH (position 37), I used QuikChange with pET-14b-α-Syn as template. The valine at position 37 was substituted with a Trp using α-Syn-V37W-5F and α-Syn-V37W-3R primers (Figure 2.4).

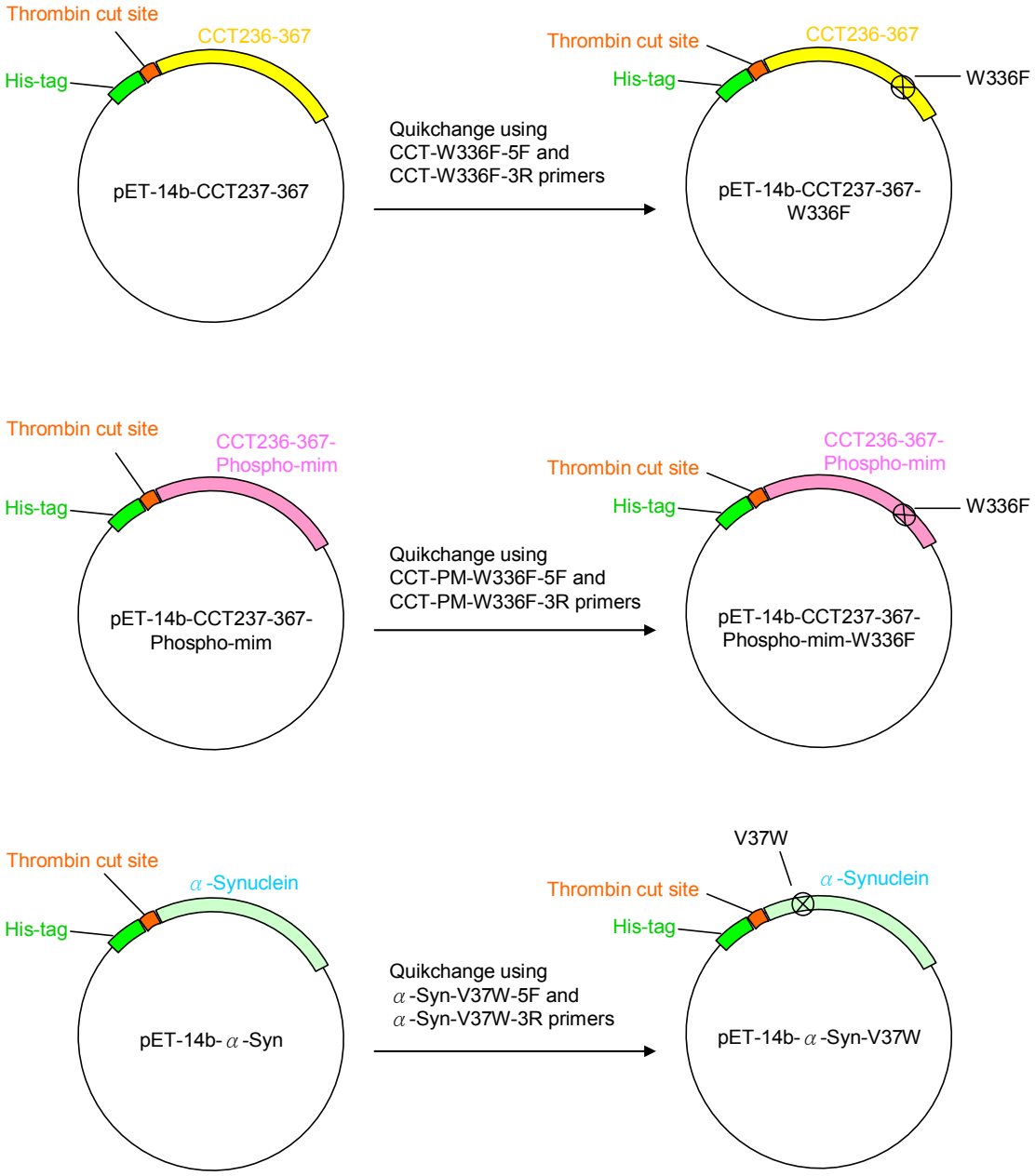

Figure 2.4 Construction of pET-14b-CCT237-367-W336F, pET-14b-CCT237-367-phospho-mimic-W336F, and pET-14b-α-Syn-V37W

2.2.4.6 pET-14b-CCT237-367-M302W and pET-14b-CCT237-367-phospho-mimic-M302W (single Trp CCT variants at position 302)

The original CCT's (WT and PM) tail domains both have two Trp residues, one in domain M and one in domain P. I engineered CCTs with a single Trp at residue 302 using two rounds of QuikChange mutagenesis. First, using pET-14b-CCT237-367-W336F and pET-14b-CCT237-367-phospho-mimic-W336F as templates, the Trp residues at position 278 were substituted into a phenylalanine with W278F-5F and W278F-3R primers. Once the sequences were confirmed, the products, pET-14b-CCT237-367-no-trp and pET-14b-CCT237-367-phospho-mimic-no-trp were then used as templates for a second round of mutagenesis to incorporate the M302W substitutions, using M302W-5F and M302W-3R primers (Figure 2.5).

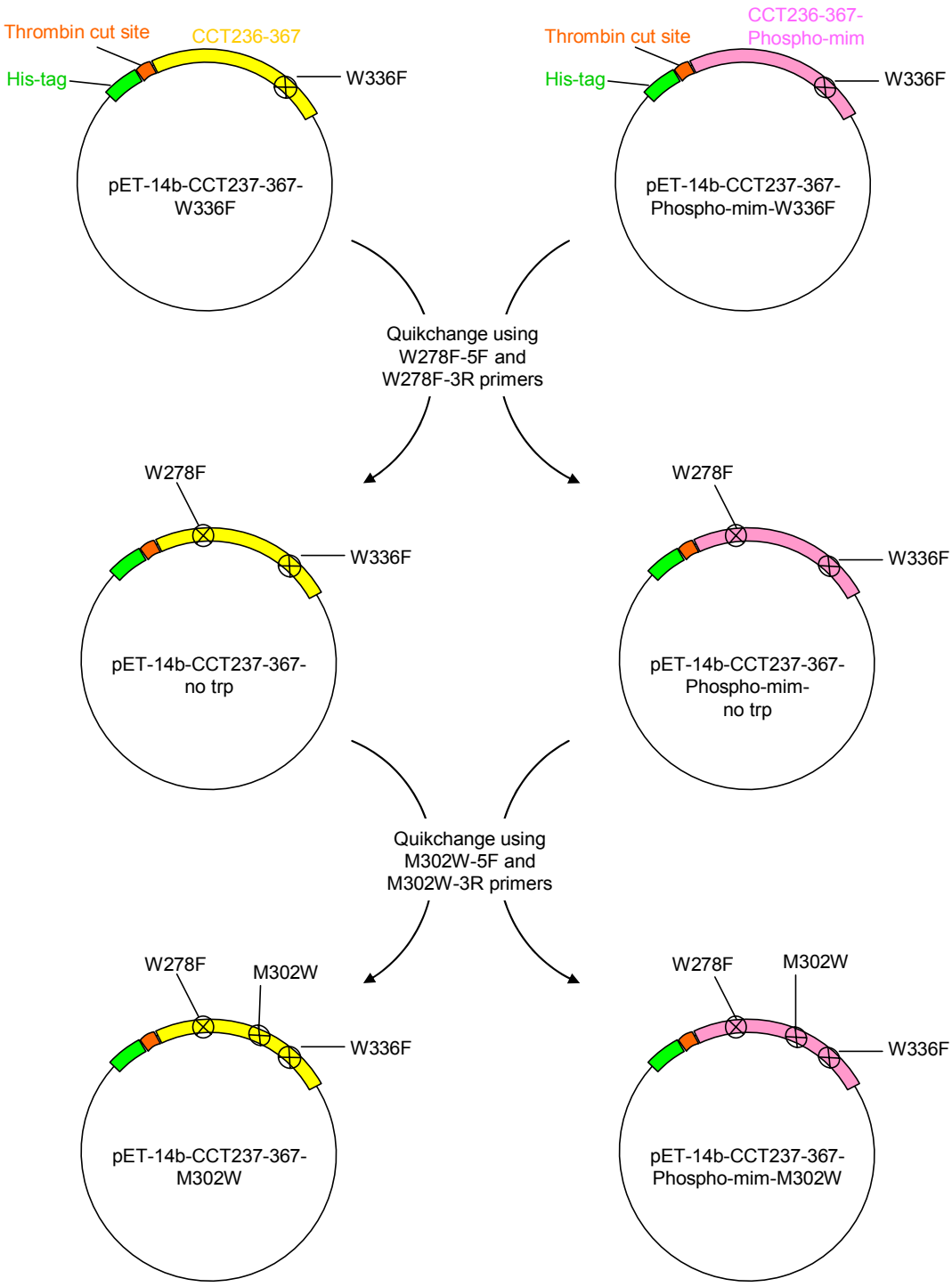

Figure 2.5 Construction of pET-14b-CCT237-367-M302W and pET-14b-CCT237-367-phospho-mimic-M302W

2.2.5 Expression of Protein via IPTG Induction using pET Vectors

After successfully obtaining colonies from pET-transformed competent Rosetta cells, I prepared a 3 mL liquid culture by inoculation with a single bacterial colony. The culture medium was LB with 100 µg/ml ampicillin and 32 µg/ml chloramphenicol. After incubating at 37˚C for 12 h with shaking, this 3 mL starter culture was the inoculum for a 30 mL LB / Amp / Cam media. After overnight at the same conditions, this 30 mL O/N culture was the inoculum for a 1 L LB / Amp / Cam media. When this culture had reached an optical density of 0.6-0.8, I induced expression of the transgene with 0.4 mM IPTG.

2.2.6 Protein Purification: His-tagged Protein Purification (Optimized Protocol)

After induction with IPTG for times and temperatures optimized for each variant, a 1 L liquid cell culture was centrifuged at 3000 x g for 10 min. All of the supernatant was aspirated and the cell pellet was either stored at -80˚C or immediately resuspended in 100 ml of lysis buffer (PBS pH 7.4, 1 mM DTT, 25 mM OG, 200 ug/mL Lysozyme, 10 ug/mL DNaseI, and battery of protease inhibitors including Leupeptin (2.5 ug/ml), Chymostatin (2 ug/ml), Antipain (1 ug/ml), Pepstatin (2 ug/ml), p-amino-benzadine (10 ug/ml), Benzamidine (10 ug/ml), and PMSF (0.5mM)). The sample was then sonicated on ice for 4 X 15 sec (with rest intervals of 15 sec in between) with a Fisher Sonic Dismembrator Model 300 at 30% output, followed by processing the 100 mL sample with an Avestin Cell Homogenizer Emulsiflex C-3 to completely lyse the cells. This whole cell homogenate was then centrifuged to separate the supernatant and the pellet

fraction. A 1:10 volume of 10X binding buffer (50 mM NaPi, 5M NaCl, 150 mM imidazole, pH 8.0) was added to the supernatant while gently vortexed to mix. The supernatant was combined with a 1/25 volume of a 50% slurry of Ni-NTA Agarose beads and transferred into two 50 mL Falcon tubes. The resulting mixture was rotated for 2 h at 4°C to ensure complete binding of His-tagged protein to the nickel-charged beads. After binding, the bead/supernatant mixture was poured into a 1 cm x 10 cm column fitted with a stopcock and left to settle at 4°C. The sample was passed through the column and the flow-through was collected and passed over the column again. The column was washed twice: first with wash buffer 1 (50 mM NaPi, 0.5 M NaCl, 25 mM imidazole, 25 mM OG, 2 mM DTT, pH 8.0), then with wash buffer 2 (50 mM NaPi, 100 mM NaCl, 25 mM Imidazole, 25 mM OG, 2 mM DTT, pH 8.0). His-tagged protein was eluted from the column with the addition of elution buffer (50 mM NaPi, 100 mM NaCl, 350 mM Imidazole, 25 mM OG, 2 mM DTT, pH 8.0) and collected in approximately 2 mL fractions. A sample of each fraction was electrophoresed on a 12% SDS-PAG to determine the fraction with the highest protein concentration. The buffer in the pooled peak fraction was then exchanged using an Amicon Ultra-4 (10,000 MWCO) centrifugal filter device with PBS (137 mM NaCl, 2.7 mM KCl, 8.1 mM Na_2HPO_4, 1.76 mM KH_2PO_4 , pH 7.4) / 25 mM OG/ 2 mM DTT at 3000 x g at 25°C until the final imidazole concentration was approximately 10-20 mM. Amicon filtered protein was aliquoted in 50 µL fractions and stored at -80˚C. All fractions of the purification process were saved at -80°C.

2.2.7 Thrombin Digestion

Purified proteins were diluted 4-fold (25mM OG → 6.25mM OG) to prevent inhibition of thrombin's enzymatic activity and thrombin was added (1 unit of thrombin to 50 µg of protein). Thrombin digestion was complete after 7 h incubation at RT and was quenched with Chymostatin, Antipain, and Leupeptin (2 µg/mL, 1 µg/mL, and 2.5 µg/mL respectively). The OG concentration was reduced to 0.1 mM via Amicon ultrafiltration, which also removed the His-tag and concentrated the proteins. All proteins after thrombin digestion would carry a short linker composed of four amino acids (GSHM) at their N-termini.

2.2.8 Sample Concentration And/Or Buffer Exchange

Amicon Ultra-4 (10, 000 MWCO) centrifugal filter devices were pre-rinsed with the same buffer as the sample, by applying the buffer to the filter column and centrifuging at 3000 x g, for 10 min at 25°C. The retentate was removed from the filter devices, and the sample applied (sample volumes up to 4 mL). The sample and filter were then centrifuged at 3000 x g) at 25°C for the time necessary to reduce the retenate volume to the desired volume. For samples that required buffer exchange, the new buffer was added to the concentrated sample in the appropriate volume. The filter walls were thoroughly rinsed with the sample, which was then removed from the device by pipeting.

2.2.9 Protein Biochemical Methods

The concentration of protein samples was determined either using the 1) Bradford method (Bradford, 1976) or 2) Nanodrop ND-1000 Spectrophotometer.

1) Standard (0-20 µg BSA) and sample volumes were adjusted to 100 µl. 1 ml of Bradford Dye Reagent (0.005% (w/v) Coomassie Brilliant Blue R, 5% (v/v) EtOH, 10% (v/v) H_3PO_4) was added while vortexing. Samples and standards were incubated for 15 min in a 37°C water bath, and the absorbance was read at 595 nm on a Beckman DU 640 Spectrophotometer.

2) 2 µL sample was used to read the absorbance at 280 nm on a Nanodrop ND-1000 Spectrophotometer. Concentration was obtained by the supplied program, based on the protein's extinction coefficient and molecular weight.

2.2.10 Chemical Analysis of Detergent β-Octylglucoside Concentration

An anthrone reaction was used to determine the concentration of OG in the final sample. This reaction is based on the formation in concentrated sulfuric acid of furfural derivatives which react with anthrone to form a blue-green color (Roe, 1955). Fresh anthrone reagent was prepared by first combining 28 mL of distilled water with 72 mL of concentrated sulfuric acid. While this mixture was still warm, 50 mg of anthrone and 1 g of thiourea was added and mixed until dissolved. Lastly, the reagent was cooled at 4˚C and aged for at least 4 h.

The reaction was carried out in Pyrex tubes. Standards (50 – 1000 µM OG) and sample volumes were adjusted to 50 µL PBS. 250 µL of cold anthrone reagent was added and mixed via vortexing. Samples and standards were heated in boiling water bath for 15 mins., cooled in a water bath for 20 mins, and the absorbance was read at 620 nm on a Beckman DU 640 Spectrophotometer.

2.2.11 Gel Electrophoresis

Proteins were separated on 12% SDS-polyacrylamide gels using Bio-Rad's Mini-PROTEAN II gel apparatus at a constant 150 V, for ~45 min in Running Buffer (25 mM Tris pH 8.3, 192 mM glycine, 0.1% (w/v) SDS) (Laemmli, 1970). After electrophoresis, gels were fixed in Coomassie stain (0.3% (w/v) Coomassie Brilliant Blue R, 45% (v/v) MeOH, 10% (v/v) HAc) for at least 1 h, destained for 10-15 min in Fast Destain (40% (v/v) MeOH, 10% (v/v) HAc), and followed by several hours in Slow Destain (7% (v/v) MeOH, 5% (v/v) HAc).

The proportions of aliquots loaded onto the SDS-polyacrylamide gel are as follows: homogenate, supernatant, pellet, flow-through, and wash fractions were 0.01% of total volume; elution, dialysis, Amicon filtration, thrombin digestion fractions were 0.1% of total volume.

2.2.12 Preparation of Small Unilamellar Vesicles (SUVs)

Appropriate volumes of different phospholipids to give various molar ratios were aliquoted from chloroform stocks to a 5 mL round bottom flask. The lipid mixture was evaporated to dryness for 25 min at 37°C, using a rotary evaporator. The dried lipids were resuspended in 0.8 mL ddH_2O and vortexed to resuspend. The suspension was sonicated with a Heat Systems Ultrasonic reservoir Processor W-375 set at 30% duty cycle, on ice for 15 min at which time the solution was clear, and was then centrifuged for 4 min at 12470 x g, 4°C to remove any residual multi-lamellar lipids.

2.2.13 Circular Dichroism Spectroscopy and Deconvolution Protocol

Far-UV C.D. spectroscopy reveals important characteristics of protein secondary structure. All measurements were taken on a Jasco J-810 spectropolarimeter using a 0.5 mm quartz cell at 25°C. The samples were in 1/5 diluted PBS buffer with a protein concentration of 10 μM and various lipid concentrations. The ionic strength of the samples was constant at ~35 mM. Each spectrum (from 190 nm – 260 nm) was measured twice at a 100 nm/min scan rate in steps of 0.5 nm, and the two were averaged and smoothed. Background spectra of the lipid vesicles in buffer were subtracted from the peptide + lipid spectra. Mean residue molar ellipticity, deg • cm^2/dmol, was calculated based on molecular masses of ~15 350 Da and 135 amino acids for CCT237-367 (WT and various Trp variants), ~16 000 Da and 135 amino acids for CCT237-367-PM (PM and various Trp variants), ~14 700 Da and 143 amino acids for α-syn, and ~14 800 Da and 143 amino acids for α-syn-V37W. The secondary structure content was deconvoluted from the CD spectra by three methods, SELCON 3, CONTINLL, and CDSSTR, which are part of the software package CDPro available at http://lamar.colostate.edu/_sreeram/CDPro (Sreerama and Woody, 2000). This program compares the input spectrum to a set of reference spectra from proteins with solved structures. The deconvolution of the input spectrum generates the percent of total structure that is helical, beta strand, turns, and unordered. The strengths and limitations of the three deconvolution programs have been reviewed (Sreerama and Woody, 1993; Sreerama and Woody, 2000; Johnson, 1999). Since CCT and α-syn spectra were noisy between 190 – 195 nm, all

values input into the CDPro were from 195 – 240 nm. The three programs used an identical set of 56 reference proteins (43 soluble proteins and 13 membrane protein). Analyzing protein CD spectra using all three methods improves the reliability of the predicted secondary structure (Sreerama and Woody, 2000). The percent of each structural mode was plotted using GraphPad Prism 5, fitting the data to the model that gave the best correlation between data and model.

2.2.14 Tryptophan Fluorescence Analyses

Spectra were recorded on a PTI-LS 100 fluorescence spectrophotometer or a Varian Cary Eclipse fluorescence spectrophotometer. For the Varian model, the recorded emission and excitation slit widths were of 10 nm, a PMT voltage of 750V, a scan rate of 600 nm/min, and data interval of 1 nm. Samples were at room temperature in a 1 cm quartz fluorescence cuvette. The excitation wavelength was 280 nm, and the emission spectra were recorded from 300 to 450 nm. The sample in dilute PBS buffer contained either 6 μM or 2 μM of protein and various lipid concentrations. In all experiments, the upper limit concentration of sonicated lipid vesicles (e.g. 720 uM) caused no interference from sample turbidity. Lipid and proteins were preincubated at room temperature for ~10 min prior to recording spectra. The fluorescence in the absence of peptide was subtracted from the fluorescence obtained in the presence of peptide + lipid. The peak fluorescence wavelength of each spectrum was obtained by manually recording the wavelength for the highest fluorescence intensity in a smoothed spectrum. The amount of fluorescence blue shift was determined by subtracting λ from λ_o, where λ is the wavelength of the peak fluorescence in the presence of

lipid vesicles, and λ_o is the wavelength of the peak fluorescence in the absence of lipid vesicles. For iodide quenching experiments, samples in dilute PBS buffer contained protein, lipid, 10 mM $Na_2S_20_3$, and the indicated concentration of NaI added from a 2.5 M stock. NaCl, which does not quench fluorescence, was added to maintain a constant ionic strength of 0.2 M. Data obtained from fluorescence spectra were plotted using GraphPad Prism 5 by choosing the model that gave the best correlation between data and model.

3 DEVELOPMENT OF A PURIFICATION PROTOCOL FOR HIS-TAGGED CCT TAILS AND α-SYNUCLEIN

3.1 Introduction

The first step in achieving the goal of comparing the lipid responses of the CCT tail and α-syn was to develop protocols for their efficient expression and purification. The hallmarks of an efficient protocol would be the acquisition of pure protein with high yield and with the fewest steps. The potential challenges when working with membrane binding proteins is their intrinsic low-water solubility and consequent requirement for detergents. The detergents, however, have the potential to interfere with the protein-lipid interactions. The account that follows describes how I managed these conflicting challenges.

3.2 Results and Discussion

3.2.1 Expression protocol for CCT Tail Domains and α-Synuclein

In my thesis work, CCT tail constructs composed of residues 237-367 are referred to as CCT(M+P) or CCT tail. My initial trial utilized a Strep-tagged CCT wild-type tail construct (prepared by Ziwei Ding). It was expressed effectively in Rosetta strain of *E. coli*. But was not purified sufficiently by a single pass on the streptactin affinity column and was very costly for large scale expression. I then prepared, with the assistance of Ziwei Ding, a His-tagged version for expression in *E. coli Rosetta* cells for protein expression. Expression was optimized for the induction of soluble protein by varying the induction time and temperature (Figure

3.1). Inducing for 2 h at 20˚C with 0.4 mM IPTG was adequate, whereas longer induction times caused protein aggregation/pelleting (Figure 3.1).

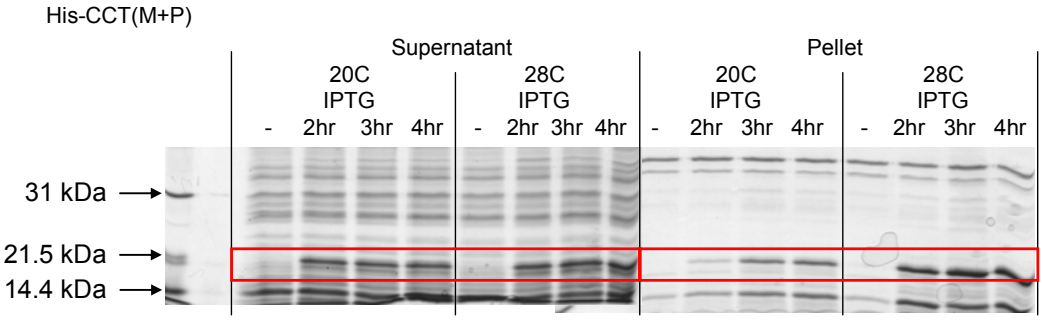

Figure 3.1 Protein Expression Test of N-terminal His-tagged CCT(M+P) Varying Temperature and Time of IPTG Induction
E. coli Rosetta cells harboring pET-14b with the CCT cDNAs were induced with 0.4 mM IPTG at either 20 ˚C or 28 ˚C for 2-4 h. Cells were lysed and fractionated as described in Methods. The expected molecular weight for His-CCT(M+P) is 17.2 kDa (outlined in red boxes. Proportional aliquots of each fraction were separated on a 12% SDS-PAGE gel and visualized by Coomassie staining.

Over-expression of the PM domain P (16S→E) variant was observed after 2 h of IPTG induction (at 20˚C) and the protein was virtually all in the soluble form. The estimated molecular weight of the PM variant is 17.9 kDa. However, according to the supernatant lane for His-CCT(M+P)-PM in Figure 3.2 A, the migration rate of this variant is retarded which is likely due to its highly acidic tail sequence. The Trp variants of the CCT tail domain were also expressed well in the soluble fraction after 2 h induction at 20˚C (data not shown).

Unlike the CCT tails, His-α-syn was not induced at 20˚C, but was expressed in soluble form at 37˚C after 2 h (Figure 3.2 B), as were the Trp variants of His-α-syn.

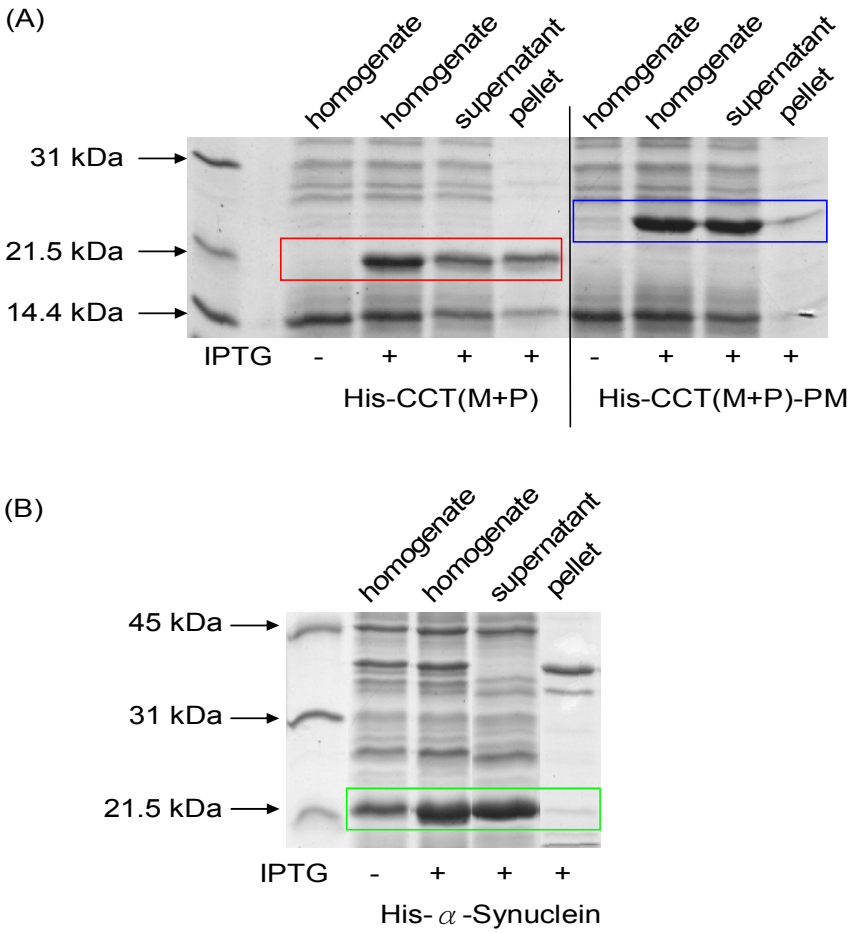

Figure 3.2 Protein Expression of N-terminal His-tagged Proteins
E. coli Rosetta cells harboring pET-14b with the CCT or α-Syn cDNAs were induced for 2 h with 0.4 mM IPTG at (a) 20 ˚C or (b) 37 ˚C. Cells were lysed and fractionated as described in Methods. The expected molecular weight for (a) His-CCT(M+P) is 17.2 kDa, His-CCT(M+P)-PM is 17.9 kDa and (b) α-Synuclein is 16.6 kDa which are outlined in red, blue and green boxes respectively. Proportional aliquots of each fraction was separated on a 12% SDS-PAGE gel and visualized by Coomassie staining.

3.2.2 Development of Nickel Affinity Chromatography Protocol

3.2.2.1 Aggregation of the CCT tail necessitates inclusion of detergent

A purification protocol was developed based on a common method exploiting the tight affinity of the imidazole ring of histidine for nickel. A purification protocol for His_6-tagged CCT(M+P) was adapted from a standard protocol in

which, after binding to Nickel-agarose and several washes to remove non-specific binding of proteins, the His-tagged protein is specifically eluted with 0.35 M imidazole (Xie *et al.,* 2004). The imidazole is typically removed immediately by dialysis or buffer exchange using an Amicon filtration unit prior to storage of pure protein at -80˚C. In an initial trial with His-CCT(M+P), 25 mM octylglucoside (OG) detergent was present in the Lysis Buffer and Wash 1 Buffer, whereas Wash 2 and Elution Buffer lacked detergent. A significant amount of protein was obtained from a single round of purification (Figure 3.3). However, the protein was not recovered after dialysis or Amicon filtration to remove imidazole (Figure 3.3). This was likely due to protein aggregation. Thus, it was apparent that an effective protocol would require some detergent in the final preparation. Which detergent would be optimal and at which concentration?

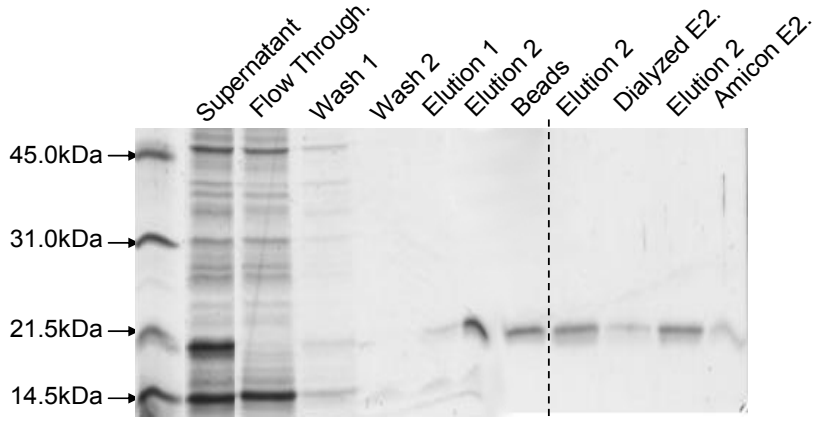

Figure 3.3 Nickel-affinity Chromatography in the Absence of Detergent Results in Loss of Soluble Protein.
His-CCT(M+P) in the soluble fraction (supernatant) of the cell lysate was purified using nickel-affinity chromatography where it eluted in the second elution fraction. Elution fraction 2 was either dialyzed against PBS buffer or centrifuged using an Amicon Ultrafiltration unit (AE2) to remove excess imidazole. Samples were subjected to 12% SDS-PAGE and visualized with Coomassie (refer to methods section 2.2.11 for proportion of aliquots loaded).

3.2.2.2 The Anionic Detergent SDS Promotes α-Helix Formation in CCT Tail Domains

The use of 2 mM anionic detergent SDS (a concentration above its critical micelle concentration (CMC), which is 1.35 mM at physiological ionic strength (Corrin and Harkins, 1947)) kept the WT CCT tail domain protein soluble during the entire process of protein isolation including cell lysis, nickel-affinity chromatography, Amicon buffer exchange, thrombin digestion, and a 30 min 100,000 x g centrifugation (Data not shown). Previous work with α-syn (Chandra *et al.,* 2003) and CCT domain M-derived peptides (Johnson *et al.,* 1998) showed that micellar concentrations of SDS can promote α-helix formation, indicative of an interaction between the proteins/peptides and SDS micelles. My goal was to generate a soluble protein that would show a lipid-dependent conformational transition, probed by C.D. Therefore I reduced the SDS to a sub-micellar concentration.

To prepare the protein for C.D. spectroscopy analysis, the final concentration of the SDS in the sample was reduced to approximately 65 μM via dialysis, which is only 3-fold molar excess over the protein and well below the CMC. Figure 3.4 compares the C.D. spectra of WT CCT tail in PBS buffer containing 65 μM SDS versus in PBS with 65 μM SDS and 50% 2,2,2-Trifluoroethanol (TFE), an established promoter of structure in peptides, including CCT M-peptides (Johnson and Cornell, 1994). Surprisingly, the SDS caused the protein to adopt α-helical conformation nearly as effectively as TFE (Figure 3.4).

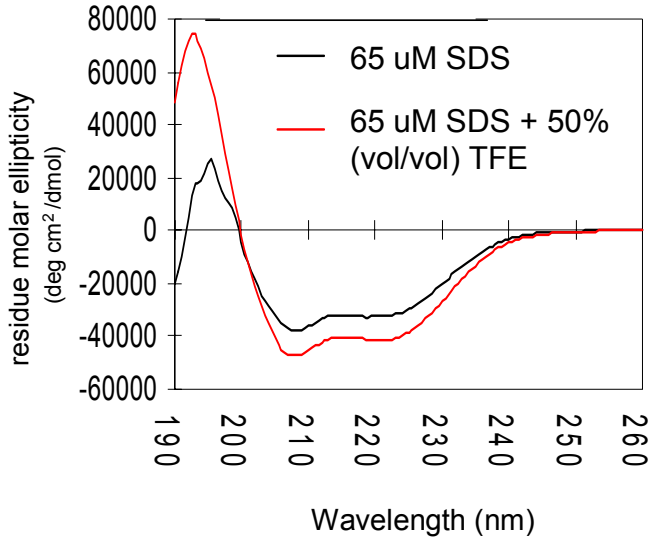

Figure 3.4 SDS Promotes α-Helix Formation in WT CCT Tail
Circular dichroism spectra of CCT(M+P) in PBS/ 0.65 μM SDS/ 2 mM DTT (dashed line) and in PBS/ 0.65 μM SDS/ 2 mM DTT with 50% trifluoroethanol solution (solid line). Peptide concentration was 20 μM in both samples.

How did the minimal SDS promote α-helicity in the CCT tail? One possibility is that the SDS monomers mimic a particular feature of TFE in which TFE molecules can aggregate around a peptides displacing water and providing a low dielectric environment that favors the formation of intrapeptide hydrogen bonds (Kumar *et al.,* 2003). SDS is a negatively charged detergent that may bind tightly to the protein and trigger the induction of helix in the CCT tail by this mechanism.

Another possibility is that the actual concentration of SDS in the final sample was greater than 65 μM, since I did not monitor the concentration of the SDS after the process of dialysis. Possible, dialysis did not reach equilibrium before I removed the sample for C.D. spectroscopy. In its micellar form it would

mimic anionic lipid vesicles as a negatively charged amphiphilic surface for CCT binding.

3.2.2.3 The Use of Non-Ionic Detergent Octyl ß-Glucoside as the Optimal Approach

Octyl ß-Glucoside (OG) is a nondenaturing, non-ionic detergent. This detergent has been useful for solubilizing membrane proteins. For most types of detergent to be removed efficient by Amicon filtration, the detergent concentration must be less than the CMC since only detergent monomers can be removed by this method. Since OG has a high CMC (25 mM), it can be readily removed by Amicon ultrafiltration provided its concentration is < 25 mM. In the optimized protocol, a concentration of 25 mM OG (above CMC) was included in every step of the purification procedure until the thrombin cleavage step where it was diluted to 6.25 mM. In the next and very last step, the concentration of OG was reduced to ~0.1 mM via Amicon ultrafiltration (see section 3.2.4).

OG helped His-CCT(M+P) to remain soluble during the nickel-affinity chromatography, the buffer exchange via Amicon filtration, as well as a 30 min 100,000 x g ultracentrifugation that immediately followed (Figure 3.5 A + D). The nickel affinity chromatography using OG as detergent was also successful with the PM variant of His-CCT(M+P) (Figure 3.5 B +E) and His-α-Syn (Figure 3.5 C + F). Hence this protocol was implemented in the purification of the various Trp variants for the CCT tail proteins and α-synuclein (Appendix C Figure C.1). The final yields of pure proteins were reported in Table 3.1.

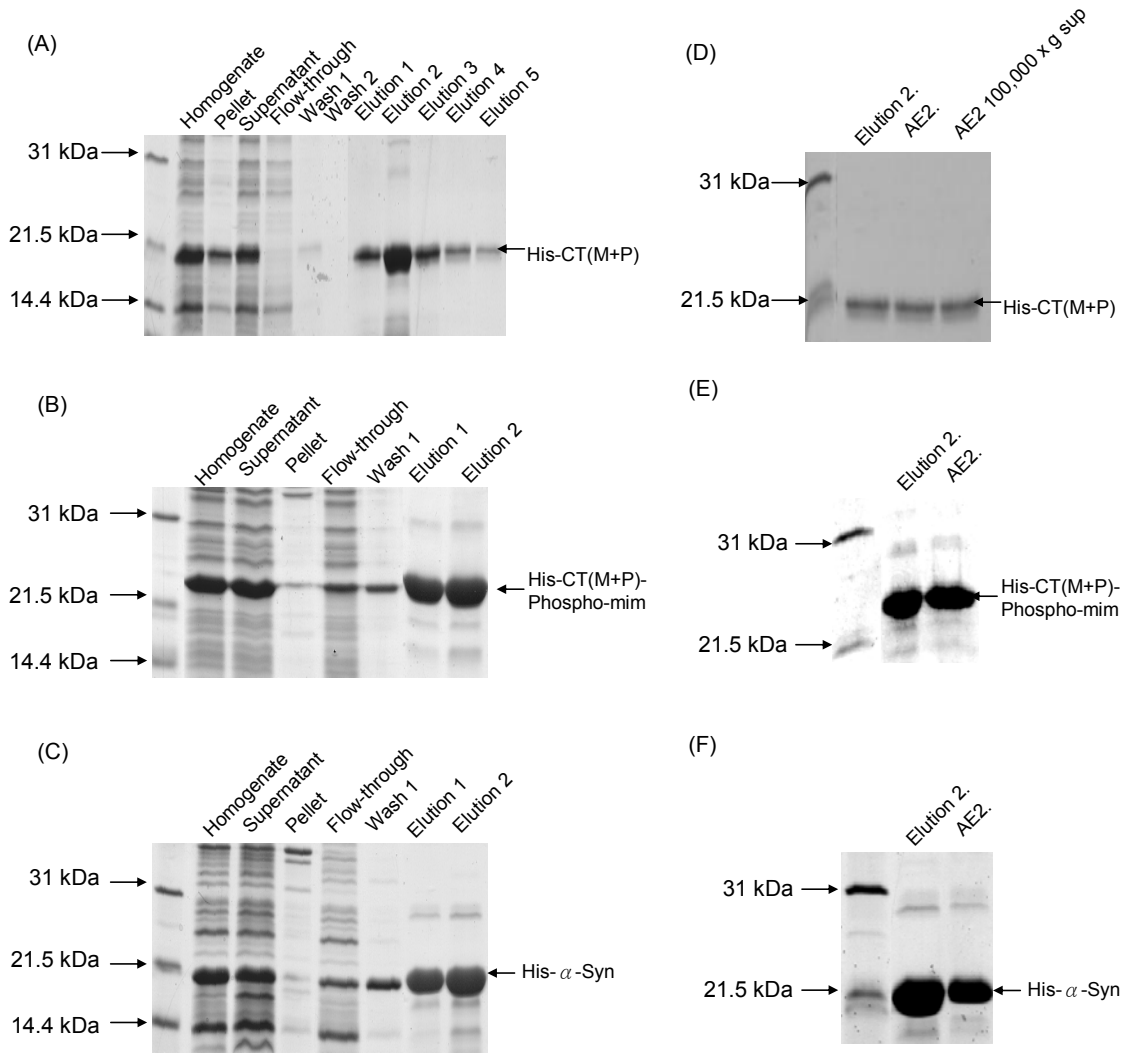

Figure 3.5 Nickel-affinity Chromatography with the Use of the Detergent OG Generates High Recovery of Soluble Protein.

(A-C) Purification progress for (A) His-CCT(M+P), (B) His-CCT(M+P)-PM, and (C) His-α-Syn. The tagged-proteins in the soluble fraction (supernatant) of the cell lysate was purified using nickel-affinity chromatography where it eluted in the first two elution fractions (with the expected Mr of (A) ~17.2 kDa, (B) ~17.9 kDa, and (C) ~16.6 kDa). (D-F) Recovery/Solubility of the purified proteins. Elution fraction 2 containing (D) His-CCT(M+P) (E) His-CCT(M+P)-PM, or (F) His-α-Syn was centrifuged using an Amicon Ultrafiltration unit (AE2) to remove excess imidazole. I also tested the solubility of (d) His-CCT(M+P) by centrifugation at 100, 000 x g, 30 min . Samples were subjected to 12% SDS-PAGE and visualized with Coomassie (refer to methods for proportion of aliquots loaded).

3.2.3 Development of Thrombin Digestion Protocol

The recommended protocol from GE Healthcare for thrombin digestion is to use one unit of enzyme for 100 µg of fusion protein when incubated in 1X PBS at 22˚C for 16 h. However, the enzymatic activity of thrombin may be affected by the presence of detergent in the sample. Therefore, I determined the optimal conditions for cleavage with respect to time, temperature, thrombin/substrate ratio, and OG concentration. With the ratio of one unit of thrombin to 50 µg of fusion protein and a four-fold dilution of sample using PBS/ 2 mM DTT/ pH 7.4 (25 mM OG→ 6.25 mM OG), I observed complete thrombin cleavage for the WT and PM CCT tail domains and α-syn after 7 h with end-over-end rotation at RT indicated by a band shift (Figure 3.6). In most trials the thrombin cleavage was faithful to the engineered site, as there was only one cleavage product. Hence this method was put into practice for the various Trp variants of CCT tail and α-syn proteins as well (Appendix C Figure C.2).

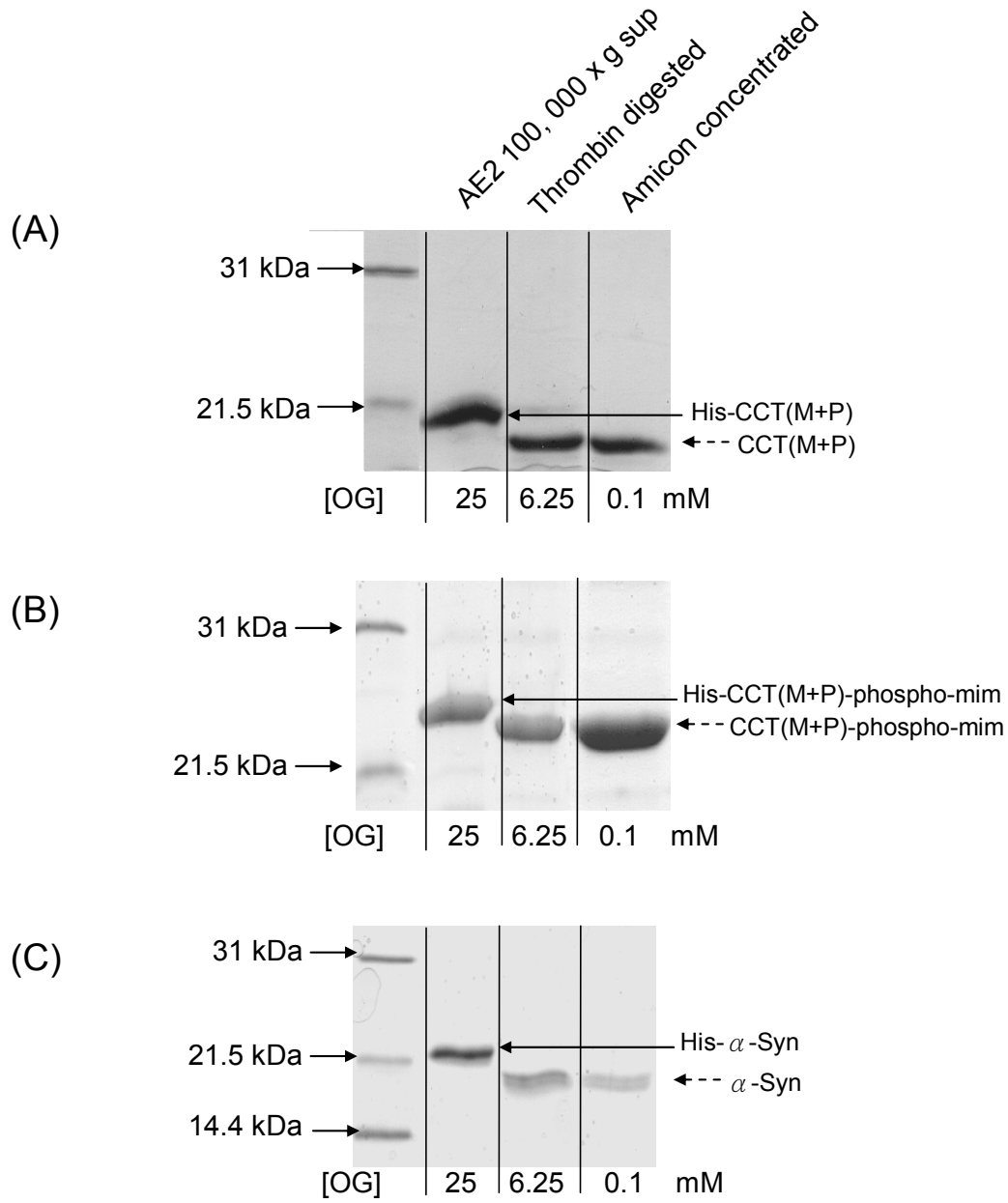

Figure 3.6 Thrombin Digestion of N-terminal His-tagged Proteins
Proteins purified via Ni chromatography and buffer-exchanged by ultrafiltration were subjected to thrombin for 7 h at 20 ˚C. The (A) CCT(M+P) (Mr 15.4 kDa), (B) CCT(M+P)-PM (Mr 16 kDa), and (C) α-Syn (Mr 14.7 kDa) were recovered after concentration with an Amicon Ultrafiltration unit (AE) to reduce OG concentration. Samples were subjected to 12% SDS-PAGE and visualized with Coomassie (proportional aliquots were loaded into each gel).

3.2.4 Potential Pitfalls of Octyl ß-Glucoside

OG is a non-ionic detergent, thus it could interfere with the analysis of protein binding to anionic vesicles either by competition with the vesicles, by modifying the properties of the vesicles, or by altering the protein conformation. The concentration of OG was determined to be < 0.4 mM for all purified CCT tail domains and α-syn protein samples. These were diluted for the C.D. measurements so the concentration of OG was ~20 μM in the sample for spectroscopy. This concentration is much less than the CMC of ~25 mM, thus it is unlikely that the OG micelles would be competing for binding of CCT and α-syn. Moreover OG does not affect the conformation of CCT when present at much higher concentrations than 0.4 mM (Taneva *et al.,* 2003). However, I cannot exclude the possibility that the OG monomers, which would partition into the lipid vesicles, might influence the charge density or order of the lipids. At low lipid concentration this would be of particular concern. The ideal condition, a detergent free preparation, would have been preferable. But given the solubility issues especially for the WT CCT tail, I had to include a minimal amount of the detergent where OG should be in its monomeric state and not affecting the proteins' secondary structure.

3.3 Concluding Discussion

A flow chart summarizing the protocol I developed for the expression and purification of all the His-tagged constructs used in this thesis is shown in Figure 3.7. Yields of pure protein ready for analysis were listed in Table 3.1. The proteins were not proteolyzed during purification, other than the specific cleavage with

Thrombin to remove the His-tag. This cleavage leaves a small peptide linker (GSHM) before the actual sequence of the CCT tail or α-syn. The linker is designed to be structure-less, so it should not interfere with conformation transitions. The chief issue of protein solubility was especially acute for the WT CCT tail protein. While SDS solved this problem, it interfered with subsequent analysis of structure transitions induced by specific lipids by substituting for the lipid. Purification with OG achieved the solubility goal. The OG concentration was reduced to < 400 μM by Amicon filtration. This was determined by means of a chemical analysis of OG concentration in the final prep. As will be shown in the next chapter, the 20 μM OG in the protein preparations for spectroscopy did not interfere with the evaluation of conformational transitions induced by lipid vesicles.

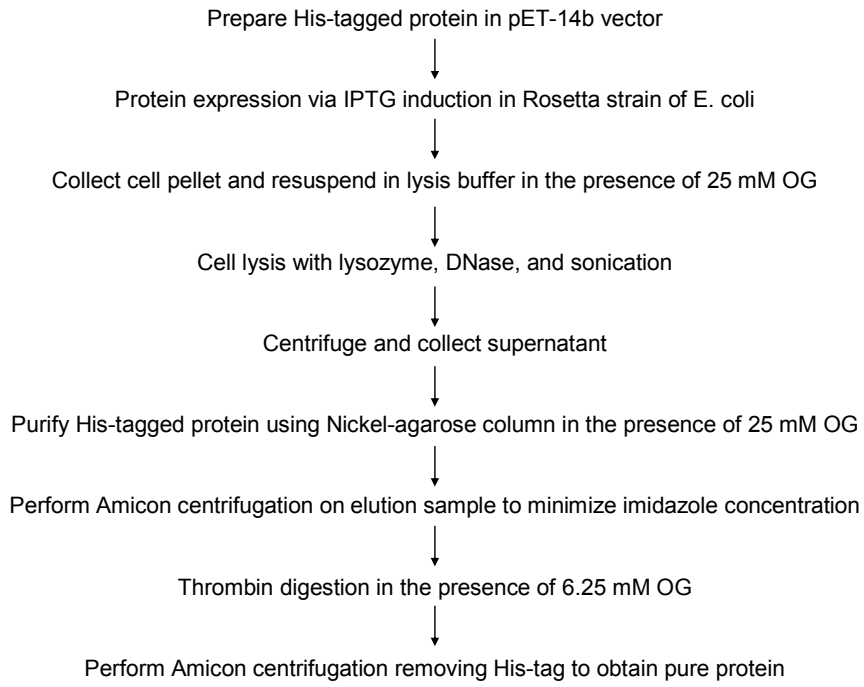

Figure 3.7 Flow Chart for Expression and Purification of His-tagged Proteins

Table 3.1 Yields of WT and Various Variants of CCT(M+P), CCT(M+P)-PM, and α-Syn Determined by Nanodrop and Amino Acid Analyses.

Sample	mg purified protein per liter E.coli cell culture
CCT(M+P) [1]	4.7 ± 0.35
CCT(M+P)-PM [1]	11 ± 0.87
α-Synuclein [1]	3.9 ± 0.73
CCT(M+P)-W336F [2]	5.2 ± 0.05
CCT(M+P)-PM-W336F [2]	8.6 ± 0.11
α-Synuclein-V37W [2]	1.0 ± 0.03
CCT(M+P)-M302W [2]	0.70 ± 0.02
CCT(M+P)-PM-M302W [2]	1.5 ± 0.10

[1] Results are based on average of one nanodrop and two amino acid analyses.
[2] Results are based on average of three nanodrop analyses.

4 COMPARATIVE INVESTIGATION OF THE LIPID INTERACTION OF CCT TAILS AND α-SYNUCLEIN

4.1 Introduction

Published work has identified many similarities between CCT tail domains and α-syn in terms of their membrane binding properties. Both proteins show selectivity for anionic vesicles, bind via a combination of electrostatic and hydrophobic interactions, and penetrate into the hydrocarbon core. However, these membrane binding properties of α-syn and CCT domain M peptides emerged from separate studies on the two proteins and utilized different methods and conditions. This makes it difficult to conclude which protein has a stronger binding strength. In fact, the lipid interactions of a complete CCT tail domain encompassing domains M+P had never been tested. Hence, in this chapter I will present my work comparing their lipid binding properties side-by-side using similar analytical methods, lipid species, and buffer conditions. As mentioned in Chapter 3, I have prepared, expressed in *E. coli,* and purified rat CCTα tail domains (WT and PM) and human α-syn. The CCT PM is a variant with all 16 serines in domain P substituted with glutamates. These sites have been identified as phosphorylated to varying degree in rat CCTα (MacDonald and Kent, 1994; Bogan *et al.*, 2005). Due to its carboxylic acid functional group, which is deprotonated at physiological pH, glutamate is often used as a mimic for phosphoserine (Wang and Kent, 1995b; Gehrig *et al.*, 2009). Wang and Kent

(1995b) showed that the PM substitution in all 16 serine residues in domain P (16S→E) reduced membrane partitioning in cells in agreement with the antagonistic effect of phosphorylation on membrane binding, indicating that the glutamate substitution is a mimic for phosphorylation. Similarly, Gehrig *et al.*(2009) found that the transfer of CCT from the nuclear to the cytoplasmic compartment requires nuclear membrane translocation and activation, which is mediated by domain M. The export of 16S→E variant was significantly reduced due to its reduced affinity for membranes (Gehrig *et al.*, 2009).

As mentioned in Chapter 1, α-syn and CCT tail domains have many features in common. However, unlike α-syn, full length CCT does not have a tendency to misfold and form fibrils in cells. Since the structures of membrane-bound α-syn and CCT tail domains (residues 237-367) appear to resemble each other, a potential factor that prevents CCT(M+P) from misfolding may be interactions with the head domain (N + C) of CCT. Hence, CCT(N+C) may serve as a molecular chaperone for CCT's tail. Comparing the tail domain of CCT with α-syn may prompt investigation in the future on the potential that CCT's domain (N+C) acts as a molecular chaperone for α-syn to reduce fibrillar aggregation *in vitro* and potentially in cells.

I have measured the response of the purified α-syn and CCT tail constructs to lipid vesicles of various compositions and lipid-to-protein molar ratio by monitoring α-helix acquisition via C.D. with spectral deconvolution and bilayer insertion via Trp fluorescence (Johnson and Cornell, 1994). While both of these are indirect methods, Joanne Johnson (1998; 2003) showed with CCT domain M

peptides that there is a strong correlation between vesicle-binding (based on a direct filter-trapping method), the induction of α-helical content (monitored by C.D.) and changes in Trp fluorescence properties.

4.2 Results

4.2.1 CCT Tail Domains Have Higher Affinity than α-Synuclein for Membranes Containing Anionic Lipids

In this section, I will show that α-syn has much lower membrane binding affinity for a model anionic lipid vesicle composed of PC/PG (1:1 mol/mol) than CCT tails. This system was chosen as a starting place for a comparison of binding affinities because both proteins have been shown to bind to vesicles of this composition (Taneva *et al.,* 2003; Zhu *et al,* 2003). The interaction was monitored by both C.D. and Trp fluorescence.

4.2.1.1 Circular Dichroism Control Experiments

At the start of my C.D. studies, I conducted several control experiments to monitor the consistency of the results. First, I explored the effect of buffers on signal to noise during the recording of C.D. spectra. I found that reducing the salt concentration in my buffer was a crucial parameter in obtaining high quality spectra (data not shown). Spectra acquired in PBS (137 mM NaCl, 2.7 mM KCl, 8.1 mM Na_2HPO_4, 1.76 mM KH_2PO_4, pH 7.4) with 0.1 mM OG and 2 mM DTT (ionic strength = 150 mM) gave high background noise below 200 nm, which is an important region for distinguishing α-helical from beta structure. All spectra (both C.D. and fluorescence for consistency) were subsequently acquired in 1/5 dilution of PBS/2 mM DTT/0.1 mM OG in water. Secondly, I tested the time dependence

of helix induction. Here, I determined that the amount of helix induction is not affected by the duration of protein/lipid incubation between 5 – 120 mins (α-syn results shown in Figure 4.1A; other proteins data not shown). Lastly, the stability of α-syn to freeze-thaw cycle was determined. Since pure α-syn is prone to aggregation and I would be thawing frozen samples for each experiment, this issue is important. I found that freeze-thaw process does not affect the stability of α-syn. The secondary structure of α-syn in the absence or presence of anionic lipid SUVs remains the same before and after one round of freeze-thaw cycle (Figure 4.1B).

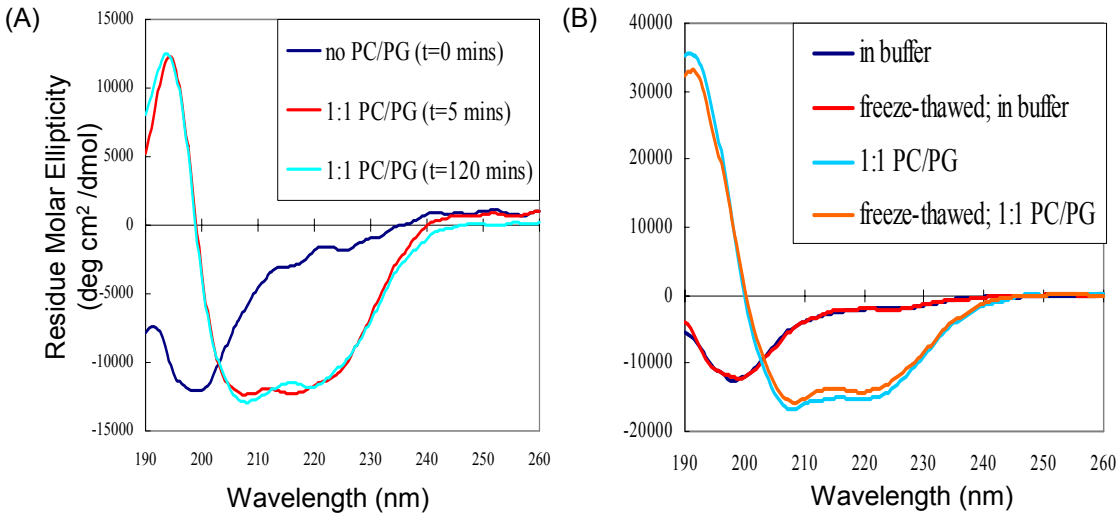

Figure 4.1 Effect of Protein/Lipid Incubation Time and the Effect of Freeze-Thaw Cycle on the Secondary Structure of α-Synuclein
C.D. spectra of purified α-syn (10 uM) in 1/5 diluted PBS acquired with a Jasco 810 spectropolarimeter at 25°C were plotted after subtraction of appropriate backgrounds. The vesicles (SUVs) used were 1:1 (mol/mol) PC/PG. Concentration of OG in the samples for spectroscopy is 20 μM. The protein was tested for its (A) incubation time dependence using a L/P molar ratio of 40 and (B) effects of freeze-thaw cycle using a L/P molar ratio of 80.

4.2.1.2 α-Synuclein Requires Higher Anionic Lipid Concentration for Helix Induction than CCT Tail Domains

Having established the optimum conditions for the C.D. experiments, I monitored the secondary structural change of each protein while varying the lipid to protein (L/P) molar ratio using 1:1 egg phosphatidylcholine (PC) / egg phosphatidylglycerol (PG) (mol/mol) SUVs (Figure 4.2). The spectra obtained were deconvoluted by a CDPro software package that consists of three distinct programs. The deconvolution generates an estimate of the percent distribution of the protein among four secondary structures: α-helix, beta strand, turns, and unordered. In the absence of any activating lipids, CCT tails and α-syn are predominately beta strand arrangement and unordered (Figure 4.3).

All proteins showed an increase in helical character with increasing lipid concentrations, as was expected from previous work (Taneva *et al.,* 2003; Zhu *et al.,* 2003). The results showed that a low L/P molar ratio (e.g. 10-20) is sufficient for the saturation of α-helix in both CCT(M+P) WT and PM variant (Figure 4.3 A and B). Whereas for the protein α-syn, a L/P molar ratio between 80-120 is required to saturate the alpha helical content (Figure 4.3 C, 4.4). The increase in the amount of alpha helical content is at the expense of beta structure, whereas the percentages of disordered and turn conformations changed only slightly.

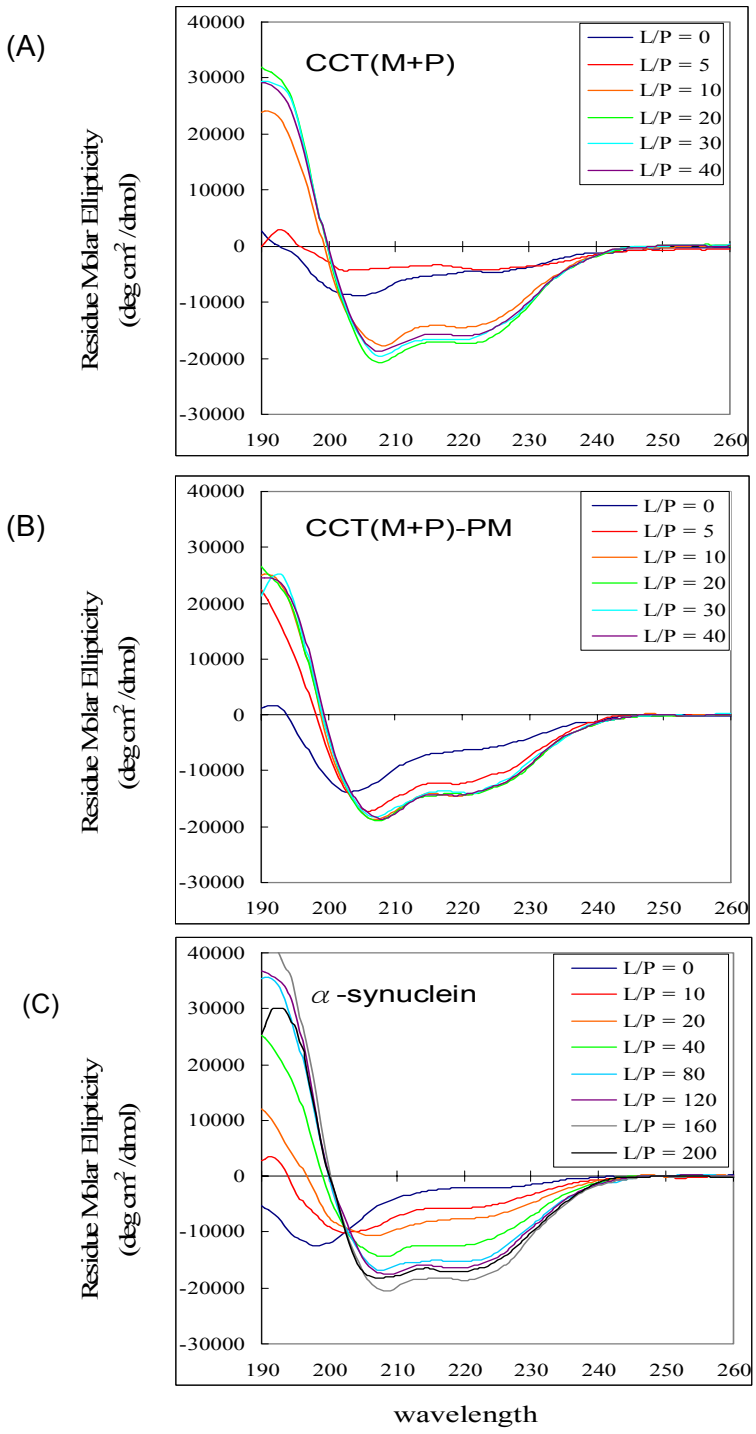

Figure 4.2 Circular Dichroism Spectra of Proteins in the Absence and Presence of Increasing Concentration of Lipid.
C.D. spectra of purified proteins (10 uM) in 1/5 diluted PBS acquired with a Jasco 810 spectropolarimeter at 25˚C were plotted after subtraction of appropriate backgrounds. The small unilamellar vesicles (SUVs) used were 1:1 (mol/mol) PC/PG. Concentration of OG in the samples for spectroscopy is ~ 20 μM.

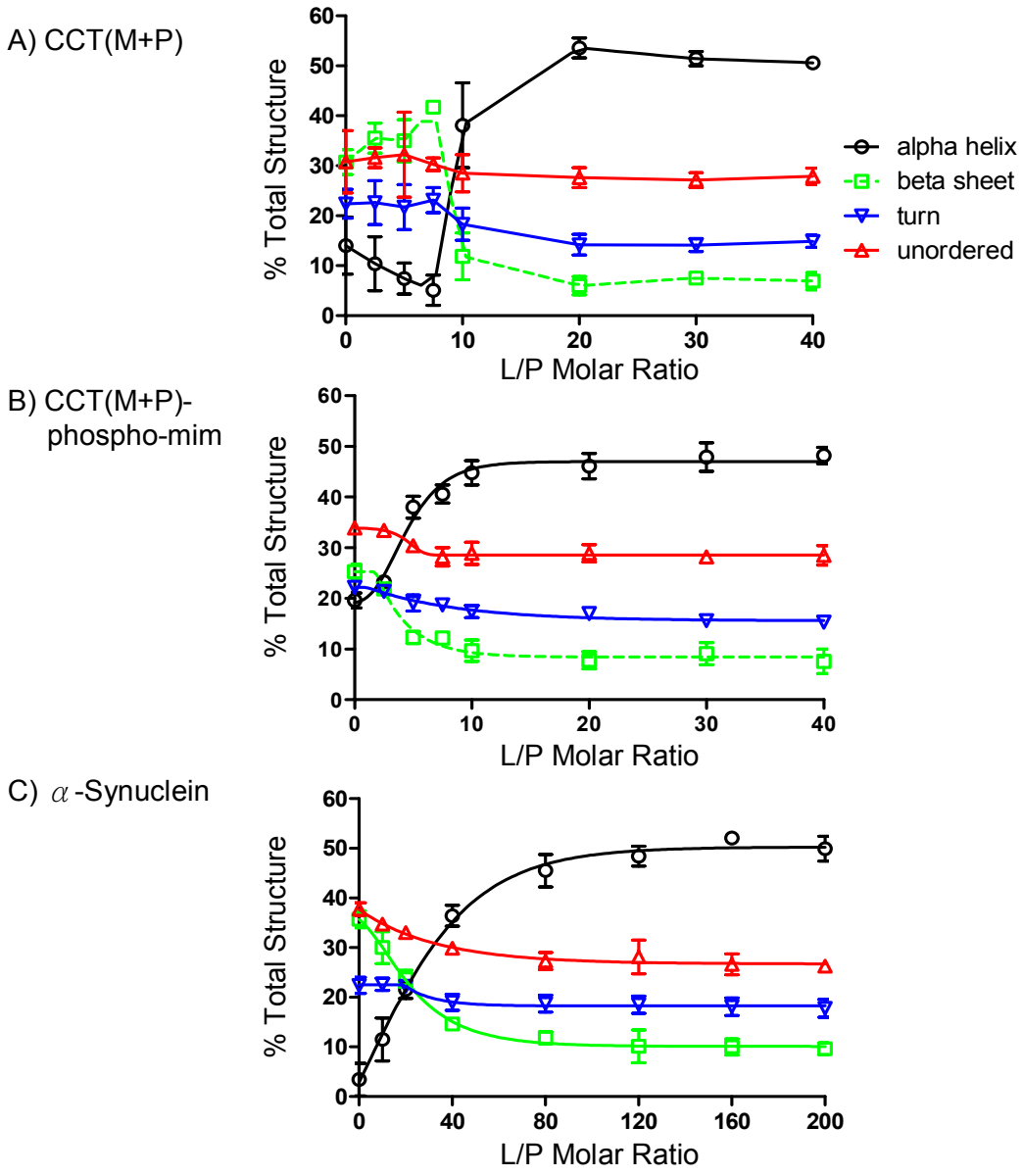

Figure 4.3 Comparison of the Effect of Lipid to Protein Molar Ratio on the Secondary Structure of WT and Phospho-Mimic CCT Tail Domains and α-Synuclein
The spectra shown in Figure 4.2 were deconvoluted by CDPro as described in Methods. Each value is the mean ± S.D. of the data from the three distinct CDPro programs. The data were fit to an asymmetric (five parameter) using GraphPad Prism 5.

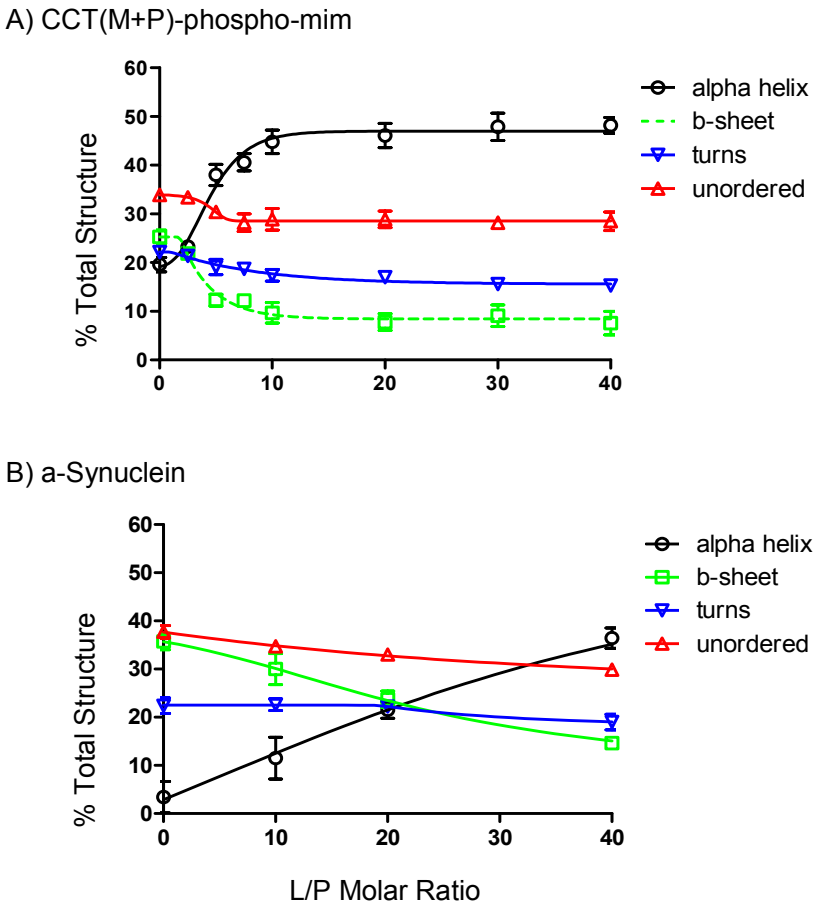

Figure 4.4 Replot of the Percent Structure Distribution Shown in Figure 4.3 for the CCT tail-PM and α-Synuclein Using the Same L/P Scale
This layout shows clearly the weaker binding of α-syn in comparison to the CCT tail construct. Vesicles are 1:1 (mol/mol) PC.PG. The data were fit to an asymmetric (five parameter) using GraphPad Prism 5.

4.2.1.3 Fluorescence Analysis Reveals CCT Tail Domain Proteins Bind More Readily than α-Synuclein to Anionic Lipids.

To confirm the findings obtained using C.D. spectroscopy showing that the CCT tail has a higher anionic vesicle affinity than α-syn, I monitored the insertion of the proteins into the bilayer by Trp fluorescence blue-shifts. This analysis does not report on conformation of the bound proteins, but rather reports on the depth of penetration of the AH. Trp has maximum wavelength absorption at 280 nm and an emission peak that ranges from 330 to 350 nm depending on the polarity of the environment. When a Trp residue is exposed to the aqueous solution, it fluoresces at a higher wavelength (~350 nm) with a lower intensity. When inserted into the hydrophobic membrane core or in our case embedded into the lipid vesicle, Trp fluoresces at a lower wavelength (~330 nm) with an increase in quantum yield. This is designated as a blue-shifted emission spectrum (Lakowicz, 2006). This “blue-shift” in the Trp fluorescence is evident if the aqueous peptide were to bind to lipid vesicles with its hydrophobic face intercalating into the membrane. Recording these emission blue-shifts also allowed us to compare the concentration of anionic lipids required for insertion

I took advantage of the single natural Trp residue in domain M of CCT (Trp-278) and created a variant by substituting W336 with Phe in domain P (CCT(M+P)-W336F and CCT(M+P)-PM-W336F). However, human α-syn contains no Trp residue, hence I have prepared a single Trp variant at Val37 (α-syn-V37W). As mentioned in Chapter 1, the helix formed by the CCT tails and α-syn would be highly amphipathic, leading to the model of peptide-vesicle interaction involving the hydrophobic face of the helical peptide interacting with

the hydrophobic membrane. Position 37 was selected for engineering a Trp variant because this residue lies in the middle of the AH (Figure. 1.6).

Figure 4.5 shows that the emission spectra of the Trp from the three proteins were slightly blue-shifted in buffer lacking lipids relative to free Trp in buffer which will show a peak at 350 nm. Peak emission wavelengths were 334 nm, 340nm, and 342 nm for (CCT(M+P)-W336F, CCT(M+P)-PM-W336F, and α-syn-V37W, respectively. Thus the Trp residues may be in somewhat apolar environments in the soluble forms (Figure 4.5). Upon gradual addition of PG anionic lipids (1:1 mol/mol PC/PG SUVs) the emission maximum shifted towards a lower wavelength, and the intensity of the fluorescence increased, indicative of a shift of the Trp residue to a more hydrophobic environment for all three proteins (Figure 4.5).

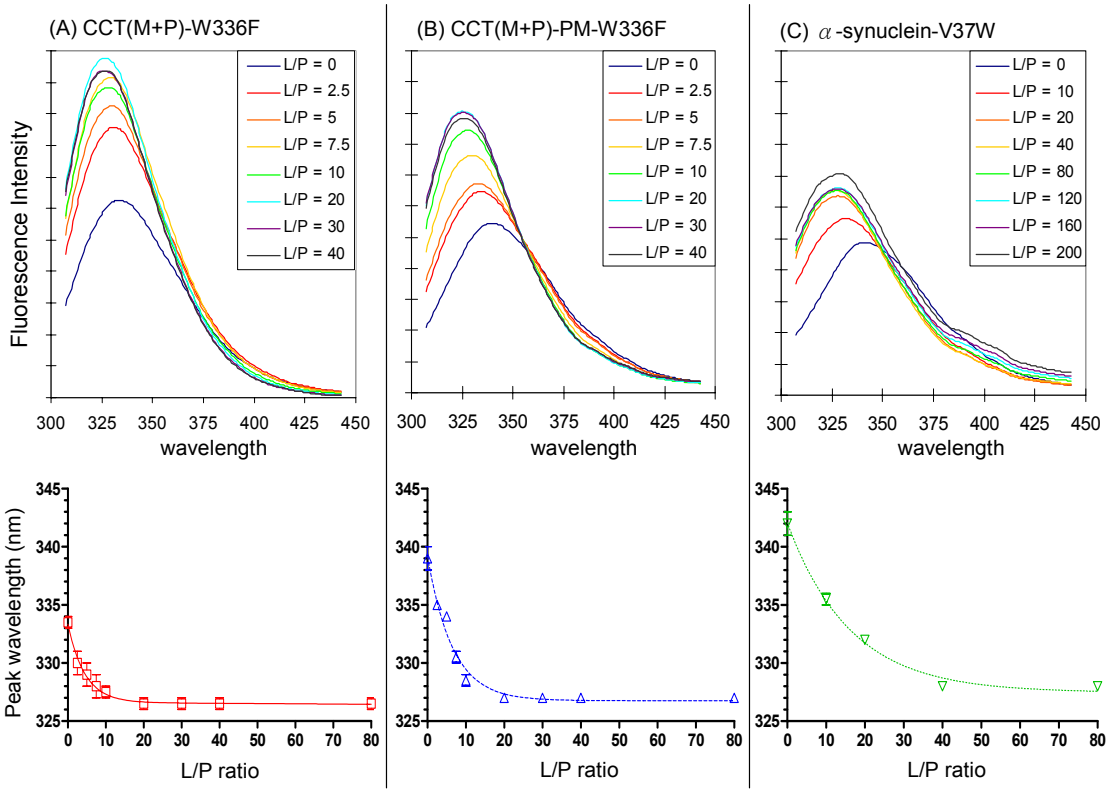

Figure 4.5 Anionic Vesicles Induce Protein Tryptophan Fluorescence Enhancement and Blue-Shift.
Tryptophan fluorescence and peak wavelength of CCT(M+P)-W336F (A) WT and (B) PM and (C) α-synuclein-V37W in diluted PBS and in diluted PBS with the presence of increasing L/P ratio of 1:1 (mol/mol) PC:PG vesicles. The excitation wavelength was 280 nm. Protein concentration was 6 uM and the concentration of OG was 6 μM in the sample for spectroscopy. The peak wavelength versus L/P ratio data was fit to a two phase exponential decay plot using GraphPad Prism 5

The wavelength at the peak of the blue-shifted spectrum was dependent on the protein examined and the concentration of anionic vesicles added. α-Syn required a higher L/P ratio for the blue-shift. An L/P ratio of 40 was required for the maximal blue shift for α-syn, whereas an L/P of 20 was sufficient for the CCT tails. However, for all three proteins, the final peak wavelength was 327-328 nm, suggesting a similar environment polarity for the Trp residues (Figure 4.5). For CCT tails, the inductions of the helical conformation in the proteins, as observed

in the C.D. experiments (Figure 4.3), correlated very well with the shifts of the Trp to a more hydrophobic environment, as observed in the fluorescence experiments, where both parameters saturated at L/P 10-20 (Figure 4.6). On the other hand, for α-syn the induction of the helical content did not correlate with the blue-shift of the Trp residue; α-syn required a L/P ratio of only 40 to reach blue-shift saturation (Figure 4.6), whereas it required at least a L/P ratio of 80 to reach helical content saturation (Figure 4.3).

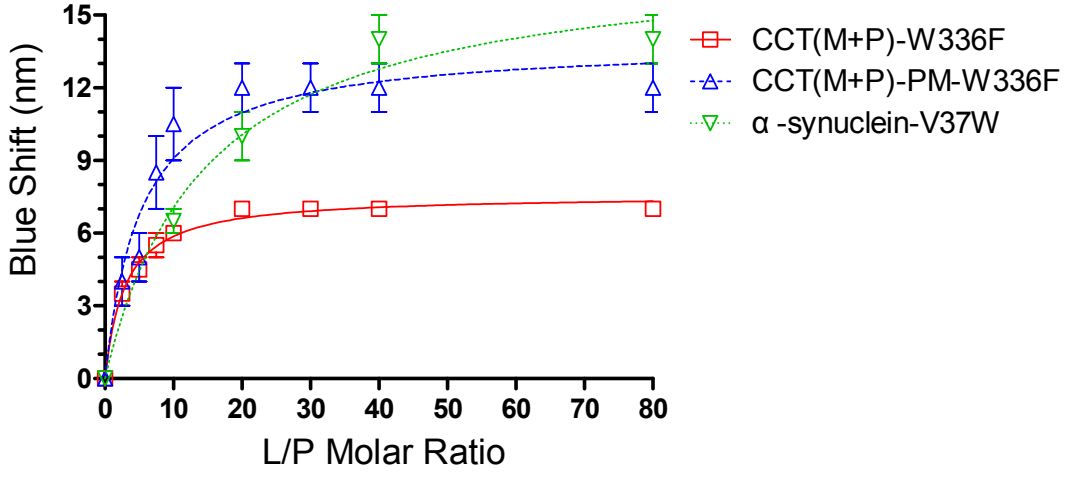

Figure 4.6 Comparison of the Effect of Lipid-to-Protein Molar Ratio on the Tryptophan Blue Shift of WT and Phospho-mimic CCT Tail Domains and α-Synuclein to Anionic Lipid SUVs

The fluorescence blue shift for each protein was obtained from the spectra shown in Figure 4.5. The equation to determine the blue shift was described in methods section. The peak fluorescence values (λ_{max}) for the proteins in the absence of lipid were 334 nm, 340 nm, and 342 nm for CCT(M+P)-W336F, CCT(M+P)-PM-W336F, and α-syn-V37W. The data represents the averages of two separate analyses. The data were fit to a one site binding (hyperbola) using GraphPad Prism 5

4.2.2 Comparison of Lipid Compositional Selectivity of WT and Phospho-mimic CCT Tails, and α-Synuclein.

In this section, I performed C.D. spectroscopy and Trp fluorescence analysis to show that all three proteins have similar dependence on the mol percent of anionic lipids in the SUVs. Additionally, I show that their anionic lipid selectivity is based on the negative charge, rather than the specific chemistry, of their head group. Moreover, I have discovered that unlike CCT tail domains, α-syn does not respond to type II lipids.

4.2.2.1 CCT Tail Domains and α-Synuclein have Similar Anionic Lipid Requirements for Helix Induction and Membrane Insertion

C.D. experiments were done to examine secondary structure changes of each protein as a function of the mol% of anionic lipid (egg PG used here) in an egg PC matrix. The L/P molar ratio was set to 120 because at this ratio using 1:1 PC/PG vesicles, the alpha helical content of all three proteins was saturated, indicating maximal binding (Figure 4.3). By controlling the L/P molar ratio, the resulting data from all three proteins would be comparable. The spectral deconvolution data are shown in figure 4.7, illustrating that an increase in alpha helical structure correlates to the increase in the mol% of anionic lipid in the lipid vesicle. The results showed that 20 mol% of egg PG is sufficient for maximal helix induction of all three proteins (Figure 4.7).

To confirm the findings obtained via C.D. spectroscopy showing that all three proteins have the same selectivity for lipid vesicle composition, I examined the binding of WT and PM CCT(M+P)-W336F and α-syn-V37W to vesicles containing various mol% PG by monitoring Trp fluorescence. Figure 4.8 shows

that the blue shifts of all three proteins are saturated when the PC matrix contains 20 mol% anionic lipid PG. Thus, the surface concentration of anionic lipid (PG) needed for induction of the helical conformation in the proteins, as observed in the C.D. experiments, correlated very well with a shift of the Trp to a more hydrophobic environment, as observed in the fluorescence experiments. Therefore, at a high lipid-to-protein ratio of 120, 20 mol% of anionic lipid will be sufficient to induce the AHs within the CCT domain M and α-syn and allow them to intercalate into the hydrophobic zone of the bilayer. The typical concentration of anionic lipid in cell membranes is 20 mol% (Leventis and Grinstein, 2010).

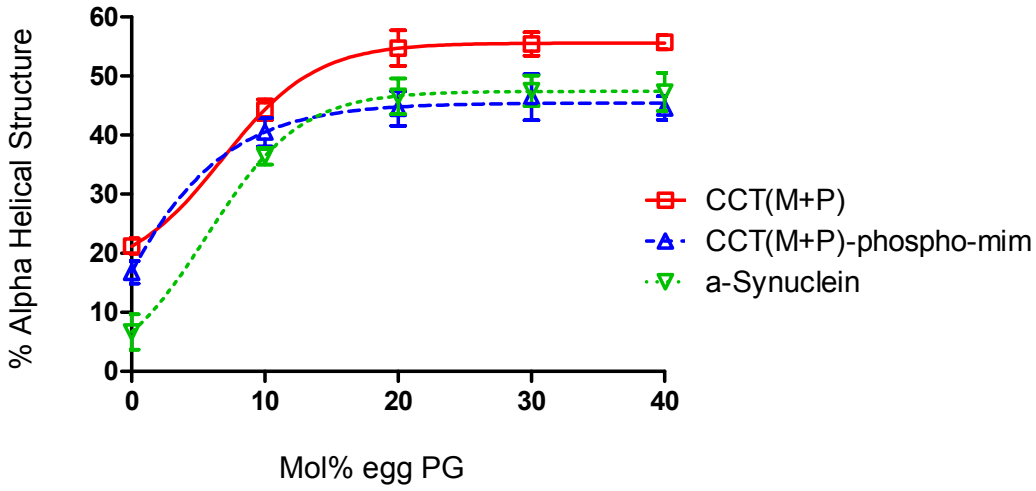

Figure 4.7 Comparison of the Effect of Various Mol% PG on the Secondary Structure of WT and Phospho-mimic CCT Tail Domains and α-Syn.
C.D. spectra were acquired for purified proteins (10 uM) in 1/5 diluted PBS. Concentration of OG in the samples for spectroscopy is 20 μM. PC was used as vesicle matrix. The lipid to protein molar ratio was kept constant at 120/1. Spectra were deconvoluted by CDPro to obtain the percent helical content. Each value is the mean ± S.D. of the data from the three distinct CDPro programs. The data were fit to a Boltzmann sigmoidal curve using GraphPad Prism 5

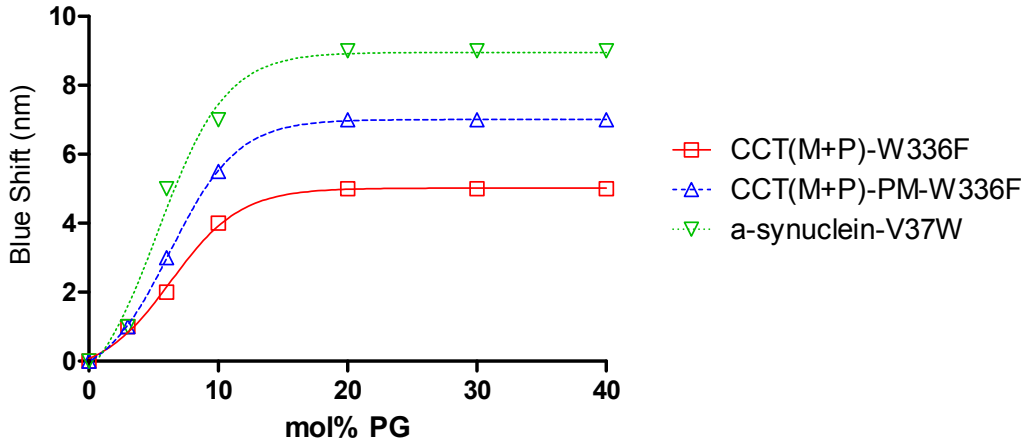

Figure 4.8 Comparison of the Effect of the Mol% of Egg PG on the Tryptophan Blue Shift of WT and Phospho-mimic CCT Tail Domains and α-Syn
Purified proteins (6 uM) were in 1/5 diluted PBS and 6 μM OG. PC was used as vesicle matrix. The lipid to protein molar ratio was kept constant at 120. The λ_{max} values for the proteins in 100% PC vesicles (0% PG) were 335, 337, and 342 for CCT WT, CCT PM, and α-syn, respectively. The equation to determine the blue shift was described in methods section. The data were fit to a Boltzmann sigmoidal curve using GraphPad Prism 5.

4.2.2.2 CCT and α-Syn Show Selectivity for Anionic Charge on Phospholipid Head-group

To confirm that the proteins are responding to the anionic lipid charge of the phospholipid head group, rather than the specific headgroup chemistry, I examined the effects of another anionic phospholipid, palmitoyl-oleoyl phosphatidylserine (POPS). To make results comparable, PC/PG and PC/POPS SUVs were both prepared at a molar ratio of 4:1 mol/mol. Varying the L/P molar ratio showed that CCT(M+P) responded similarly to both PG and POPS (Figure 4.9, other proteins not shown). The percent helix obtained from the deconvolution spectra varied similarly as a function of the lipid concentration. This confirms that the charge on the anionic lipid, which promotes electrostatic interaction, is an

important component in lipid selectivity for both CCT and α-syn membrane binding domain.

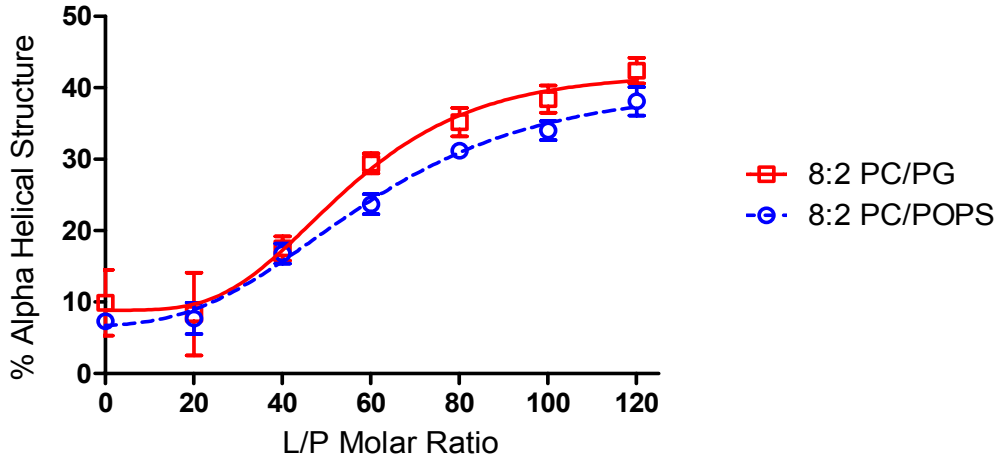

Figure 4.9 Comparison of the Effect of Different Anionic Lipid Vesicles on the Secondary Structure of CCT (M+P).
C.D. spectra were acquired for purified CCT(M+P) (10 uM) in 1/5 diluted PBS and 20μM OG containing vesicles composed of either 4:1 (mol/mol) PC/PG or PC/POPS. The spectra were deconvoluted by CDPro to obtain the percent helical content. Each value is the mean ± S.D. of the data from the three distinct CDPro programs. The data were fit to an asymmetric (five parameter) model using GraphPad Prism 5.

4.2.2.3 Only CCT Tail Domains Respond to Type II Lipids

Previous studies have shown that CCT will respond to the negative curvature strain created by type II lipid such as 1,2-dioleoyl-*sn*-glycero-3-phosphoethanolamine (DOPE) (Davies *et al.*, 2001). However, little is known about how α-syn responds to type II lipids. To investigate the response of the three different proteins to this class of lipids in parallel, SUVs consisting of a 1,2-dioleoyl-*sn*-glycero-3-phosphocholine (DOPC) / DOPE at a molar ratio of 2:3 mol/mol were used in C.D. spectroscopy. In this experiment, the results suggest that even at a high L/P molar ratio (e.g. 120), α-syn does not take on significant

alpha helical conformation, whereas CCT domain M + P peptides do (Figure 4.10).

Even though the WT and the PM variant of CCT(M+P) are characterized to have a significant increase in alpha helical content in the presence of type II lipids, their responses are weak compared to those obtained using anionic lipids SUVs (Figure 4.3 + 4.10). When compared to the response to anionic lipids, the CCT domain M + P proteins require a much higher L/P molar ratio of type II lipids to reach maximal helix induction and show less alpha helical contents at saturation.

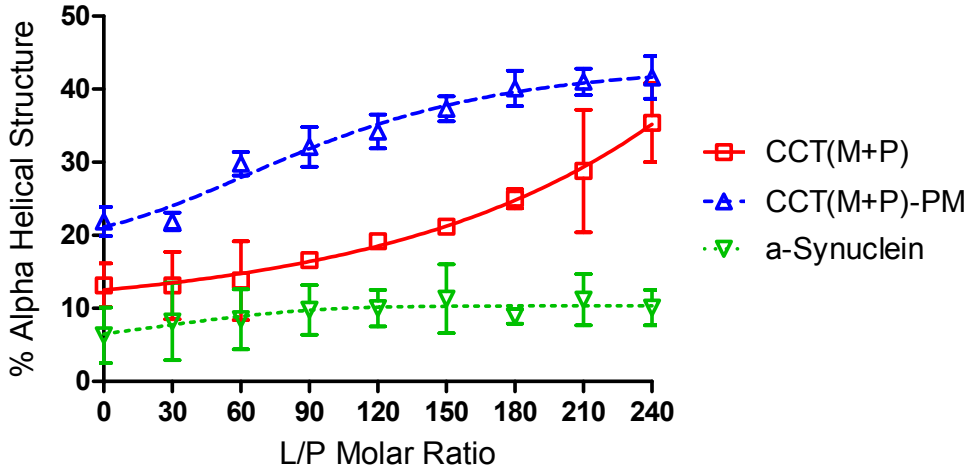

Figure 4.10 Comparison of the Effect of Type II Lipid (DOPE) on the Secondary Structure of WT and Phospho-mimic CCT Tail Domains and α-Synuclein.
C.D. spectra were acquired for purified proteins(10 uM) in 1/5 diluted PBS and 20 μM OG. The vesicles composed of a 2:3 molar ratios of DOPC/DOPE. The spectra were deconvoluted by CDPro to obtain the percent helical content. Each value is the mean ± S.D. of the data from the three distinct CDPro programs. The data were fit to an asymmetric (five parameter) model using GraphPad Prism 5

4.2.3 CCTs and α-Synuclein Bind with Similar Extent of Bilayer Penetration

The Trp environments of the three proteins (WT and PM CCT(M+P)-W336F, and α-syn-V37W) were also monitored by its accessibility to fluorescence quenchers. An aqueous phase quencher, in this case iodide, will quench the fluorescence of Trp upon collision with the molecule (Eftink, 1991, Lakowicz, 2006). If the Trp is not accessible to the aqueous environment, as is the case if the residue is buried in a membrane or in the interior of a protein, the effect of the aqueous quenchers will be greatly diminished.

4.2.3.1 Anionic Lipid Vesicles Shield CCT Tails and α-Synuclein from Aqueous Iodide Quenching

Figure 4.11 panels a-c show the spectra of CCT(M+P)-W336F WT and PM and α-syn-V37W in diluted PBS buffer + 0.2 M NaCl. The presence of NaCl does not quench fluorescence and was incorporated to maintain a constant ionic strength among all samples. When NaCl was replaced by NaI, the aqueous quencher, a reduction in the fluorescence intensity was observed. Figure 4.11 panels d-f show the spectra of the proteins in similar buffer containing 1:1 PC/PG vesicles, with their characteristic blue-shifted peaks below 330 nm. Here, the addition of iodide resulted in a much lower reduction in fluorescence intensity. These results suggest that the anionic vesicles shield the proteins' Trp from the aqueous iodide and confirm that the Trp residues intercalate the hydrophobic core of the vesicles.

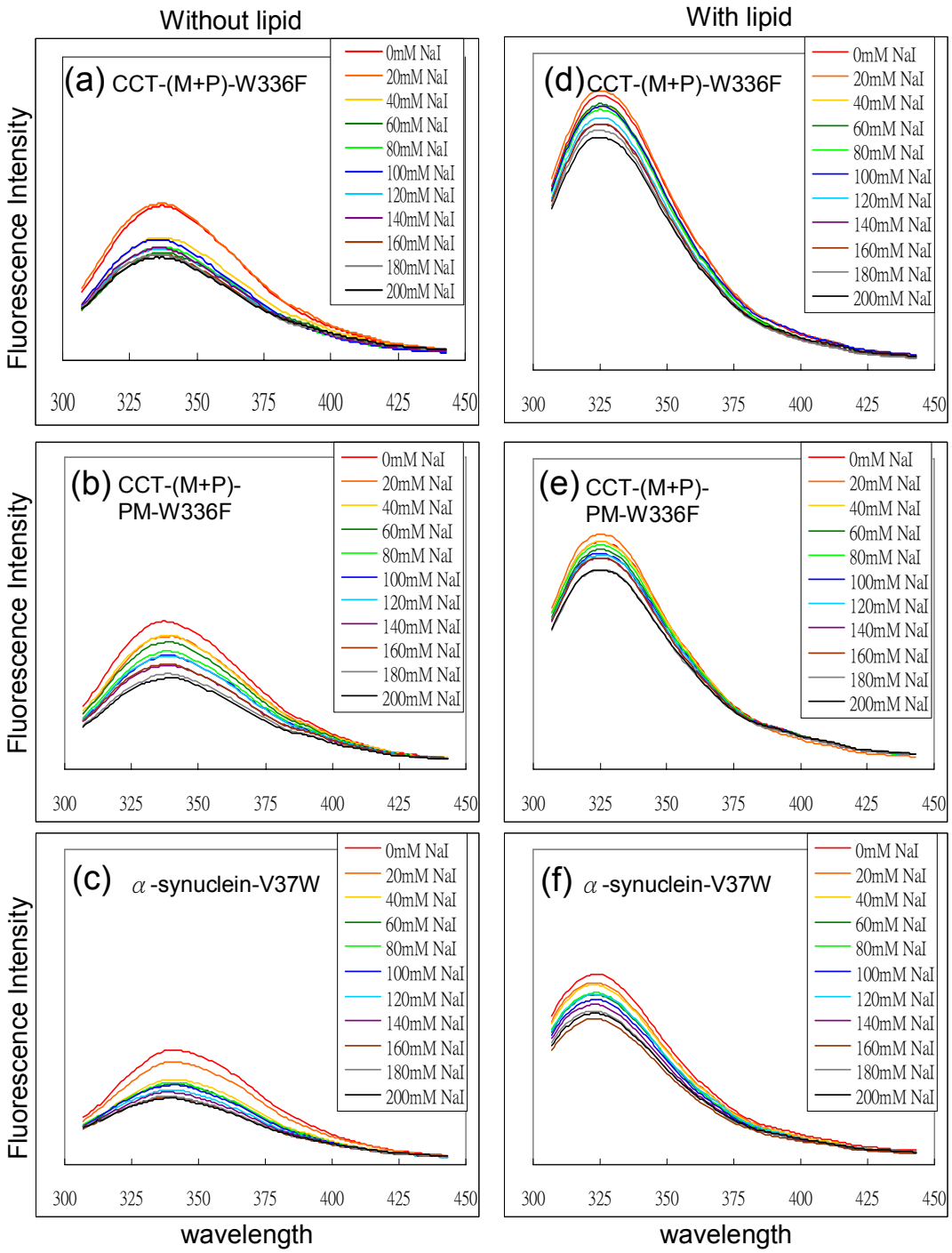

Figure 4.11 Quenching of Tryptophan Fluorescence in CCT Tails and α-Synuclein by Aqueous Iodide.
The protein concentrations were 6 uM and the OG concentration were 6 μM. Unquenched proteins were in 1/5 diluted PBS + 0.2 M NaCl. Quenching of proteins was done by increments of 0.02 M NaI up to 0.2 M NaI. Panels a-c, proteins are in buffer. Panels d-f, proteins are in the presence of 0.5 mM 1:1 (mol/mol) PC/PG SUVs.

By converting the fluorescence quenching results into a Stern-Volmer plot, I could analyze the data quantitatively. The Stern-Volmer plot relates the fluorescence quenching to the concentration of the quencher using the following equation: $F_o / F = K_{sv}$ [quencher] +1, where F_o is the peak fluorescence intensity in the absence of quencher, F is the peak fluorescence intensity in the presence of quencher, and K_{sv} is the Stern-Volmer quenching constant obtained as the slope of a plot of F_o / F versus [quencher] (Lakowicz, 2006). When the Trp is inaccessible to the quencher, the low fluorescence quenching probability will be indicated by a small Stern-Volmer quenching constant K_{sv}. In Figure 4.12, the Stern-Volmer plots of iodide quenching for the three proteins in buffer and in the presence of 1:1 PC/PG SUVs are shown. In buffer only, the WT and PM CCT tail domains show similar slopes (2.5 and 2.9 respectively) compared to the slope for α-syn (3.7). This suggests that the CCT Trp residues reside in a similar environment whereas the α-syn Trp residue, having a higher K_{sv} value, is likely to be in a more hydrophilic setting. This is in agreement with the more blue-shifted Trp fluorescence maxima for the CCT tails versus α-syn (Figure 4.5). In the presence of anionic lipids, the slope is much lower for all three proteins suggesting the Trp is much less accessible to the aqueous environment. Again, the slopes for the CCT tail domains (~0.85) are smaller than that of α-syn (1.4) when the proteins are in the presence of anionic lipids. However, when comparing the magnitude of change between the slopes obtained from buffer only and in the presence of 1:1 PC/PG SUVs, the result suggests that the Trp from the three

proteins have similar degrees of shielding from the anionic lipids by inserting into the hydrophobic region of the SUVs to a similar depth.

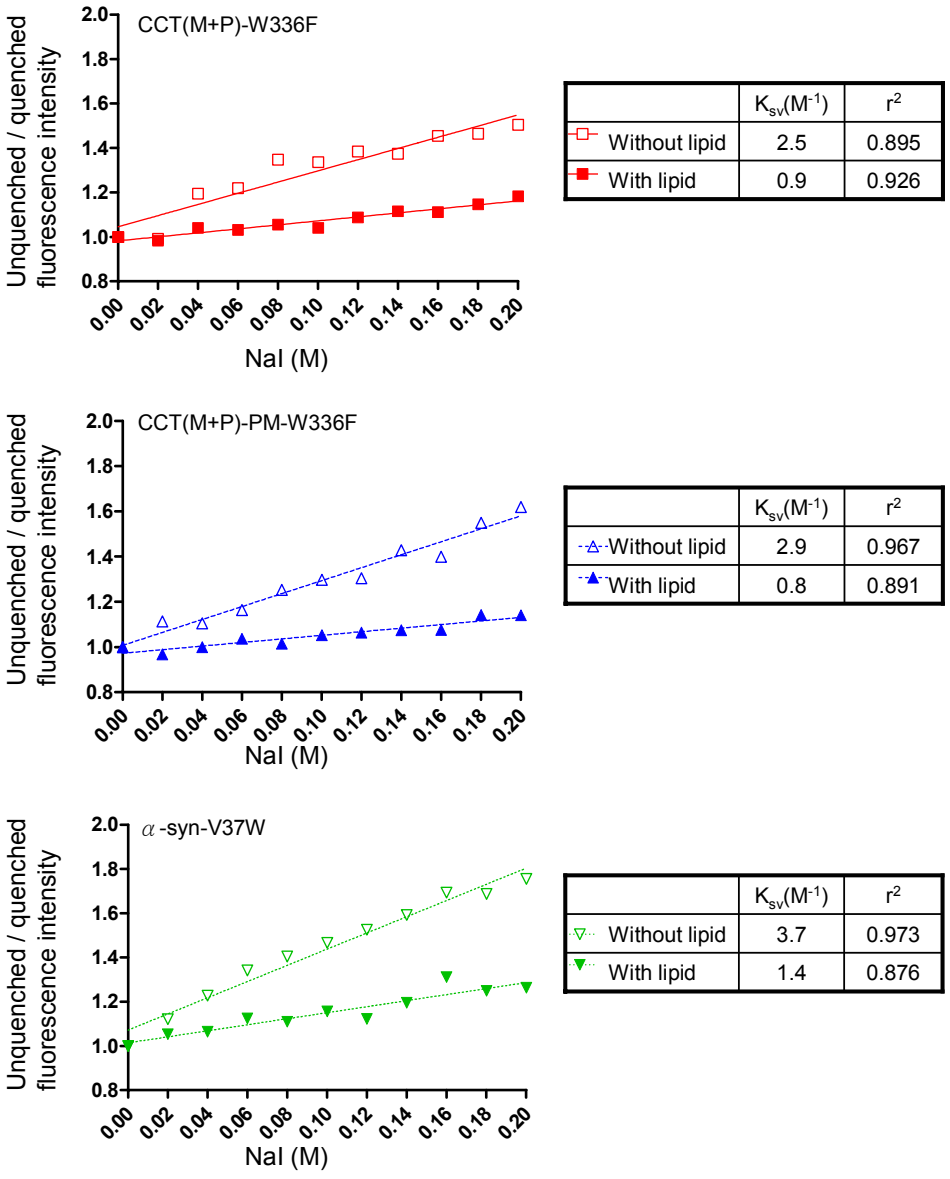

	$K_{sv}(M^{-1})$	r^2
Without lipid	2.5	0.895
With lipid	0.9	0.926

	$K_{sv}(M^{-1})$	r^2
Without lipid	2.9	0.967
With lipid	0.8	0.891

	$K_{sv}(M^{-1})$	r^2
Without lipid	3.7	0.973
With lipid	1.4	0.876

Figure 4.12 Stern-Volmer Plot for Iodide Quenching of Tryptophan Fluorescence. Samples contained 6 uM protein in 1/5 diluted PBS (w/o lipids samples), or in the presence of 0.5 mM vesicles composed of egg 1:1 (mol/mol) PC/PG (with lipids). Iodide concentration was as indicated. The ionic strength was kept constant at 0.2 M by the addition of NaCl. The data were fit to a linear regression line using GraphPad Prism 5

4.2.4 How Does the Phospho-mimic Modification Affect CCT's Domain M?

Finally, I investigated in more detail how phosphorylation mimicry of domain P affects domain M's membrane binding ability. By creating a domain M variant with a single C-terminal Trp substitution, I showed that this tail region penetrates into the lipid hydrocarbon core to the same degree in both WT and PM CCT tails.

4.2.4.1 The Phospho-mimic Variant has Lower Helical Structure Saturation than WT CCT Tail Domain.

Both WT and PM CCT(M+P)-W336F helical structures saturate at approximately 20 mol% PG (Figure 4.7). However, at saturating lipid concentration, the PM variant has a significantly lower percentage of helical structure compared to the wild-type (~45% versus 55%). There could be two possible explanations for this. One possibility is that the degree of alpha helical induction is proportional to the depth of domain M penetration into the lipid vesicles (Figure 4.13 A). The acidic tail on the PM domain P could cause charge repulsion with the anionic lipids and limit domain M insertion into the bilayer. However, data described above argue against this notion since fluorescence blue-shifts and Trp quenching results indicated that Trp-278 in both WT and PM W336F variants penetrate the lipid vesicles to a similar extent. The second possibility is that the additional negative charge on the tail of PM domain P increases the tail disorder and hinders helix formation on the adjacent C-terminus of domain M (Figure 4.13 B). This would imply that the N-terminal segment of domain M of both WT and PM CCTs bind in an equivalent fashion and penetrate

into the vesicles with equal depth, but they differ in the helix content of the C-terminal segment of domain M.

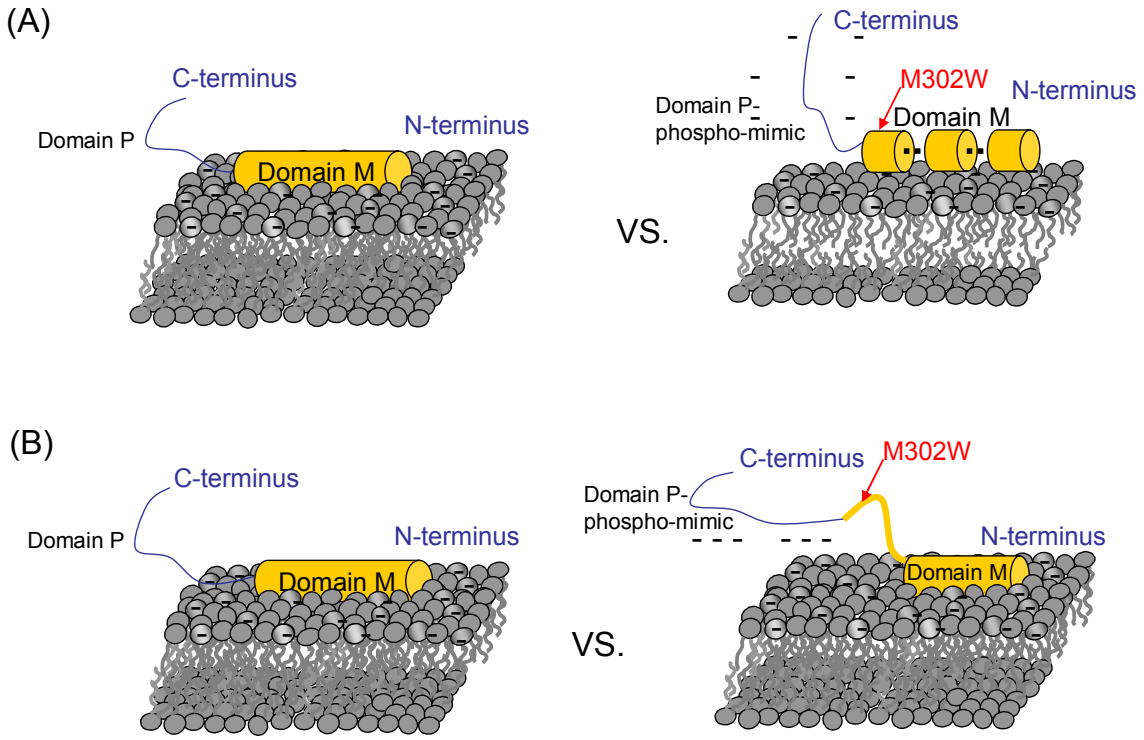

Figure 4.13 Amphipathic Helix Insertion Model vs. Domain M C-terminus Disorder Model
(A) Degree of helical induction is proportional to the depth of domain M penetration into the membrane. (B) Additional negative charge on the tail of PM variant domain P increases the tail disorder and hinders helix formation on the adjacent C-terminus of domain M.

To explore the second mechanism (Figure 4.13 B) I monitored fluorescence shifts in a Trp engineered into the C-terminal segment of domain M at M302W. If the helical content of domain M helix is affected by the phosphorylation status of the tail, then we would expect that the penetration depth of this Trp-302 would be lower in CCT(M+P)-PM than in the WT CCT tail.

The methionine at position 302 (see sequence in Figure 1.6) was changed into a Trp while substituting the Trp residues at 278 in domain M and 336 in

domain P with phenylalanine residues. I compared the lipid response of both CCT tail proteins by blue-shift analysis and by shielding from iodide quenching.

4.2.4.2 Wild-type and Phospho-mimic CCT(M+P)-M302W shows Identical Blue-Shift Induced by Anionic Lipid

The emission spectra for the two soluble proteins in buffer showed the emission peaks were at 341 nm for WT and 344 nm for the PM variant (Figure 4.14 C + D) suggestive of a somewhat apolar environment in the absence of lipid, as was observed with Trp-278. Upon addition of PC/PG (1/1) SUVs the emission spectra for both CCT tails blue-shifted to a plateau of 333 nm, indicative of burial in the bilayer. The concentration of anionic lipid vesicles needed for blue-shift saturation was 60 μM (i.e. lipid to protein ratio of 30) (Figure 4.15).

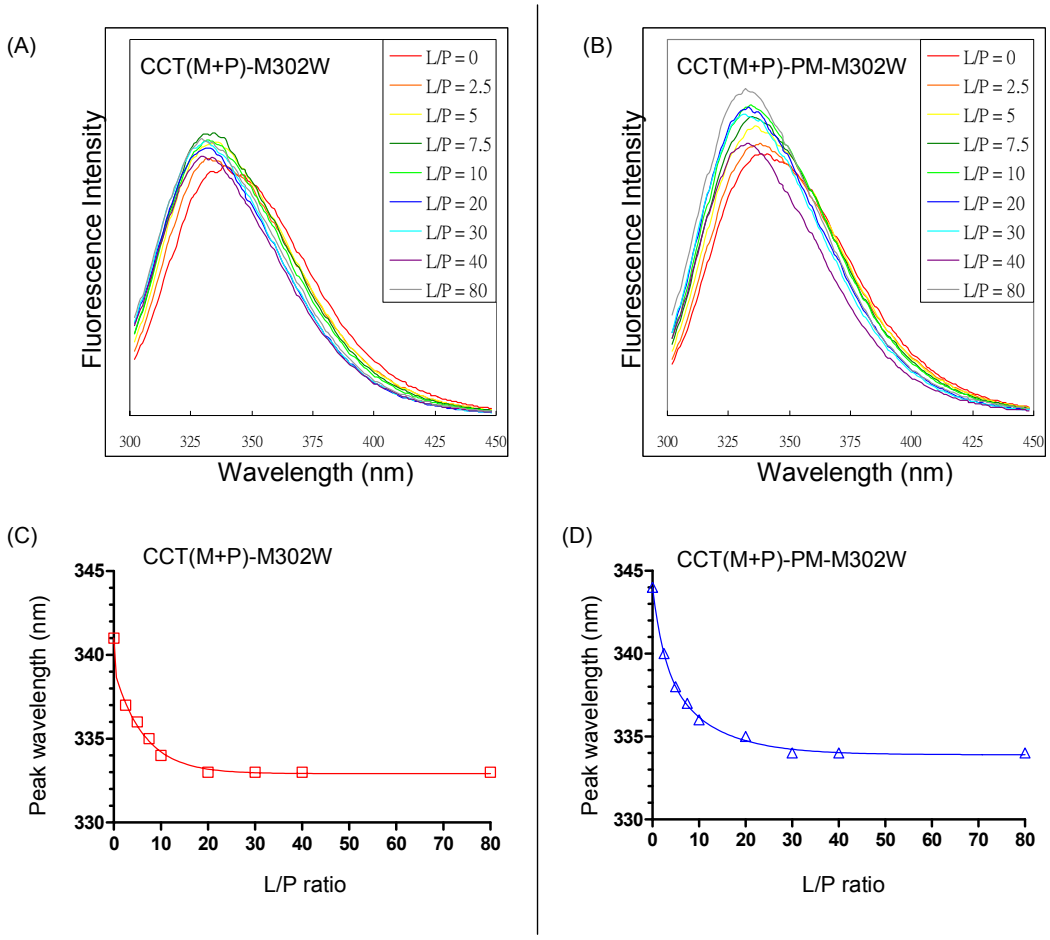

Figure 4.14 Anionic Vesicles Induce Protein Tryptophan Fluorescence Enhancement and Blue-Shift Indicating Membrane Penetration of Trp 302
Fluorescence spectra were acquired in 1/5 diluted PBS, 5 μM OG and/or increasing L/P ratio of 1:1 (mol/mol) PC:PG vesicles. Protein concentration was 2 uM. In the panels at the bottom, peak wavelengths of each protein were plotted at each L/P ratio. Data represents averages of two separate analyses. The data were fit to a two phase exponential decay model using GraphPad Prism 5.

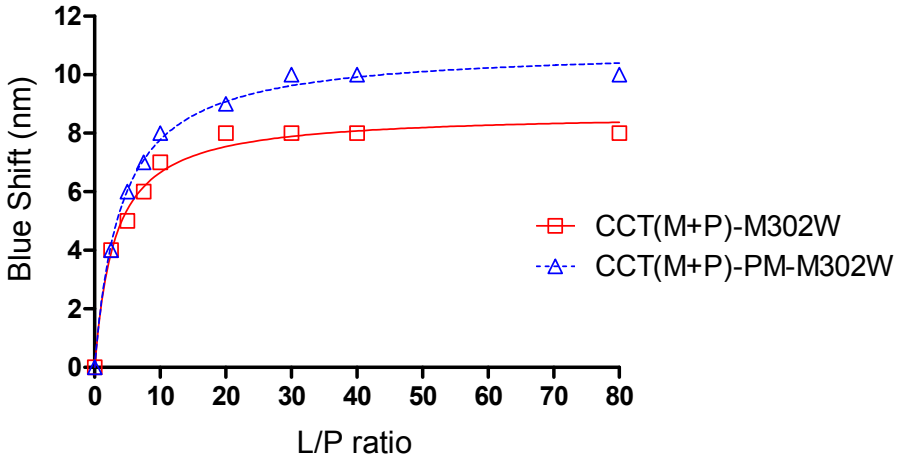

Figure 4.15 Comparison of the Effect of Lipid-to-Protein Molar Ratio on the Tryptophan-302 Blue-Shift of WT and Phospho-mimic CCT(M+P)-M302W
The spectra in Figure 4.14 are replotted as blue shift *vs.* L/P molar ratio; Vesicles were 1:1 (mol/mol) PC/PG. The equation to calculate the blue shift is provided in methods section, page 41. Data represent the averages of two separate analyses. The data was fit to a one site binding (hyperbola) model using GraphPad Prism 5

4.2.4.3 Similar Lipid Composition Promotes WT and PM CCT(M+P)-M302W Interaction with the Membrane

I determined the dependence on the mol % anionic lipid for insertion of Trp-302, using fluorescence blue-shift analysis. The Trp emissions were blue-shifted as a function of increasing mol% of anionic lipid PG (figure 4.16 panels C + D). Figure 4.17 showed that both WT and PM CCT tails, at L/P ratio of 50, required at least 40 mol% of PG for Trp-302 to fully penetrate into the lipid vesicle. In addition, the blue-shift curves for the two proteins are comparable suggesting the C-terminus of the two domain Ms would require the same lipid composition for membrane insertion.

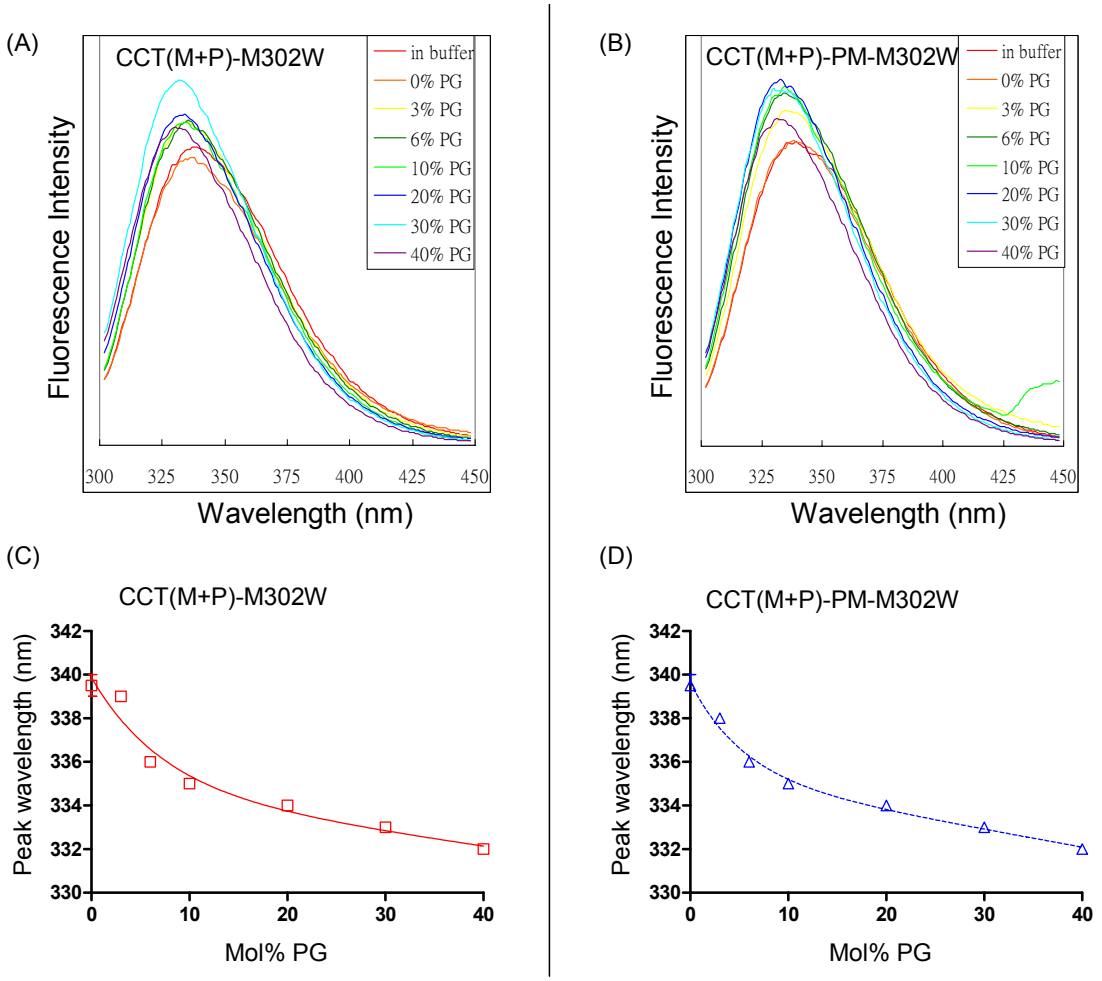

Figure 4.16 Effect of Increasing Anionic Lipid on Trp-302 Fluorescence
Proteins (2 uM) in 1/5 diluted PBS, 5 μM OG, and PC vesicles containing the indicated mol% egg PG vesicles. The lipid-to-protein molar ratio was kept constant at 50. The peak wavelengths at each L/P ratio in the spectra shown in a and b were determined as described in Methods section, and were plotted as a function of mol% PG in c and d. Data represents average of two separate analyses. The data were fit to a two phase exponential decay plot using GraphPad Prism 5

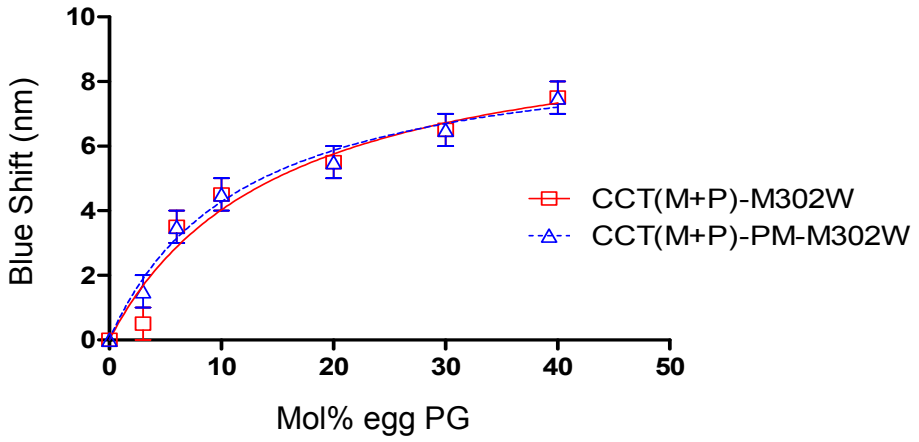

Figure 4.17 Comparison of the Effect of Increasing PG Content on Trp-302 Blue-shifts in WT and Phospho-mimic CCTs.
Spectra were acquired with purified proteins (6 uM) in 1/5 diluted PBS, 6 μM OG. PC was used as vesicle matrix. The lipid to protein molar ratio was kept constant at 50. Data represent average of two separate analyses. The data were fit to a Boltzmann sigmoidal curve using GraphPad Prism 5

4.2.4.4 Aqueous Iodide Quenching Shows WT and PM CCT M302W Intercalates Equally into the Hydrophobic Core of the Membrane

If aqueous iodide quenching of Trp-302 were different for the WT versus PM CCT, this would support model B in Figure 4.13. Figure 4.18 shows that in the absence of lipid vesicles there was approximately 40% reduction in the intensities of the fluorescence for both the WT and PM CCT tails by 0.2 M sodium iodide. In the presence of PC/PG vesicles the spectra of both proteins show characteristic blue-shifted peaks. (Figure 4.18, panels C and D). For both proteins, iodide quenching was very similar, showing only approximately 20% quenching. The Trp-302 quenching results for the two proteins were also analyzed by Stern-Volmer plots (Figure 4.19).

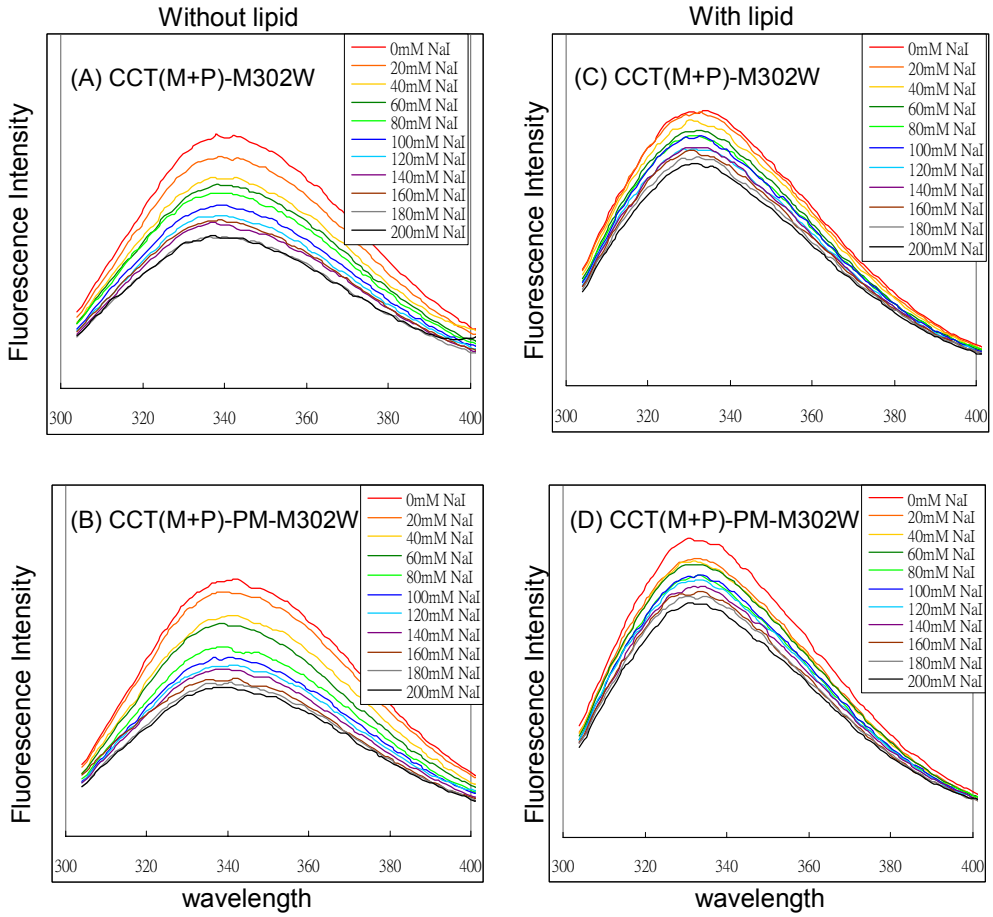

Figure 4.18 Quenching of Tryptophan Fluorescence in CCT Domain M C-terminus by Aqueous Iodide.
The protein concentrations were 2 μM and the OG concentrations were 6 μM. Unquenched proteins were in in 1/5 diluted PBS + 0.2 M NaCl. Quenching of proteins was done by increments of 0.02 M NaI up to 0.2 M NaI and 5 μM OG. diluted PBS. Panels a-b, proteins are in buffer. Panels c-d, proteins are in the presence of 0.16 mM 1:1 (mol/mol) PC/PG SUVs.

An overlay of the Stern-Volmer plots for WT and PM CCT M302W indicated the environments of the two proteins are identical with respect to iodide accessibility in both the absence (K_{sv}, of 3.4 *vs* 3.8) or presence (K_{sv},= 1.24 *vs* 1.16) of anionic lipid vesicles (Table 4.1). These results suggest that in the presence of anionic vesicles, Trp-302 of both proteins intercalates into the hydrophobic core of the lipid vesicles and hence shield themselves from the

aqueous iodide quencher. Thus model B in Figure 4.13 is not supported by this data.

Comparing Stern-Volmer data for Trp-278 and Trp-302 (Table 4.1) shows that the slopes ($K_{sv,}$) for Trp-302 are higher than Trp-278. This is true for both in the absence and presence of lipid (Figure 4.12, Table 4.1). This implies that Trp-302 is buried less in both the soluble and membrane-associated forms. Hence, Trp-302 may be located in a more disordered region compared to Trp-278.

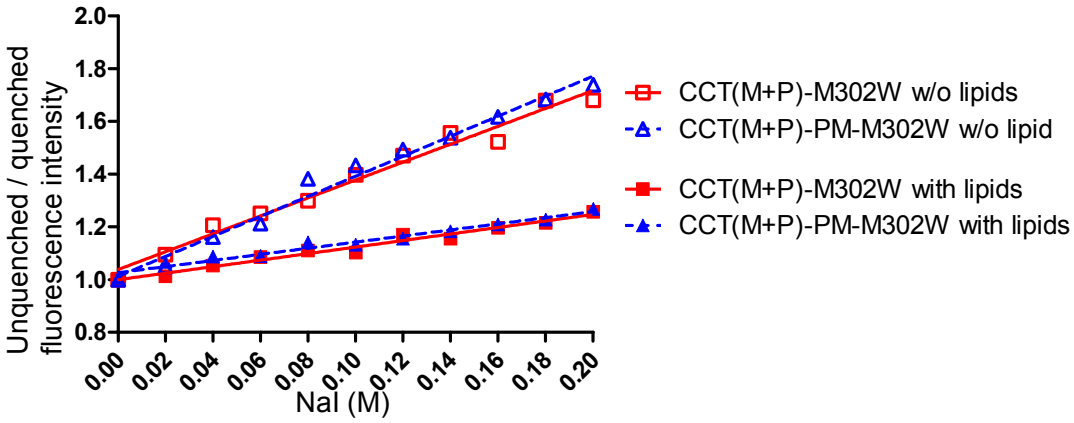

Figure 4.19 Stern-Volmer Plot for Iodide Quenching of Tryptophan-302 Fluorescence
Samples contained 2 uM peptide in diluted PBS (w/o lipids samples), or in the presence of 0.16 mM vesicles composed of egg 1:1 (mol/mol) PC/PG (with lipids). Iodide concentration was as indicated. The ionic strength was kept constant at 0.2 M by the addition of NaCl. The data was fit to a linear regression line using GraphPad Prism 5

Table 4.1 Stern-Volmer Iodide Quenching Constants for WT and Phospho-mimic CCTs: a Comparison of Quenching of Trp-278 with Trp-302.

Sample CCT(M+P)	Trp monitored	K_{sv} (M^{-1})	
		– lipid	+ lipid
Wildtype	278	2.5	0.9
	302	3.4	1.24
Phospho-mimic Variant	278	2.9	0.8
	302	3.8	1.16

r^2 values for the linear regressions were > 0.89

4.3 Discussion

I have used C.D. to compare the secondary structure and fluorescence to compare the membrane interactions of CCT's tail domains (M+P) and α-syn, which are known to have an AH with membrane-binding properties. The results of these spectroscopic experiments have led to four major conclusions about the membrane-binding characteristics of WT and PM CCT tail domains and α-syn.

4.3.1 CCT Tail Domains and α-Synuclein Conversion to α-Helices, Promoted by Lipids, Occurs at the Expense of Beta Structure.

CCT tail: C.D. studies with short domain M peptides suggested that they are predominately disordered in buffer (Taneva *et al.*, 2003). In contrast, the C.D. analyses in this thesis showed that both the CCT tails and α-syn contain some structure in the absence of lipids; 25-35% beta strand is obtained from the deconvoluted spectra. The ProfSec secondary structure prediction of domain P's sequence strongly predicts an unstructured segment (Rost and Eyrich, 2001).

According to my C.D. spectroscopy data, the percentages of disordered and turn conformations remain relatively unchanged regardless of the amount of lipids present. These data suggest that the beta structure is most likely to reside in domain M of the soluble CCT tail. The blue-shifted fluorescence peak emission wavelength of the Trp residue (Trp-278) in both soluble WT and PM CCT(M+P) also support this idea. The Trp residue may be located in a moderately hydrophobic setting created by interactions with nearby residues.

Previous studies have shown that domain M of CCT inhibits the catalytic domain in CCT's soluble form (Friesen *et al.,* 1999). Thus, domain M's inhibitory conformation contains beta structure. It is possible that these beta strands may form direct inhibitory contacts with the adjacent catalytic domain active site.

This beta structure is converted into long helical structures by lipid binding. The lipid vesicles that caused a change in the fluorescence properties of the tail domains also promoted the helical conformation. There was a close correlation between the lipid to protein ratio required, or mol % anionic lipid required, for maximum induction of helix and for complete Trp fluorescence blue shift. In summary, my results suggest that the induction of AH and the insertion of the tail domain occur at a relatively low L/P ratio (10-20) and require lipid vesicles composed of a low mol% of anionic lipids (20 mol%), which is the typical anionic content of a cell membrane.

α-Synuclein: This protein, like CCT tail domains, adopts a helical conformation at the expense of beta structure upon addition of anionic lipid. However, unlike domain M of CCT, α-syn requires a significantly higher

concentration of anionic lipid for both helix induction and membrane insertion (lipid-to-protein ratio of 80 and 40, respectively). When examining the alpha helical content of α-syn, the data suggest that this protein has almost no helical tendencies in the absence of lipid, thus it is less primed to bind membranes in an alpha helical conformation (Figure 4.4 and 4.7). For α-syn to bind membranes as an α-helix, it requires a higher lipid concentration to break its beta-strand character and to make up for the entropy loss of its completely disordered portions. This idea was supported by secondary structure prediction systems such as ProfSec, indicating that α-syn has a lower tendency for alpha helical conformation (Figure 4.21) and would require a bigger boost to change its propensity from beta strand and unordered conformations to helical content.

In summary, α-syn has a much weaker affinity than the CCT(M+P) and CCT(M+P)-PM proteins for anionic lipid vesicles. The binding curve in Figure 4.20 makes this clearly evident. I constructed this curve by equating the lipid-dependent change in α-helical content (from Figure 4.3) with membrane binding. Partition constants (K_p) can be extrapolated from these graphs (K_p = 1/[L] at 50% bound). There is a 6-fold difference between the K_p values calculated for CCT(M+P)-PM and α-syn (39,000 *vs.* 6,110, respectively; Figure 4.20).

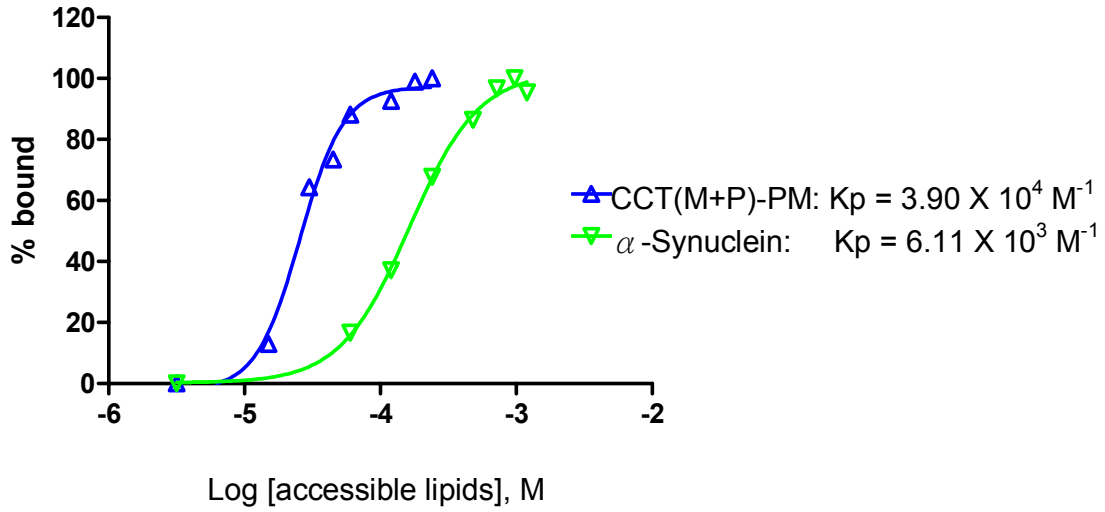

Figure 4.20 Binding Curve of CCT(M+P)-PM and α-Synuclein for PC/PG (1/1) vesicles] The CDPro results shown in Figure 4.3 B and C were converted into a binding curve. % Bound = 100 (% α-helix – I) / (F – I) where I is % α-helical structure at no lipid and F is maximum % α-helical structure obtained. Kp = 1 / [accessible lipids] where accessible lipid is 0.6 of total lipid. Top and bottom values were constrained to 100 and 0 %, respectively. The data were fit to an Sigmoidal dose-response (variable slope) model using GraphPad Prism 5.

Although my Stern-Volmer analysis of the environment of Trp-37 in α-syn suggested that it binds more superficially than Trp-278 in CCT, it is not sound logic to conclude that α-syn binds more superficially to anionic lipid vesicles than the CCT tails. To investigate this, one would need to examine the accessibility of many positions throughout the CCT tails and α-syn.

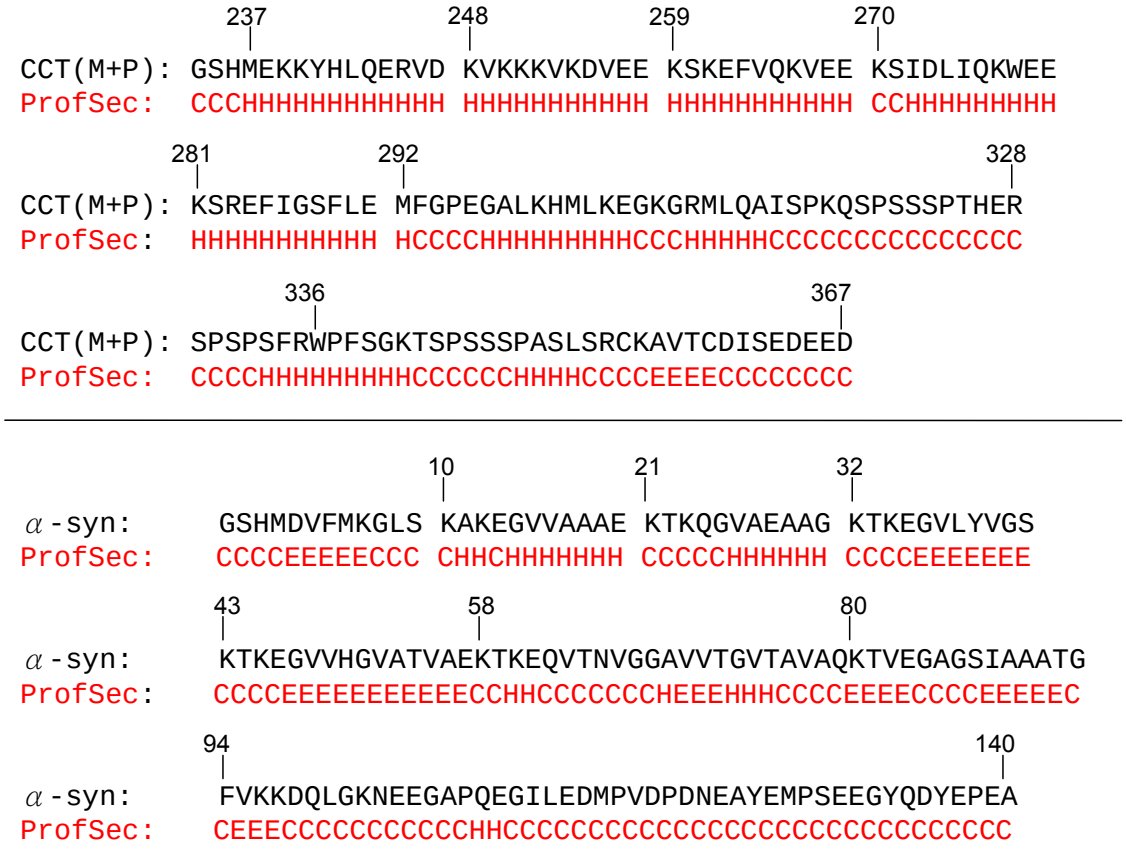

Figure 4.21 ProfSec Secondary Structure Prediction of CCT(M+P) and α-Synuclein
Individual amino acid were assigned a secondary structure prediction of either H = alpha helix, E = beta strand, or C = coil conformation. This prediction system was provided by Aberystwyth University Computation Biology Group.

4.3.2 α-Synuclein and CCT Tails Differ in Their Response to Type II Lipids

Although the unsaturated PC and PE used here are zwitterionic (neutral) phospholipids that exhibit similar electrostatic properties, they differ in their head group size, orientation and bilayer packing parameters. The smaller head group volume of PE relative to its larger hydrocarbon chains volume creates an inverted cone structure. This is in contrast to PC, which retains a cylindrical geometry, ideal for bilayer packing. The cone-shaped geometry of DOPE tends to create

voids between lipid molecules in a bilayer, which leads to compensatory effects including high negative curvature strain. Davies and colleagues (2001) have shown that the activation of CCT by unsaturated PE, classified as type II lipids, correlates with this negative curvature strain. CCT activation by type II lipids is weaker than the activation by anionic lipids (Taneva *et al.,* 2005), in that a higher molar concentration is required to achieve activation. My C.D. spectroscopy results examining the tail domains of WT and PM CCT also showed that 2:3 molar ratio of DOPC/DOPE SUVs induce α-helix conformation at a high lipid-to-protein ratio (Figure 4.10). However, compared to the results using anionic lipids as activators, it was observed that CCT tail domains have significantly less affinity for type II lipids. This trend was also observed when examining domain M peptides showing a much weaker response to type II lipids compared to anionic lipid vesicles (Johnson *et al.,* 1998).

A previous study also looked at PE's effect on α-syn's vesicle binding abilities and helical induction (Jo *et al.*, 2000). In their study, however, the researchers replaced PC with PE in acidic multilamellar vesicles (PE/POPA 1:1) and observed an increase in the binding of α-syn to those vesicles as well as its α-helicity. Because the anionic lipid would antagonize the effects of the PE on curvature strain induction, this study did not duplicate my analyses, in which I used DOPE in DOPC vesicles devoid of any PG. C.D. spectroscopy showed that α-syn does not acquire additional helix conformation even at a lipid-to-protein ratio of 240. Hence, my findings indicate α-syn does not respond to the negative curvature strain provided by type II lipids.

4.3.3 Phospho-Mimic Modification Does Not Affect the Structure or Membrane Binding of the Proximal Portion of the M Domain

One of the challenges when comparing the WT and the PM CCT's tail domains was to distinguish between the models for their different maximum helical response. As mentioned previously, the difference may be due to either (1) domain M's depth of penetration into the hydrocarbon core of the vesicles or (2) the hindering of helix formation on the C-terminus of domain M caused by the acidic tail of PM domain P. Trp fluorescence data investigating Trp-278 (natural Trp residue in domain M) and M302W (Trp residue engineered into the C-terminus of domain M) concluded that both WT and PM variants share identical characteristics, namely their affinity for anionic lipids, lipid composition preference, and similar depth of intercalation into the lipid bilayer. Thus another model is required to explain helical content differences. The N-terminus of domain M has a large number of positively charged residues. As domain M changes conformation into α-helix upon addition of activating lipids, the disordered, negatively charged phospho-mimic domain P may interact with the positively charged residues at the N-terminus of domain M. Instead of disrupting the helix formation in the C-terminus of domain M, the PM domain P may prevent the formation of α-helix at the N-terminus, hence reducing the overall helical content in domain M.

4.3.4 C-terminal Limit of Domain M Includes Residue 302

Up to this time, there has been little indication for the C-terminal boundary of CCT's membrane binding domain (M). Previous analyses of the structure and lipid selectivity of domain M have ultilized synthetic peptides that terminate at

residue 293 or 299, while monitoring the natural Trp residue at position 278 (Johnson *et al.,* 1998; Taneva *et al.*, 2003). In working with the Trp variant M302W, I found that domain M extends to at least residue 302. In both WT and PM version of the CCT tail, I showed that Trp-302 undergoes fluorescence blue-shifts and is shielded from iodide quenching in the presence of SUVs; i.e. this residue penetrates into the SUVs hydrophobic core of the bilayer. The additional negative charge in domain P in CCT(M+P)-PM did not affect the penetration at Trp-302, suggesting this residue is part of the membrane binding domain, regardless of CCT's phosphorylation status.

5 CONCLUDING DISCUSSION

My thesis work contributed to the discovery that CCT tail domains (membrane binding and phosphorylation domains) and α-syn, although sharing similar properties such as sequence motifs, have important differences in lipid responses. Like CCT tails, α-syn bound to anionic vesicles, and the same anionic content (20 mol%) was required for either CCT or α-syn. However, α-syn required a higher lipid molar concentration for binding, as assessed by the lipid concentration required for conversion to an alpha helix or intercalation into lipid vesicles. Another key difference emerging from my results was that while CCT binds (weakly) to type II lipids, α-syn does not bind these lipids. Thus, CCT tails possess a higher affinity for both anionic and type II lipids than α-syn.

Why does α-synuclein bind more weakly than CCT tails to anionic lipids? To answer this, we should consider the membrane-binding mechanism of amphipathic helical proteins. The first step in binding involves electrostatic attraction of protein positive charges towards the negative charged membrane surface and intimate contact with the lipid head-group region. In this lower dielectric environment, helix induction is promoted, as there is less competition with water for hydrogen bonding along the peptide backbone (Drin and Antonny, 2010; Cornell and Taneva, 2006). Alpha helical conformation would then propagate from helical nucleation sites throughout the length of α-syn or CCT domain M. Once the amphipathic region becomes fully α-helical, the protein will

penetrate deeper towards the hydrocarbon core, so that the hydrophobic residues on the non-polar face are shielded from water. The main difference between CCT tails and α-syn may lie in their propensity for alpha helical conformation as predicted by ProfSec and other programs (Figure 4.21). For CCT tail, more than 60% of the residues are predicted to be alpha helical even in its soluble form, whereas α-syn has <20%. One of the factors antagonizing membrane binding of the AH peptides is entropy, as they become *more ordered* upon binding. Membrane binding of α- syn will be associated with a greater unfavourable ΔS than that for the CCT tail, since the latter is more ordered (e.g. more helical) in its soluble form. This is supported not only by the predictions, but also my C.D. data (Figure 4.3). The unfavourable entropy change will shift the binding equilibrium towards the soluble form more so for α-syn than CCT.

Another factor influencing membrane affinity corresponds to the hydrophobic contribution from the non-polar face of the AH. Cornell and Taneva (2006) have calculated that the mean hydrophobicity for CCT residues 242-293 is slightly greater than that of α-syn (0.45 *vs.* 0.27 kcal/mol). Hence the free energy from the hydrophobic component of CCT tail will drive the equilibrium towards membrane bound state more so than α-syn.

Why does α-synuclein not bind at all to type II lipids? And what is the driving force of CCT tail's interaction with type II lipids? Type II lipids are phospholipids with small head-groups, such as DAG and unsaturated PE. In vesicles composed of PC and unsaturated PE, surface gaps exist between the head-groups of the phospholipids, creating instability. This instability is countered

by a tendency of the monolayer to curl towards the aqueous phase, but this is not compatible with maintaining a bilayer arrangement. Thus type II lipids create negative curvature strain and increase lipid packing pressure in an effort to eliminate packing gaps. CCT binding to type II lipids vesicles via its AH would reduce the negative curvature strain and packing pressure due to its elimination of the surface gaps upon insertion as a helix. α-Syn may not bind to type II lipid vesicles because the non-polar face of its AH is less bulky than that of CCT's domain M. α-Syn contains only 1 aromatic residue whereas the hydrophobic face of the CCT domain M contains 5 aromatic residues. Thus α-syn binding to these vesicles would be less effective in reducing negative curvature strain than CCT. As well, the high packing pressure on the membrane surface might be too great a barrier, and this is supported by the requirement of α-syn for looser surface packing, as I discuss next.

Another hypothesis for α-syn lack of affinity for type II lipids is because it requires vesicles with positive curvature, whereas CCT does not. Middleton and Rhoades (2010) showed that vesicle curvature has a strong effect on the binding affinity of α-syn. α-Syn showed a 15-fold binding preference for SUVs with a diameter of only 46 nm compared to LUVs of diameter 160nm. Thus α-syn requires vesicles with high positive curvature, which translates into loose lipid packing at the surface. The PC/DOPE vesicles I used were likely of increased diameter compared to the anionic SUVs, due to negative curvature strain, and this would prevent the creation of the loosely packed, positive curved membrane surface that α-syn demands.

How does the phospho-mimic modification impact the helical content of the adjoining M domain? The difference in maximal helical content between the WT (55%) and PM variant (45%) upon binding to anionic lipid containing SUVs suggested that the PM modification has either altered the membrane binding ability of domain M or the secondary structure of domain M. Yet, Trp fluorescence analyses and iodide quenching experiments monitoring a natural Trp residue in the middle of domain M suggested both WT and PM CCT(M+P) insert an equal depth into lipid vesicle. Similarly, monitoring a Trp variant at the C-terminus of domain M showed the two CCT tail domains insert equally into the vesicle and also demonstrate this segment of residues to be alpha-helical in structure. Thus, it can be concluded that the PM modification must use another mechanism to reduce the amount of helical content present in domain M. Our current hypothesis is that it interacts electrostatically with the highly basic region at the N-terminus of domain M, and lowers the α-helical propensity of this region.

Two other possibilities for the lack of effect of the PM should be mentioned. Firstly the PM may be a poor substitute for the phosphoserine, as has been confirmed in the comparison of the effects of PM versus phosphoserine of the fibrillation of α-syn (Paleologou *et al.*, 2008). Secondly, it is conceivable that the phosphoserines interact with some element within the CCT head domain (N+C), explaining why no influence of the PM is observed in this study with the tail domain.

Where does domain M of CCT end? Work in this thesis also demonstrates that the C-terminal limit of domain M extends to residue M302. By substituting M302 into a Trp, fluorescence blue shifts and iodide quenching data revealed that this residue penetrates into the core of lipid vesicles. My results suggest that this residue resides on the hydrophobic face of a very long AH and intercalates into the membrane hydrocarbon core.

Significance and Future Directions. By examining CCT(M+P) and α-syn side-by-side, I was able to compare their affinity for various lipid vesicles and how the binding induces structural change. This will serve as a stepping stone to further studies aimed at stabilizing α-syn helical structure and/or preventing its mis-folding. The catalytic domain of CCT might suppress beta structure that progresses into aggregated intermediates in domain M. In doing so, it could act as a molecular chaperone to prevent misfolding of the CCT tail. Since the CCT tail resembles α-syn, one possibility is that a chimera between the CCT head domain and α-syn might bind α-syn monomers and interrupt the process of oligomerization and fibrillization. Moreover if CCT tails on their own can forge interactions with α-syn, then this interaction might block the fibrillation of α-syn, while promoting α-helical content. The investigation of CCT as a potential inhibitor of α-syn fibrillization will be worthwhile from the viewpoint of the evolution of AH motifs in proteins. Future research examining the question of why some intrinsically disordered AH motifs mis-fold into amyloid while others do not may provide insight into mechanisms for promoting α-helical conformation of α-syn and ultimately be useful in the treatment of Parkinson’s disease.

REFERENCES

Arnold, R. S. & Cornell, R. B. (1996) Lipid Regulation of CTP: phosphocholine Cytidylyltransferase: Electrostatic, Hydrophobic, and Synergistic Interactions of Anionic Phospholipids and Diacylglycerol. *Biochemistry* 35, 9917-24.

Arnold, R. S., DePaoli-Roach, A. A. & Cornell, R. B. (1997) Binding of CTP:phosphocholine Cytidylyltransferase to Lipid Vesicles: Diacylglycerol and Enzyme Dephosphorylation Increase the Affinity for Negatively Charged Membranes. *Biochemistry* 36, 6149-56.

Biere, A.L., Wood, S.J., Wypych, J., Steavenson, S., Jiang, Y., Anafi, D., Jacobsen, F.W., Jarosinski, M.A., Wu, G.M., Louis, J.C., Martin, F., Narhi, L.O., and Citron, M. (2000) Parkinson's Disease-associated α-Synuclein is More Fibrillogenic than β- and γ-Synuclein and Cannot Cross-seed its Homologs. *J. Biol. Chem.* 275, 34574–79

Bogan, M.J., Agnes, G.R., Pio, F., and Cornell, R.B. (2005) Interdomain and Membrane Interactions of CTP: phosphocholine Cytidylyltransferase Revealed via Limited Proteolysis and Mass Spectrometry. *J Biol. Chem.* 280, 19613-19624

Bradford, M. (1976) A Rapid and Sensitive Method for the Quantitation of Microgram Quantities of Protein Utilizing the Principle of Protein-dye Binding. *Anal Biochem.* 72, 248-253.

Burré, J., Sharma, M., Tsetsenis, T., Buchman, V., Etherton, M.R., and Südhof, T.C. (2010) α-Synuclein Promotes SNARE-Complex Assembly in Vivo and in Vitro. *Science* 329, 1663-67.

Bussell, R. and Eliezer, D. (2003) A Structural and Functional Role for 11-mer Repeats in α-Synuclein and Other Exchangeable Lipid Binding Proteins. *J. Mol. Biol.* 329, 763-778.

Cabin, D.E., Shimazu, K., Murphy, D., Cole, NB., Gottschalk, W., McIlwain, K.L., Orrison, B., Chen, A., Ellis, C.E., Paylor, R., Lu, B., and Nussbaum, R.L. (2002) Synaptic Vesicle Depletion Correlates with Attenuated Synaptic Responses to Prolonged Repetitive Stimulation in Mice Lacking - α-Synuclein. *J. Neurosci.* 22, 8797-807.

Chandra, S., Chen, X., Rizo, J., Jahn, R., and Sudhof, T.C. (2003) A Broken α-Helix in Folded α-Synuclein. *J. Biol. Chem.* 278, 15313-18.

Conway, K.A., Harper, J.D., Lansbury, P.T. (1998) Accelerated In Vitro Fibril Formation by a Mutant α-Synuclein Linked to Early-onset Parkinson Disease. *Nat. Med.* 4,1318–20

Conway, K.A., Lee, S.J., Rochet, J.C., Ding, T.T., Williamson, R.E., and Lansbury, P.T. Jr. (2000) Acceleration of Oligomerization, Not Fibrillization, is a Shared Property of Both α-Synuclein Mutations Linked to Early–onset Parkinson's Disease. *PNAS* 97, 571-576.

Cornell, R. B. (1991a) Regulation of CTP:phosphocholine Cytidylyltransferase by Lipids. 1. Negative Surface Charge Dependence for Activation. *Biochemistry* 30, 5873-80.

Cornell, R.B. (1991b) Regulation of CTP:phosphocholine Cytidylyltransferase by Lipids. Surface Curvature, Acyl Chain Length and Lipid Phase Dependence for Activation. *Biochemistry* 30, 5881-5888.

Cornell, R.B. (1998) How Cytidylyltransferase Uses an Amphipathic Helix to Sense Membrane Phospholipid Composition. *Biochem. Soc. Trans.* 26, 539-544

Cornell, R.B., Kalmar, G.B., Kay, R.J., Johnson, M.A., Sanghera, J.S., and Pelech, S.L. (1995) Functions of the C-terminal Domain of CTP: phosphocholine Cytidylyltransferase. Effects of C-terminal Deletions on Enzyme Activity, Intracellular Localization and Phosphorylation Potential. *Biochem. J*. 310, 699-708.

Cornell, R. B. and Northwood, I. C. (2000) Regulation of CTP:phosphocholine cytidylyltransferase by amphitropism and relocalization. *Trends Biochem Sci* 25, 441-7.

Cornell, R.B. and Taneva, S.G. (2006) Amphipathic Helices as Mediators of the Memrbane Interaction of Amphitropic Proteins, and as Modulators of Bilayer Physical Properties. *Curr Protein Pept Sci.* 7, 539-52

Corrin, M.L., and Harkins, W.D. (1947) The Effect of Salts on the Critical Concentration for the Formation of Micelles in Colloidal Electrolytes. *ACS*. 69, 683-688

Craig, L., Johnson, J.E., and Cornell, R.B. (1994) Identificatio of the Membrane-binding Domain of Rat Liver CTP: phosphocholine Cytidylyltransferase using Chymotrypsin Proteolysis. *J Biol. Chem.* 269, 3311-3317

Cuervo, A.M., Stefanis, L., Fredenburg, R., Lansbury, P.T., and Sulzer, D. (2004) Impaired Degradation of Mutant a-Synuclein by Chaperone-mediated Autophagy. *Science* 305, 1292–1295

Davidson, W., Jonas, A., Clayton, D., and George, J.M. (1998) Stabilization of α-Synuclein Secondary Structure Upon Binding to Synthetic Membranes. *J. Biol. Chem.* 273, 9443-9449.

Davies, S.M., Epand, R.M., Kraayenhof, R., and Cornell, R.B. (2001) Regulation of CTP: phosphocholine Cytidylyltransferase Activity by the Physical Properties of Lipid Membranes: an Important Role for Stored Curvature Strain Energy. *Biochemistry* 40, 10522-10531.

Dennis, M.K., Taneva, S.G., and Cornell, R.B. (2011) The Intrinsically Disordered Nuclear Localization Signal and Phosphorylation Segments Distinguish the Membrane Affinity of Two Cytidylyltransferase Isoforms. *J Biol. Chem.* Paper in Press

Ding, T.T., Lee, S.J., Rochet, J.C., and Lansbury, P.T. Jr. (2002) Annular α-Synuclein Protofibrils are Produced when Spherical Protofibrils are Incubated in Solution or Bound to Brain-derived Membranes. *Biochemistry* 41, 10209-10217.

Drin, G. and Antonny, B. (2010) Amphipathic Helices and Membrane Curvature. *FEBS Lett.* 584, 1840-7.

Dunne, S.J., Cornell, R.B., Johnson, J.E., Glover, N.R., and Tracy, A.S. (1996) Structure of the Membrane Binding Domain of CTP: phosphocholine Cytidylyltransferase. *Biochemistry* 35, 11975-11984.

Eftink, M.R. (1991) Fluorescence Techniques for Studying Protein Structure. *Methods Biochem. Anal.* 35, 127-205.

Eliezer, D., Kutluay, E., Bussell, R. Jr., and Browne, G. (2001) Conformational Properties of α-Synuclein in its Free and Lipid-associated States. *J. Mol. Biol.* 307, 1061-73.

Feany, M.B. and Bender, W.W. (2000) A Drosophila Model of Parkinson's Disease. *Nature* 404, 394-398.

Fink, A.L. (2006) The Aggregation and Fibrillation of α-Synuclein. *Acc. Chem. Res*. 39, 629-634.

Fiscus, W.G. and Schneider, W.C. (1966) The Role of Phospholipids in Stimulating Phosphorylcholine Cytidylyltransferase Activity. *J Biol. Chem.* 241, 3324-3330

Fredenburg, R.A., Rospigliosi, C., Meray, R., Kessler, J., Lashuel, H, Eliezer, D., Lansbury, P.T. (2007) The Impact of the E46K Mutation on the Properties of α-Synuclein in its Monomeric and Oligomeric States. *Biochemistry* 46, 7107-7118.

Friesen, J.A., Campbell, H.A., Kent, C. (1999) Enzymatic and Cellular Characterization of a Catalytic Fragment of CTP: phosphocholine Cytidylyltransferase Alpha. *J Biol. Chem*. 274, 13384-13389

Gehrig, K., Morton, C.C., and Ridgeway, N.D. (2009) Nuclear Export of the Rate-limiting Enzyme in Phosphatidylcholine Synthesis is Mediated by its Membrane Binding Domain. *J. Lipid Res.* 50, 966-976.

Georgieva, E.R., Ramlall, T.R., Borbat, P.P., Freed, J.H., and Eliezer, D. (2008) Membrane-bound α-Synuclein Forms an Extended Helix: Long-distance Pulsed ESR Measurements Using Vesicles, Bicelles and Rodlike Micelles. *J. Am. Chem. Soc.* 130, 12856-57.

Georgleva, E.R., Ramlall, T.R., Borbat, P.P., Freed, J.H., and Eliezer, D. (2010) The Lipid-binding Domain of Wild Type and Mutant α-Synuclein: Compactness and Interconversion between the Broken and Extended Helix Forms. *J. Biol. Chem.* 285, 28261-74.

Giasson, B.I., Duda, J.E., Quinn, S.M., Zhang, B., Trojanowski, J.Q., and Lee, V.M. (2002) Neuronal α-Synucleinopathy with Severe Movement Disorder in Mice Expressing A53T Human α-Synuclein. *Neuron* 34, 521-33.

Giasson, B.I., Uryu, K., Trojanowski, J.Q., Lee, V.M. (1999) Mutant and Wild Type Human α-Synucleins Assemble into Elongated Filaments with Distinct Morphologies In Vitro. *J. Biol. Chem.* 274, 7619–22

Houweling, M., Cui, Z., Anfuso, C.D., Bussiere, M., Chen, M.H. & Vance, D.E. (1996) CTP: phosphocholine cytidylyltransferase is both a nuclear and cytoplasmic protein in primary hepatocytes. *Eur. J. Cell. Biol.* 69, 55-63.

Houweling, M., Jamil, H., Hatch, G.M., Vance, D.E. (1994) Dephosphorylation of CTP-phosphocholine Cytidylyltransferase is Not Required for Binding to Membranes. *J Biol. Chem*. 269, 7544-7551

Jao, C.C., Der-Sarkissian, A., Chen, J., and Langen, R. (2004) Structure of Membrane-bound α-Synuclein Studied by Site-directed Spin Labeling. *Proc. Natl. Acad. Sci.* 101, 8331-6.

Jo, E., McLaurin, J., Yip, C.M., St. George-Hyslop, P., and Fraser, P.E. (2000) α-Synuclein Membrane Interactions and Lipid Specificity. *J Biol. Chem.* 275, 34328-34334

Johnson, J.E., and Cornell, R.B. (1994) Membrane-binding Amphipathic Alpha-helical Peptide Derived from CTP:phosphocholine Cytidylyltransferase. *Biochemistry* 33, 4327-4335

Johnson, J.E., Aebersold, R., and Cornell, R.B. (1997) An Amphipathic Alpha-helix is the Principle Membrane-embedded Region of CTP: phosphocholine Cytidylyltransferase. Identification of the 3-(trifluoromethyl)-3- (m-[125I]iodophenyl) Diazirine Photolabeled Domain. *Biochim Biophys Acta.* 1324, 273-84

Johnson, J.E., Rao, N.M., Hui, S., and Cornell, R.B. (1998) Conformation and Lipid Binding Properties of Four Peptides Derived from the Membrane-binding Domain of CTP:phosphocholine Cytidylyltransferase. *Biochem*istry 37, 9509-9519

Johnson, J.E., Xie, M., Singh, L.M.R., Edge, R., and Cornell, R.B. (2003) Both Acidic and Basic Amino Acids in an Amphitropic Enzyme, CTP: phosphocholine Cytidylyltransferase, Dictate its Selectivity for Anionic Membranes. *J Biol. Chem.* 278, 514-522

Johnson, W.C. (1999) Analyzing Protein CD for Accurate secondary Structures. *Proteins* 35, 307-312.

Kennedy, E. P. & Weiss, S. B. (1956) Function of Cytidine Coenzymes in the Biosynthesis of Phospholipids. *J Biol. Chem.* 222, 193-215.

Kent, C. (1997) CTP:phosphocholine cytidylyltransferase. *Biochim Biophys Acta* 1348, 79-90.

Kruger, R., Kuhn, W., Müller, T., Woitalla, D., Graeber, M., Kösel, S., Przuntek, H., Epplen, J.T., Schöls, L., and Riess, O. (1998) Ala30Pro Mutation in the Gene Encoding a-Synuclein in Parkinson's Disease. *Nat. Genet.* 18, 106–108

Kumar, S., Modig, K., and Halle, B. (2003) Trifluoroethanol-Induced β → α Transition in β-Lactoglobulin: Hydration and Cosolvent Binding Studied by ^{2}H, ^{17}O, and ^{19}F Magnetic Relaxation Dispersion. *Biochemistry* 42, 13708-13716.

Weinhold, P. A., Rounsifer, M. E. & Feldman, D. A. (1986) The Purification and Characterization of CTP:Phosphorylcholine Cytidylyltransferase from Rat Liver. *J Biol. Chem.* 261, 5104-5110.

Laemmli, U. K. (1970) Cleavage of Structural Proteins during the Assembly of the Head of BacteriophageT4. *Nature* 227, 680-685.

Lakowicz, J. R. (2006) *Principles of Fluorescence Spectroscopy 3rd edition*, Springer, New York., pp. 201-216.

Larsen, K.E., Schmitz, Y., Troyer, M.D., Mosharov, E., Dietrich, P., Quazi, A.,Z., Savalle, M., Stefanis, L., and Sulzer, D. (2006) α-Synuclein Overexpression in PC12 and Chromaffin Cells Impairs Catecholamine Release by Interfering with a Late Step in Exocytosis. *J. Neurosci*. 26, 11915-22.

Lee, H-J., Choi, C., and Lee, S-J. (2002) Membrane-bound α-synuclein has a high aggregation propensity and the ability to seed the aggregation of the cytosolic form. *J Biol. Chem.* 277, 67-678.

Lee, J., Johnson, J., Ding, Z., Paetzel, M., Cornell, R.B. (2009) Crystal Structure of a Mammalian CTP: Phosphocholine Cytidylyltransferase Catalytic Domain Reveals Novel Active Site Residues within a Highly Conserved Nucleotidyltransferase Fold. *J Biol. Chem*. 284, 33535-48

Leventis, P.A., and Grinstein, S. (2010) The Distribution and Function of Phosphatidylserine in Cellular Membranes. *Annu. Rev. Biophys.* 9, 407-27.

Li, J., Uversky, V., Fink, A.L. (2001) Effect of Familial PD Point Mutations A30P and A53T on the Structural Properties, Aggregation and Fibrillation of Human α-Synuclein. *Biochemistry* 40, 11604-11613.

Lykidis, A., Baburina, I. & Jackowski, S. (1999) Distribution of CTP:phosphocholine cytidylyltransferase (CCT) isoforms. Identification of a new CCT beta splice mutant. *J Biol. Chem.* 274, 26992-7001.

MacDonald, J.I. and Kent, C. (1994) Identification of Phosphorylation Sites in Rat Liver CTP: phosphocholine Cytidylyltransferase. *J Biol. Chem.* 269, 10529-10537

Masliah, E., Rockenstein, E., Veinbergs, I., Mallory, M., Hashimoto, M., Takeda, A., Sagara, Y., Sisk, A., and Mucke, L. (2000) Dopaminergic Loss and Inclusion Body Formation in α-Synuclein Mice: Implications for Neurodegenerative Disorders. *Science* 287, 1265-1269.

Middleton, E.R., and Rhoades, E. (2010) Effects of Curvature and Composition on α-Synuclein Binding to Lipid Vesicles. *Biophys. J*. 99, 2279-88.

Northwood, I. C., Tong, A. H., Crawford, B., Drobnies, A. E., and Cornell, R. B. (1999) Shuttling of CTP: phosphocholine Cytidylyltransferase Between the Nucleus and Endoplasmic Reticulum Accompanies the Wave of Phosphatidylcholine Synthesis During the G(0)→G(1) Transition. *J Biol. Chem.* 274, 26240-26248.

Nuscher, B., Kamp, F., Mehnert, T., Odoy, S., Haass, C., Kahle, P.J., and Beyer, K. (2004) α-Synuclein has a High Affinity for Packing Defects in a Bilayer Membrane. *J. Biol. Chem.* 279, 21966-21975.

Paleologou KE, Schmid AW, Rospigliosi CC, Kim HY, Lamberto GR, Fredenburg RA, Lansbury PT Jr, Fernandez CO, Eliezer D, Zweckstetter M, Lashuel HA. (2008) Phosphorylation at Ser-129 but not the Phosphomimics S129E/D Inhibits the Fibrillation of Alpha-Synuclein. *J.Biol. Chem.* 283, 16895-16905

Park, Y.S., Gee, P., Sanker, S., Schurter, E.J., Zuiderweg, E.R. & Kent, C. (1997) Identification of functional conserved residues of CTP:glycerol-3-phosphate cytidylyltransferase. Role of histidines in the conserved HXGH in catalysis. *J. Biol. Chem.* 272, 15161-15166.

Perrin, R.J. *et al*. (2000) Interaction of Human α-Synuclein and Parkinson's Disease Mutants with Phospholipids. *J. Biol. Chem.* 275, 34393-98.

Polymeropoulos, M.H., Lavedan, C., Leroy, E.,, Ide, S.E., Dehejia, A., Dutra, A., Pike, B., Root, H., Rubenstein, J., Boyer, R., Stenroos, E.S., Chandrasekharappa, S., Athanassiadou, A., Papapetropoulos, T., Johnson, W.G., Lazzarini, A.M., Duvoisin, R.C., Di Iorio, G., Golbe, L.I., and Nussbaum, R.L. (1997) Mutation in the a-Synuclein Gene Identified in Families with Parkinson's Disease. *Science* 276, 2045–2047

Roe, J.H. (1955) The Determination of Sugar in Blood and Spinal Fluid with Anthrone Reagent. *J. Biol. Chem.* 212, 335-343.

Rospigliosi, C.C., McClendon, S., Schmid, A.W., Ramlall, T.F., Barre, P., Lashuel, H.A., and Eliezer, D. (2009). E46K Parkinson's-linked Mutation Enhances C-terminal-to-N-terminal Contacts in α-Synuclein. *J. Mol. Biol.* 388, 1022–32

Rost B, and Eyrich VA. (2001) EVA: Large-scale Analysis of Secondary Structure Prediction. *Proteins* 45, Suppl 5, 192-199.

Sambrook, J., Fritsch., E.F., and Maniatis, T. (1989) *Molecular cloning: a Laboratory Annual.* Cold Spring Harbor Laboratory, Cold Spring Harbor, N.Y.

Singleton, A.B., Farrer, M., Johnson, J., Singleton, A., Hague, S., Kachergus, J., Hulihan, M., Peuralinna, T., Dutra, A., Nussbaum, R., Lincoln, S., Crawley, A., Hanson, M., Maraganore, D., Adler, C., Cookson, M.R., Muenter, M., Baptista, M., Miller, D., Blancato, J., Hardy, J., and Gwinn-Hardy, K. (2003) a-Synuclein Locus Triplication Causes Parkinson's Disease. *Science* 302, 841

Soper, J.H., Roy, S., Stieber, A., Lee, E.,Wilson, R.B., Trojanowski, J.Q., Burd, C.G., and Lee, V.M. (2008) α-Synuclein-induced Aggregation of Cytoplasmic Vesicles in *Saccharomyces cerevisiae*. *Mol. Biol. Cell* 19, 1093–103

Spillantini, M.G., Schmidt, M.L., Lee, L.M., Trojanowski, J.Q., Jakes, R., and Goedert, M. (1997) a-Synuclein in Lewy bodies. *Nature* 388, 839–840

Sreerama, N., and Woody, R.W. (1993) A Self-Consistent Method for the analysis of Protein Secondary Structure from Circular Dichroism. *Anal. Biochem.*, 209, 32-44.

Sreerama, N. and Woody, R.W. (2000) Estimation of protein secondary structure from CD spectra: Comparison of CONTIN, SELCON and CDSSTR methods with an expanded reference set. *Anal. Biochem.* 282, 252-260.

Taneva, S., Johnson, J.E., and Cornell, R.B. (2003) Lipid-induced Conformation Switch in the Membrane Binding Domain of CTP:phosphocholine Cytidylyltransferase: a Circular Dichroism Study. *Biochemistry* 42, 11768-11776

Taneva, S.G., Patty, P.J., Frisken, B.J., and Cornell, R.B. (2005) CTP:Phosphocholine Cytidylyltransferase Binds Anionic Phospholipid Vesicles in a Cross-bridging Mode. *Biochemistry* 44, 9382-9393.

Ulmer, T.S., Bax, A., Cole, N.B., and Nussbaum, R.L. (2005) Structure and Dynamics of Micelle-bound Human α-Synuclein. *J. Biol. Chem.* 280, 9595-603.

Uversky, V., Li, J., and Fink, A.L. (2001) Evidence for a Partially Folded Intermediate in α-Synuclein Fibril Formation. *J. Biol. Chem.* 276, 10737.

Volles, M.J. and Lansbury, P.T. (2003) Zeroing In on the Pathogenic Form of α-Synuclein and its Mechanism of Neurotoxicity in Parkinson's Disease. *Biochemistry* 42, 7871-7878.

Wang, Y. and Kent, C. (1995a) Identification of an Inhibitory Domain of CTP:Phosphocholine Cytidylyltransferase. *J Biol. Chem.* 270, 18948-18952

Wang, Y and Kent, C. (1995b) Effects of Altered Phosphorylation Sites on the Properties of CTP: phosphocholine Cytidylyltransferase. *J Biol. Chem.* 270, 17843-17849

Wang, Y., MacDonald, J. I., and Kent, C. (1993) Regulation of CTP: phosphocholine Cytidylyltransferase in HeLa Cells. Effect of Oleate on Phosphorylation and Intracellular Localization. *J Biol. Chem.* 268, 5512-5518,

Wang, Y., MacDonald, J.I., and Kent, C. (1995) Identification of the Nuclear Localization Signal of Rat Liver CTP:phosphocholine Cytidylyltransferase. *J Biol. Chem.* 270, 354-360

Watkins, J.D., and Kent, C. (1991) Regulation of CTP:phosphocholine Cytidylyltransferase Activity and Subcellular Location by Phosphorylation in Chinese Hamster Ovary Cells. The Effect of Phospholipase C Treatment. *J. Biol. Chem*. 266, 21113-7.

Weinreb, P.H., Zhen, W., Poon, A.W., Conway, K.A., and Lansbury, P.T. Jr. (1996) NACP, a Protein Implicated in Alzheimer's Disease and Learning, is Natively Unfolded. *Biochemistry* 35, 13709–15

Wood WB. (1966) Host Specificity of DNA Produced by Escherichia Coli: Bacterial Mutations Affecting the Restriction and Modification of DNA. *J Mol Biol.* 16, 118-33.

Xie, M., Smith, J. L., Ding, Z., Zhang, D. & Cornell, R. B. (2004) Membrane binding modulates the quaternary structure of CTP:phosphocholine cytidylyltransferase. *J Biol. Chem.* 279, 28817-25.

Yang, W., Boggs, K.P., and Jackowski, S. (1995) The Association of Lipid Activators with the Amphipathic Helical Domain of CTP: phosphocholine Cytidylyltransferase Accerlates Catalysis by Increasing the Affinity of the Enzyme for CTP. *J Biol. Chem.* 270, 23951-23957

Yonetani, M., Nonaka, T., Masuda, M., Inukai, Y., Oikawa, T., Hisanaga, S., and Hasegawa, M. (2009). Conversion of Wild-type α-Synuclein into Mutant-type Fibrils and its Propagation in the Presence of A30P Mutant. *J. Biol Chem.* 284, 7940–50

Zarranz, J.J., Alegre, J., Gómez-Esteban, J.C., Lezcano, E., Ros, R., Ampuero, I., Vidal, L., Hoenicka, J., Rodriguez, O., Atarés, B., Llorens, V., Gomez Tortosa, E., del Ser, T., Muñoz, D.G., and de Yebenes, J.G. (2004) The New Mutation, E46K, of a-Synuclein Causes Parkinson and Lewy Body Dementia. *Ann. Neurol*. 55, 164–173

Zhu, M., and Fink, A.L. (2003) Lipid Binding Inhibits α-Synuclein Fibril Formation. *J. Biol. Chem*. 278**,** 16873-77.

Zhu, M., Li, J., and Fink, A.L. (2003) The Association of α-Synuclein with Membranes Affects Bilayer Structure, Stability, and Fibril Formation *J. Biol. Chem.* 278, 40186-40197.

APPENDICES

Appendix A: PCR And Thermocycling Reaction Conditions

Table A 1 PCR Reaction Components

Template DNA	Various	100 ηg
Forward Primer	Various	100 ηg
Reverse Primer	Various	100 ηg
dNTPs	dATP, dTTP dCTP,dGTP	250 μM each (final)
10X Reaction Buffer		5 μl
ddH_2O		to 50 μl
polymerase	*PfuTurbo*	2.5 U

Table A 2 PCR conditions

95°C	2 min	
95°C	1 min	x 24 cycles
58°C	1 min	
72°C	2 min/kb template length	
72°C	5 min	
4°C	∞	

QuikChange Site Directed Mutagenesis

Table A 3 QuikChange Site Directed Mutagenesis Reaction Components

Template DNA	Various	50 ηg
Forward Primer	Various	125 ηg
Reverse Primer	Various	125 ηg
dNTPs	dATP,dTTP dCTP, dGTP	2.5 mM each (final)
10x Reaction Buffer		5 µl
ddH_2O		to 50 µl
DNA polymerase	*PfuTurbo*	2.5 U

Table A 4 QuikChange Site Directed Mutagenesis Thermocycling Conditions

94°C	6 min	
94°C	1 min	x 24 cycles
50°C	1 min	
68°C	2 min/kb template length	
68°C	15 min	
4°C	∞	

Appendix B: Oligonucleotide Primers

Primer Design for PCR

- analyzed using Premiere Biosoft NetPrimer software

NAME:	**DESCRIPTION:**
NdeI-CT237-5F	Forward primer for pET-14b-CCT237-367 and pET-14b-CCT237-367-phospho-mimic

Y M H M E K K Y H L Q E

5' GG TAC ATG CAT ATG GAA AAG AAA TAC CAC TTG CAA GAA CG 3'

237 238 239 240 241 242 243 244

↑ inserted NdeI site

Annealing Sequence to CCT

# of Bases in Annealing Sequence: 26	**GC Content in Annealing Sequence:** 38.46%	**Annealing Sequence T_M:** 63.2°C
Total # of Bases: 40	**Total GC Content:** 40%	**Total T_M:** 77.93°C

NAME:	**DESCRIPTION:**
Modified T7	Reverse primer complementary to T7 region of pET-14b

STOP Q E A

5' GG TTA TGC TAG TTA TTG CTC AGC G 3'

Annealing Sequence to T7 termination region

# of Bases in Annealing Sequence: 24	**GC Content in Annealing Sequence:** 45.8%	**Annealing Sequence T_M:** 60.78°C

NAME:	DESCRIPTION:
BamH1-Stop-CT367-phospho-mimic-3R	Reverse Primer for pET-14b-CCT237-367-phospho-mimic

D E E D E E I D

5' ACT GTC AAG GGA TCC TTA GTC CTC TTC ATC CTC TTC GAT GTC AC 3'

367 336 335 334 333 332 331 330

Annealing Sequence to PM CCT

# of Bases in Annealing Sequence: 26	GC Content in Annealing Sequence: 50%	Annealing Sequence T_M: 64.58°C
Total # of Bases: 44	**Total GC Content:** 47.7%	**Total T_M:** 81.66°C

NAME:	DESCRIPTION:
T7-prom20-5F	Forward primer for making pET-14b-α-Syn

5’ TAA TAC GAC TCA CTA TAG GGA G 3’

Annealing Sequence to T7 promotor region

# of Bases in Annealing Sequence: 22	GC Content in Annealing Sequence: **40.9**	Annealing Sequence T_M: 49.1°C

NAME:	DESCRIPTION:
pT7-7ClaI-3R	Reverse primer for making pET-14b-α-Syn

5’ G TAT CTC GAG T CAT GTT TGA CAG CTT ATC ATC G 3’

↑ inserted XhoI site

Annealing Sequence to pT7-7 plasmid

# of Bases in Annealing Sequence:	GC Content in Annealing Sequence:	Annealing Sequence T_M: °C
Total # of Bases:	Total GC Content:	Total T_M: °C

Primers Design for QuikChange Mutagenesis

- T_M: 81.5 +0.41(%GC)-(675/N)-% mismatch; N=primer length in bases

NAME:	DESCRIPTION:
CCT-W336F-5F	Forward primer for WT CCT W336F substitution

↓ mutated trp→phe

E R S P S P S F R **F** P F S G K

5' GAG CGC TCC CCC TCC CC**A AG**C TTT CGG T**TT** CCC TTC TCT GGC AAG AC 3'

327 328 329 330 331 332 333 334 335 336 337 338 339 340 341

↑ inserted HindIII site (Pro and Ser are conserved)

# OF BASES: 47	GC CONTENT: 61.7%	MISMATCH: 10.6%	T_M: 81.8°C

NAME:	**DESCRIPTION:**
CCT-W336F-3R	Reverse primer for WT CCT W336F substitution

↓ mutated trp→phe

K G S F P **F** R F S P S P S R E

5'GT CTT GCC AGA GAA GGG **AA**A CCG AAA GCT TGG GGA GGG GGA GCG CTC3'

341 340 339 338 337 336 335 334 333 332 331 330 329 328 327

inserted HindIII site (Pro and Ser are conserved) ↑

# OF BASES: 47	**GC CONTENT:** 61.7%	**MISMATCH:** 10.6%	**T_M:** 81.8°C

NAME:	**DESCRIPTION:**
CCT-PM-W336F-5F	Forward primer for PM CCT W336F substitution

↓ mutated trp→phe

E R E P E P E F R **F** P F E G K

5' GAG CGC GAA CCC GAG CCT GAA TT**C** CGG T**TT** CCC TTC GAA GGC AAG AC 3'

327 328 329 330 331 332 333 334 335 336 337 338 339 340 341

↑ inserted EcoRI site (Glu and Phe are conserved)

# OF BASES: 47	**GC CONTENT:** 59.6%	**MISMATCH:** 6.4%	**T_M:** 85.1°C

NAME:	**DESCRIPTION:**
CCT-PM-W336F-3R	Reverse primer for PM CCT W336F substitution

↓ mutated trp→phe

K G E F P **F** R F E P E P E R E

5' GT CTT GCC TTC GAA GGG **AA**A CCG **G**AA TTC AGG CTC GGG TTC GCG CTC 3'

341 340 339 338 337 336 335 334 333 332 331 330 329 328 327

↑ inserted EcoRI site (Glu and Phe are conserved)

# OF BASES: 47	**GC CONTENT:** 59.6%	**MISMATCH:** 6.4%	**T_M:** 85.1°C

NAME:	**DESCRIPTION:**
α-Syn-V37W-5F	Forward primer for α-Syn V37W substitution

↓ mutated val→trp

G K T K E G W L Y V G S

5' GGA AAG ACA AAA GAG GGT **TGG** CTC TAT GTA GGC TCC 3'

31 32 33 34 35 36 37 38 39 40 41 42

# OF BASES: 36	**GC CONTENT:** 50%	**MISMATCH:** 8.3%	**T_M:** 74.9°C

NAME:	**DESCRIPTION:**
α-Syn-V37W-3R	Reverse primer for α-Syn V37W substitution

↓ mutated val→trp

S G V Y L W G E K T K G

5' GGA GCC TAC ATA GAG **CCA** ACC CTC TTT TGT CTT TCC 3'

42 41 40 39 38 37 36 35 34 33 32 31

↑ inserted EcoRI site (Glu and Phe are conserved)

# OF BASES: 36	**GC CONTENT:** 50%	**MISMATCH:** 8.3%	**T_M:** 74.9°C

NAME:	**DESCRIPTION:**
W278F-5F	Forward primer for WT and PM CCT W278F

↓ mutated trp→phe

D L I Q K **F** E E K S R E F I F S F

5' GAC CTC ATC CAG AAG T**TT** GAG GAG AAG TCC CGA GA**A** TTC ATT GGA AGT TTC 3'

273 274 275 276 277 278 279 280 281 282 283 284 285 286 287 288 289

inserted EcoRI site (Glu and Phe are conserved) ↑

# OF BASES: 51	**GC CONTENT:** 45.1%	**MISMATCH:** 5.9%	**T_M:** 80.9°C

NAME:	**DESCRIPTION:**
W278F-3R	Reverse primer for WT and PM CCT W278F

↓ mutated trp→phe

F S F I F E R S K E E **F** K Q I L D

5' GAA ACT TCC AAT GAA TTC TCG GGA CTT CTC CTC **AA**A CTT CTG GAT GAG GTC 3'

289 288 287 286 285 284 283 282 281 280 279 278 277 276 275 274 273

↑ inserted EcoRI site (Glu and Phe are conserved)

# OF BASES: 51	**GC CONTENT:** 45.1%	**MISMATCH:** 5.9%	**T_M:** 80.9°C

NAME:	**DESCRIPTION:**
M302W-5F	Forward primer for WT and PM CCT M302W

↓ mutated phe→trp

G A L K H **W** L K E G K

5' GGA GCG CTG AAG CAC **TG**G CTG AAA GAG GGA AAA GG 3'

297 298 299 300 301 302 303 304 305 306 307

# OF BASES: 35	**GC CONTENT:** 57.1%	**MISMATCH:** 5.7%	**T_M:** 79.9°C

NAME:	**DESCRIPTION:**
M302W-3R	Reverse primer for WT and PM CCT M302W

↓ mutated phe→trp

K G E K L **W** H K L A G

5' CC TTT TCC CTC TTT CAG C**CA** GTG CTT CAG CGC TCC 3'

307 306 305 304 303 302 301 300 299 298 297

# OF BASES: 35	**GC CONTENT:** 57.1%	**MISMATCH:** 5.7%	**T_M:** 79.9°C

Appendix C: Purification of WT and PM CCT Tails and α-Synuclein Tryptophan Variants

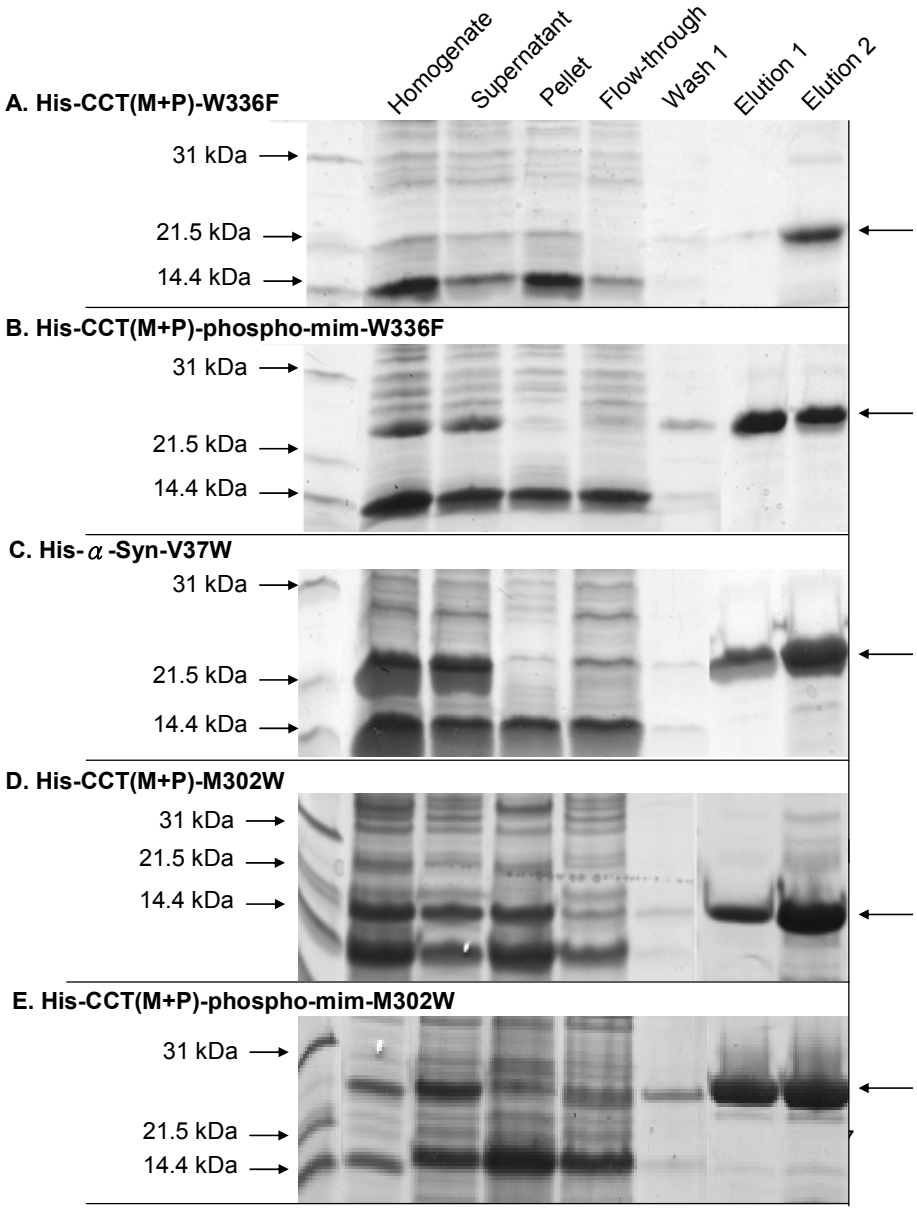

Figure C.1 Nickel-Affinity Chromatography with the Use of the Detergent OG Generates High Recovery of Soluble His-tagged Tryptophan Variants
Over-expressed His-tagged tryptophan variants were enriched in the soluble fraction (supernatant) after cell lysis. The tagged-proteins were purified using nickel-affinity chromatography where they eluted in the first two elution fractions (arrow on the right marks the position of each construct). Samples were subjected to 12% SDS-PAGE and visualized with Coomassie (refer to methods for proportion of aliquots loaded)

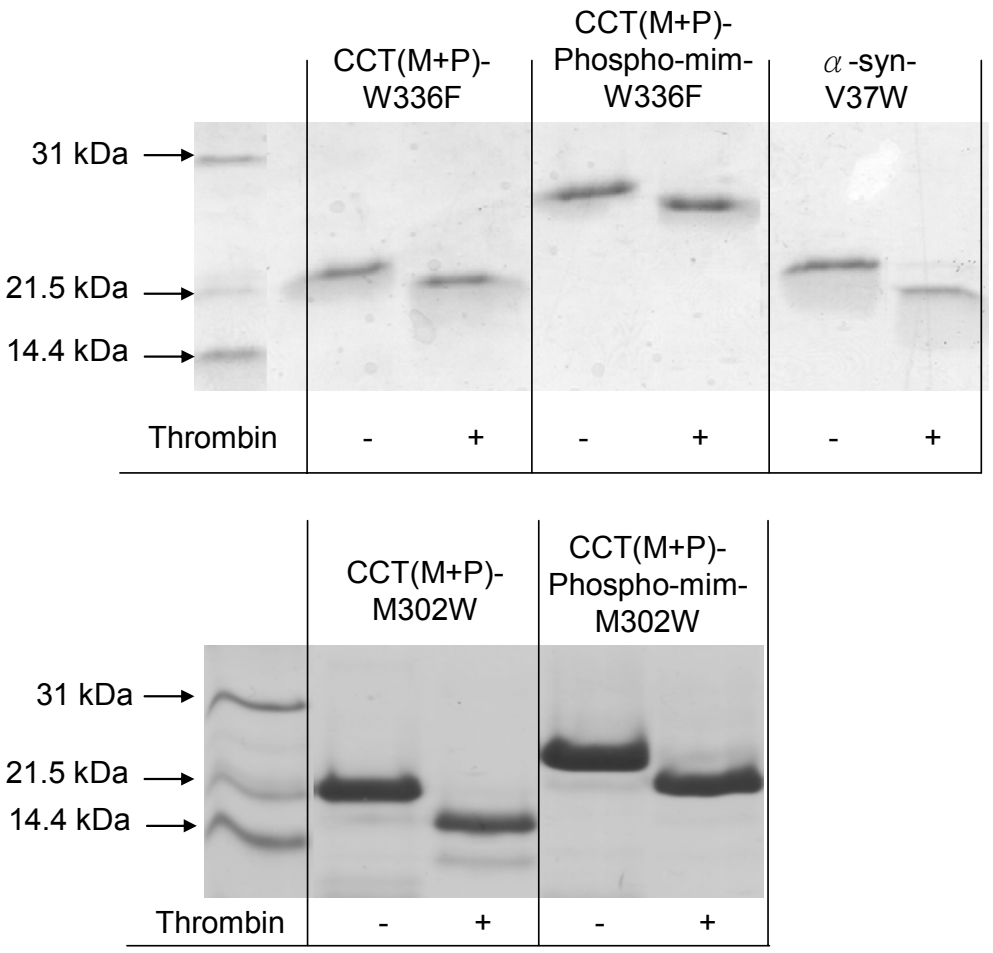

Figure C.2 Thrombin Digestion of N-terminal His-tagged Tryptophan Variants
Elution fraction #2 of each tryptophan variant was subjected to thrombin digestion where the His-tag was cleaved. The tryptophan variants were then subjected to Amicon Ultrafiltration to reduce OG concentration. Samples were run on 12% SDS-PAGE and visualized with Coomassie (proportional aliquots were loaded into each gel).